DUAL-TARGETED INHIBITORS OF BACTERIAL RNA POLYMERASE

By

CHIH-TSUNG LIN

A dissertation submitted to the

School of Graduate Studies

Rutgers, The State University of New Jersey

In partial fulfillment of the requirements

For the degree of

Doctor of Philosophy

Graduate Program in Chemistry and Chemical Biology

Written under the direction of

Richard H. Ebright

And approved by

_____

_____

_____

_____

New Brunswick, New Jersey

October, 2020

ABSTRACT OF THE DISSERTATION

Dual-targeted inhibitors of bacterial RNA polymerase

by CHIH-TSUNG LIN

Dissertation Director:

Richard H. Ebright

Resistance to antibacterial agents has become a grave threat to public safety and human health. In this work, in hopes of helping to combat this ever-increasing threat, we have designed, synthesized, and characterized two novel classes of compounds that inhibit the bacterial RNA polymerase (RNAP) enzyme and, as a result, inhibit bacterial growth. These compounds are dual-targeted inhibitors of bacterial RNAP. Through the covalent conjugation of two non-identical bacterial RNAP inhibitors, each having a distinct binding site on the bacterial RNAP enzyme, we have created compounds that can bind to two different sites on the enzyme, either in parallel or simultaneously. As a result, these dual-targeted inhibitors are able to overcome a resistance substitution that would prevent a single-target inhibitor from binding to the enzyme – making it much more difficult for a bacterium to develop resistance to these novel compounds.

The first dual-targeted inhibitors examined in this work, Class I inhibitors, are composed of a first moiety, which binds to the rifamycin/sorangicin (Rif/Sor) binding site on bacterial RNAP, that is covalently-linked to a second moiety, which binds to the immediately adjacent GE23077 (GE) binding site on bacterial RNAP. The two moieties in one molecule of a Class I dual-targeted inhibitor are able to interact

simultaneously with one molecule of bacterial RNAP through the two neighboring binding sites. Several Class I dual-targeted inhibitors were synthesized through the conjugation of Rif-derivatives or Sor-derivatives to derivatives of GE, to yield RifaGEs or SoraGEs, respectively. Biochemical experiments demonstrate that Class I dual-targeted inhibitors potently inhibit *Escherichia coli* (*E. coli*) RNAP, and are able to overcome resistance arising from a substitution in either the Rif/Sor binding site or the GE binding site. The crystal structure of *Thermus thermophilus* (*Tth*) RNAP in complex with a SoraGE demonstrates that both moieties on Class I dual-targeted inhibitor interact simultaneously with each of their binding sites on RNAP.

Class II dual-targeted inhibitors, the other primary focus of this study, are composed of a first moiety, which binds to the Rif binding site, that is covalently-linked to a second moiety, which binds to the non-adjacent binding site of the Nα-aroyl-N-aryl-phenylalaninamides (AAPs) on bacterial RNAP. Since the binding sites are non-adjacent, two molecules of a Class II dual-targeted inhibitor are able to bind simultaneously to every one molecule of bacterial RNAP. Several Class II dual-targeted inhibitors were been synthesized through the conjugation of Rif-derivatives to AAP-derivatives, to yield RifaAAPs. Biochemical experiments demonstrate that RifaAAPs potently inhibit *Mycobacterium tuberculosis* (*Mtb*) RNAP, exhibit potent antibacterial activity against *Mtb* in culture, and overcome resistance arising from a substitution in either the Rif binding site or the AAP binding site. The crystal structure of *Mtb* RNAP in complex with a RifaAAP indicates that every one molecule of bacterial RNAP has two molecules of RifaAAP bound to it, one located at the Rif binding site and one located at the AAP-binding site.

This work provides a basis for developing new inhibitors of bacterial RNAP that can overcome the most common mechanism of rifampin-resistance in clinical isolates. Dual-targeted inhibitors may play an important role in development of new antibiotics that could overcome the serious threat of clinical antibiotic resistance.

Acknowledgements

I would like to express my sincere thanks to my advisor, Dr. Richard Ebright, for his support and mentorship during the running of my graduate research. I am extremely grateful to Dr. Ebright for accepting me into the Ebright's lab and offering me a good research platform in antibacterial drug development. I have benefited from Dr. Ebright's guidance in conducting outstanding research, creative thinking, and cautious scientific attitude. It was my honor to be a Ph.D. student in the Ebright's lab.

I would also like to thank my dissertation committee members, Dr. Eddy Arnold, Dr. Wilma Olson, and my outside committee Dr. Bryce Nickels, for taking the time to serve on my committee and reviewing this work. During every annual committee meeting, Dr. Arnold and Dr. Olson always provided valuable suggestions that are important for me to carry out and finish this work.

I want to give special thanks to Dr. Yon Ebright and Dr. David Degen for their help and guidance in organic synthesis, biochemical assay, and protein purification. I appreciate your patience and the great amount of time both of you had spent on me. Additionally, I am also grateful to the previous and current structural biologists in the Ebright's lab, Dr. Yu Zhang, Dr. Wei Lin, and Mr. Yu Liu, for their work in crystallizing RNA polymerase in complex with SoraGEs and RifaAAPs.

I would also like to express my gratitude to each of the previous and current members I have interacted with in the Ebright's lab, Dr. Yu Feng, Dr. Juan Shen, Dr. Miaoxin Lin, Dr. Libing Yu, Dr. Chengyuan Wang, Dr. Jared Winkelman, Dr. Soma Mandal, Dr. Meliza Talaue, Dr. Vadim Molodtsov, Dr. Adam Hasemeyer, Dr.

Abhishek Mazumder, Dr. Hanif Vahedian-Movahed, Ms. Shuang (Carol) Liu, Ms. Ruiheng Yin, Ms. Shuya Yang, Ms. Yuxuan Wang, Mr. Pengpeng Wu, for their support and advice throughout my graduate studies.

Finally, I would like to convey my deepest thanks to my parents and families. All of you always stand by me and provide all the help that I need over the years. Especially, I deeply appreciate my dearest wife, Yu-Fen Huang. Without her care, encouragement, patience, and love, I could not have completed this Ph.D. degree. Therefore, I want to share my joy and glory with her. I would also like to thank my lovely daughter and son, Charlotte and Christopher, for their love and accompanying during my Ph.D. study at Rutgers.

Dedication

Dedicated to my dearest wife Yu-Fen Huang

Table of Contents

List of Figures

List of Tables

Chapter 1:

Introduction

The resistance to antimicrobials has been a critically-important, global issue, threatening public safety and human health (Marston et al., 2016). According to statistics from the Centers for Disease Control and Prevention (CDC), antibiotic-resistance affects at least 2.8 million people, and kills 35,000 people in the U.S. every year (CDC, 2019). Worldwide, antimicrobial resistance leads to 700,000 deaths each year (World Health Organization, 2019a). By 2050, the forecasting mortality of antibacterial drug resistance may be as high as 10 million people per year (World Health Organization, 2019a). Today, nearly all major pathogenic bacteria have developed resistance against one or more clinically-used antibiotics. There is an urgent need to develop novel antimicrobial drugs and to redesign current antibiotics in order to counteract bacterial resistance (Brown and Wright, 2016).

Tuberculosis (TB), which is globally recognized as one of the top ten infectious diseases, was responsible for 10 million infections and 1.5 million deaths in 2018 (World Health Organization, 2019b). TB is currently a treatable disease via multi-drug combination therapy. The standard treatment for TB infection is typically a six-month course of four different antibiotics in parallel: isoniazid, ethambutol, pyrazinamide, and rifampin (Rif) (World Health Organization, 2019b). TB's slow-growing and non-replicating bacterial cells make it extremely difficult to cure TB-infected patients (Barry et al., 2009). Drug-resistant TB is currently becoming another serious crisis (Riley, 1993; World Health Organization, 2019b). Although the resistance happens naturally over time via genetic mutation, misuse and

mismanagement of antibiotics during the long-period therapy for TB are also speeding up the rate of resistance development.

Among the four different antibiotics for TB treatment, rifampin (Rif) is one of the two most potent TB drugs, with the ability to kill the *Mycobacterium tuberculosis* (*Mtb*) bacterium (Mitchison, 2000). Nevertheless, resistance to Rif is one of the most common causes of multidrug-resistant TB (MDR TB) and extensively drug-resistant TB (XDR TB) (Gillespie, 2002; Floss and Yu, 2005; Madariaga et al., 2008). According to a 2019 WHO estimate, approximately half a million cases of rifampin-resistant or multidrug-resistant TB occurred globally in 2018 (World Health Organization, 2019b). Typically, Rif inhibits bacterial growth through binding to the Rif site on bacterial RNA polymerase (RNAP) (Campbell et al., 2001). Resistance to Rif is primarily associated with the substitution of an amino acid residue within its binding pocket on the RNAP enzyme (Ovchinnikov et al., 1983; Jin and Gross, 1988; Tupin et al., 2010). The residue substitution in the Rif pocket prevents or reduces the binding of Rif to RNAP, such that Rif can no longer inhibit the enzyme and, therefore, no longer kill the bacterium.

In view of the grave and growing threat to public health posed by drug-resistant TB and other drug-resistant bacteria, the development of novel bacterial RNAP inhibitors is an important strategy to overcome antibacterial resistance (Brown and Wright, 2016). However, the discovery of new antibacterial agents that function through a new, non-Rif target, on RNAP faces several challenges, including time constraints, expense, and high levels of risk. To address these difficulties, in this work, two classes of dual-targeted bacterial RNAP inhibitors have been designed, synthesized, and characterized. Through the conjugation of two different bacterial

RNAP inhibitors, possessing different inhibitory mechanisms and different binding targets, a dual-targeted inhibitor is able to be a single molecule with dual functionalities. This results in the ability to suppress or overcome resistant substitutions arising in one of the binding targets (reviewed in Bremner et al., 2007; Pokrovskaya et al., 2010; Tevyashova et al., 2015; Klahn et al., 2017; Domalaon et al., 2018). This approach of designing dual-action inhibitors could be a means to efficiently combat the ever-increasing number of antibiotic-resistant bacterial pathogens.

1.1 Bacterial RNA Polymerase

Bacterial RNA polymerase (RNAP) is the indispensable enzyme responsible for bacterial transcription. It can synthesize RNA from a template DNA and NTPs, transferring the genetic information encoded in DNA into RNA. RNAP is conserved in all living organisms. Bacterial RNAP, archaeal RNAP, and eukaryotic RNAP I, RNAP II, and RNAP III are classified as a conserved protein family, termed the "multi-subunit RNAP family" (Ebright, 2000; Darst, 2001; Cramer, 2002; Borukhov and Nudler, 2003). Bacterial RNAP is the model system of choice for comprehensive structural and mechanistic studies.

The core bacterial RNAP enzyme, a large molecule with molecular mass about 400 kDa, is composed of five conserved subunits (β, β', α^{I}, α^{II}, and ω; Figure 1). The high-resolution crystal structure of bacterial RNAP core enzyme was first determined in *Thermus aquaticus* (*Taq*) (Zhang et al., 1999). The core enzyme has dimensions of 150 Å x 115 Å x 110 Å and a shape similar to a crab claw (Zhang et al., 1999; Ebright, 2000). The two pincers of the crab claw are made up of the two

largest subunits: β and β'. Between the two pincers of crab claw is the active-center cleft. The β' subunit is the largest subunit, with a molecular mass of about 160 kDa. It comprises one of the pincers of crab claw, and part of the base of active-center cleft and catalytic center (Chakraborty, et al., 2012; Murakami and Darst, 2003). The β subunit is the second largest subunit, with a molecular mass of about 155 kDa. It forms the other pincer of crab claw, and also the other part of the base of the active-center cleft (Naryshkin et al., 2000; Mekler et al., 2002; Zhang et al., 2012).

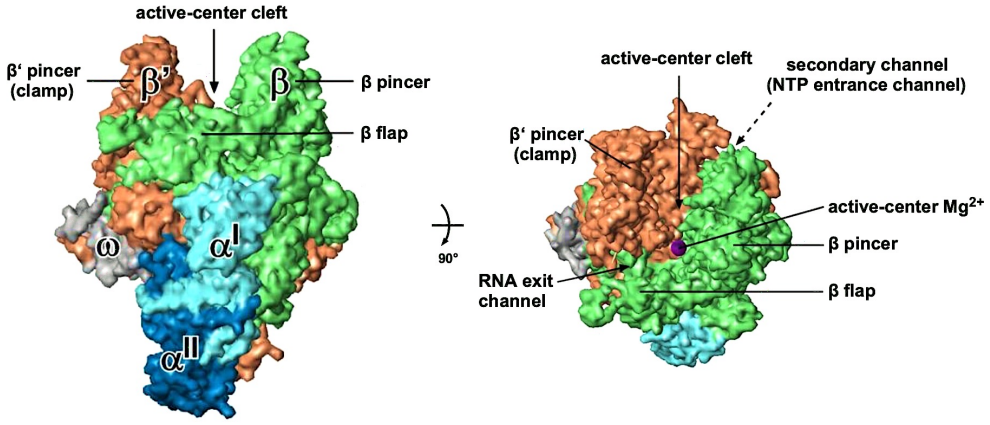

Figure 1. Structure of RNAP core enzyme (α^{I} subunit, light blue surface; α^{II} subunit, dark blue surface; β subunit, green surface; β' subunit, brown surface; ω subunit, gray surface; active-center Mg^{2+}, violet sphere) (Image modified from Wang, 2008; Lin, 2017)

The active-center cleft, which is about 25 Å in diameter in the open state and 40 Å in depth from the protein surface to the active center, is the location of transcription occurrence (Ebright, 2000). At the base of the active-center cleft is the location of active-center site and catalytic-center Mg^{2+} ion (Zhang et al., 1999; Sosunov et al., 2003). The active-center site is the starting site of RNA synthesis. During transcription, the space of the active-center cleft is sufficient to accommodate duplex DNA such that both β and β' subunit are able to interact with partially unwound DNA and the RNA product. Through the catalytic Mg^{2+}, the reaction of phosphodiester bond formation can occur with ribonucleoside triphosphate (NTP)

(Zhang et al., 1999; Sosunov et al., 2003).

The bacterial RNAP core enzyme contains two α subunits, α^{I} and α^{II}, which are located far away from the active-center cleft. Although α^{I} and α^{II} have identical sequences, α^{I} and α^{II} interact with different and specific subunits on RNAP. Generally, the α^{I} subunit primarily interacts with β subunit, and the α^{II} subunit interacts with β' subunit. The composition of each α subunit is a N-terminal domain (αNTD) connected to a C-terminal domain (αCTD) through a 14-residue flexible linker (Wang et al., 1997). The function of the α subunit is to initiate the assembly of RNAP through the dimerization of αNTD and the interaction of β and β' subunit, or to interact with upstream promoter elements and some transcription regulators through αCTD (Ross, et al., 1993; Hudson, et al., 2009).

The pincer of the β' subunit, which is also called "the clamp", plays an important role in transcription. The clamp is able to control the opening and the closing of the active-center cleft (Cramer et al., 2001; Gnatt et al., 2001; Murakami and Darst, 2003; Chakraborty et al., 2012). The duplex DNA is only allowed to load into the active-center cleft while the clamp is opening. The most essential component to control the movement of clamp is named "hinge", which is located at the base of the β' pincer (Mukhopadhyay et al., 2008; Srivastava et al., 2011). Additionally, there are two major channels within the RNAP enzyme. The NTP entrance channel, which is also called secondary channel (Zhang et al., 1999; Ebright, 2000; Korzheva et al., 2000), is formed via parts of both the β and β' subunits. Through this channel, the NTPs can reach the active-center during transcription. The other channel is the RNA exit channel, which is also formed via parts of both the β and β' subunits (Ebright, 2000; Korzheva et al., 2000; Vassylyev et al., 2002). The RNA exit channel provides

a pathway for nascent RNA product to exit the enzyme.

The ω subunit is the smallest subunit in RNAP. The position of ω subunit is close to the β' pincer base and distal to the active-center cleft. The ω subunit is not necessary for the function of RNAP, but it is helpful to assemble RNAP through latching the N-terminus and C-terminus of β' subunit together (Minakhin et al., 2001).

The RNAP core enzyme is unable to perform specific, promoter-dependent transcription initiation by itself. It must assemble an additional subunit, the σ subunit, to form the RNAP holoenzyme and perform promoter-dependent transcription (Figure 2) (Darst et al., 2001; Gross et al., 1998). The function of the σ subunit is to direct a RNAP to bind to a specific sequence on promoter DNA, recognize the transcription start site, and unwind promoter DNA (Ruff et al., 2015). In nature, there are multiple types of σ subunits in various bacteria. σ^{70} (molecular mass 70 kDa) is the primary σ factor in *Escherichia coli* (*E. coli*) (Lonetto et al., 1992). It contains five conserved regions: σR1.1, σR2, σR3, the σR3/σR4 linker, and σR4 (Campbell et al., 2002; Mekler et al., 2002; Vassylyev et al., 2002). Within the RNAP holoenzyme, σR1.1 is flexible, highly negatively charged, and positioned inside the active-center cleft. It can serve as a DNA mimic until template DNA is allowed to access to the active-center and displace σR1.1 (Mekler et al., 2002). σR2 interacts with the β' subunit pincer and is positioned within and above the RNAP active-center. σR3 interacts with the base of the β subunit and σR4 binds to the tip of the β flap (Campbell et al., 2008). The σR3/σR4 linker is also highly negatively charged and occupies the RNA-exit channel (Murakami et al., 2002; Vassylyev et al., 2002). During transcription, it must be displaced from the RNA-exit channel so that the extension of RNA product during transcription elongation is able to occur smoothly (Mekler et al., 2002).

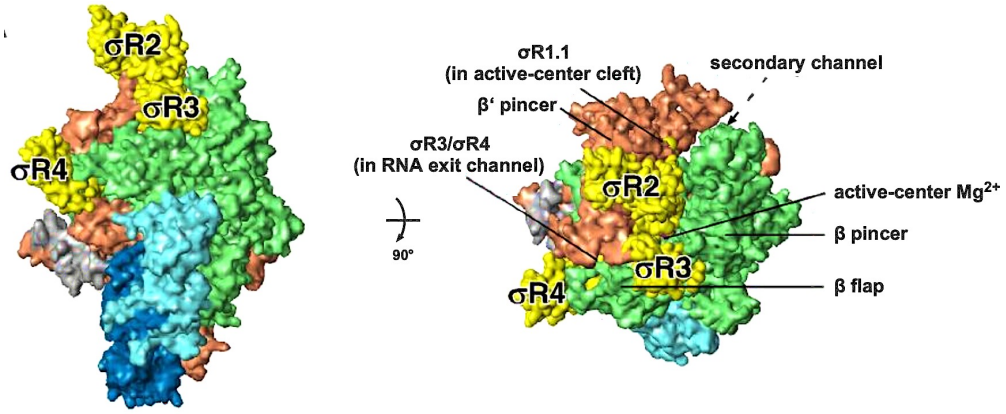

Figure 2. Structure of RNAP holoenzyme (α^{I} subunit, light blue surface; α^{II} subunit, dark blue surface; β subunit, green surface; β' subunit, brown surface; ω subunit, gray surface; σ factors, yellow surface) (Image modified from Wang, 2008; Lin, 2017)

1.2 Transcription

Transcription is an essential, and the most regulated step, in gene expression. In general, there are three sequential steps within the entire promoter-dependent transcription cycle: initiation, elongation, and termination (Figure 3) (Record et al., 1996; deHaseth et al., 1998; Murakami and Darst, 2003; Saecker et al., 2011). In order to maintain bacterial life and cell replication, all three phases are indispensable.

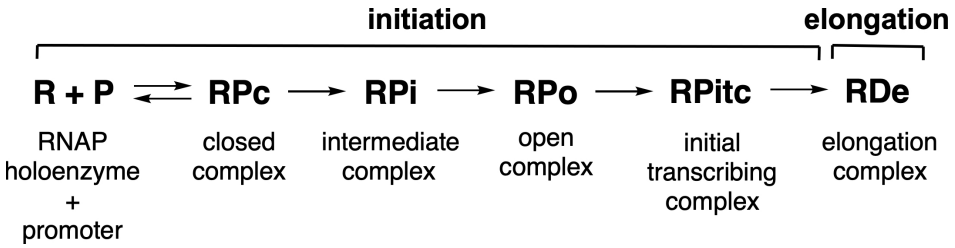

Figure 3. The schematic diagram of bacterial transcription process

1.2.1 Initiation

Transcription initiation begins with the RNAP core enzyme associated with a transcription initiation factor σ subunit to form the RNAP holoenzyme (Gross et al.,

1998; Darst et al., 2001). In the presence of DNA, each region of the σ subunit on RNAP holoenzyme can recognize and interact with the specific binding area on promoter to subsequently generate the RNA polymerase-promoter closed complex (RPc). During the phase of RPc, the duplex DNA stays outside the active-center cleft. To avoid the dissociation or isomerization of the RPc, the σR1.2 and σR2 specific interact with the -10 element of promoter DNA; σR4 specific interacts with the -35 element of promoter DNA (Mekler et al., 2002; Murakami et al., 2002; Vassylyev et al., 2002). Next, with the opening of β' clamp, the promoter DNA can be loaded into the active-center cleft of RNAP and σR1 displaced to form the RNAP-promoter intermediate complex (RPi) (Murakami and Darst, 2003). After the phase of RPi, the RNAP unwinds ~13 base pairs of double-stranded DNA surrounding the transcription start site to create a single-stranded "transcription bubble" and generate the RNAP-promoter open complex (RPo) with a closed β' clamp (Saecker et al., 2011).

After the formation of RPo, RNAP is able to begin the synthesis of RNA products in the presence of nucleoside triphosphates (NTPs). Initially, RNAP undergoes several rounds of abortive initiation, producing and releasing short RNA transcripts 2 to 9 nucleotides in length (Kapanidis et al., 2006; Revyakin et al., 2006). Once the RNAP initiates the synthesis of abortive RNA product, the status of RNAP changes from RPo to the RNAP-promoter initial transcribing complex (RPitc). Generally, the abortive initiation occurs for several rounds. This process occurs by a "scrunching" mechanism, where RNAP remains stationary on DNA, then the abortive RNA is synthesized via unwinding and pulling the downstream DNA into RNAP before passing the nucleotides through the RNAP active site in each nucleotide addition cycle (Kapanidis et al., 2006; Revyakin et al., 2006). Once an abortive RNA product 10 to 15 nucleotides in length is produced, the RNA transcript is able to

displace the σR3/σR4 linker from the RNA exit channel, resulting in destabilization of the binding between the σ subunit and RNAP core enzyme (Record et al., 1996; Mekler et al., 2002; Murakami and Darst, 2003; Mooney et al., 2005; Saecker et al., 2011). Therefore, the σ subunit can potentially be released from RNAP. Meanwhile, RNAP breaks its interactions with the promoter DNA, escaping from it and forming a transcription elongation complex (TEC or RDe) (Korzheva et al., 2000; Vassylyev et al., 2007a).

1.2.2 Elongation

During transcription elongation, under the status of RDe, the size of transcription bubble on DNA is maintained with 11 nucleotides, and the RNA-DNA hybrid is roughly 9 to 10 base pairs. By using the "stepping" mechanism, RNAP can translocate along the DNA template without DNA scrunching (Abbondanzieri et al., 2005). Within each nucleotide-addition cycle, the correct nucleotide substrate initially enters into RNAP through the secondary channel and binds to the pre-insertion site on RNAP (Vassylyev et al., 2007b). Subsequently, the correct nucleotide is delivered to the insertion site (i+1 site or A site). The hydroxyl group on the 3'-end of a nascent RNA chain in the i site (P site), which binds to the template-strand DNA, undergoes the substitution nucleophilic bi-molecular reaction (S_N2 reaction) and attacks the α-phosphate group of the nucleotide substrate in i+1 site (Erie et al., 1992). Typically, RNA synthesis during elongation occurs through the formation of a phosphodiester bond and the release of pyrophosphate byproduct (Liu, et al. 2016). Finally, the RNAP translocates by one nucleotide to continue the next nucleotide-addition cycle (Record et al., 1996; Richardson and Greenblatt, 1996).

1.2.3 Termination

Termination is the ultimate step in transcription. To stop the RNA synthesis, typically, RNAP needs to encounter a transcription terminator and release the RNA product via dissociation from template-strand DNA. There are two types of transcription termination (Richardson and Greenblatt, 1996; von Hippel, 1998). The first type is factor-independent termination, i.e., hairpin-mediated termination, wherein the intrinsic termination sequences in DNA can cause the formation of an RNA hairpin with G-C-rich base-pairs during transcription elongation, resulting in destabilization of the RDe complex, and release of the RNA product (Richardson and Greenblatt, 1996; von Hippel, 1998; Nudler, 1999). The second type of termination is factor-dependent termination. In this case, the termination factor protein, Rho, binds to a specific sequence of the RNA product, resulting in destabilization of the RDe complex, and release of the RNA transcript (Brennan et al., 1987; Richardson and Greenblatt, 1996; von Hippel, 1998).

1.3 Bacterial RNA Polymerase inhibitors and their targets

Bacterial RNA polymerase (RNAP) is a proven target for the development of antimicrobials (Darst, 2004; Chopra et al., 2007; Mukhopadhyay et al., 2008; Ho et al., 2009; Mariani et al., 2009; Srivastava et al., 2011; Ma et al., 2016). In order to discover novel broad-spectrum antibacterial agents, there are several features of bacterial RNAP that make it a suitable drug target. First, because bacterial RNAP is an essential enzyme for bacterial survival, targeting it can be an efficient approach to kill the bacterium. Second, the sequences of bacterial RNAPs are highly conserved across bacterial species (Ebright, 2000; Lane et al., 2010), and can therefore provide a basis

of broad-spectrum activity for drug candidates. Third, the sequences of bacterial RNAPs differ from the sequences of human RNAPs (Ebright, 2000; Darst, 2001; Cramer, 2002; Lane et al., 2010a; Lane et al., 2010b), which can be an opportunity for the development of inhibitors that selectively inhibit bacterial RNAP but not human RNAP. Therefore, bacterial RNAP represents an excellent target for the development of novel antibiotics.

Several different bacterial RNAP inhibitors are currently in clinical use or are under investigation. These inhibitors are able to halt transcription within a bacterium by binding to specific sites on bacterial RNAP, including the rifamycin/sorangicin binding site, the switch-region, the bridge-helix/trigger-loop, and the RNAP active-center "i and i+1 sites" (Campbell et al., 2001; Ho et al., 2009; Degen et al., 2014; Zhang et al., 2014; Lin et al., 2017; Lin et al., 2018). Because these binding sites represent distinct mechanisms to inhibit the enzyme, and do not overlap each other, inhibitors that function through these different sites would not be expected to exhibit cross-resistance with one another.

1.3.1 Rifamycins

Rifamycins are a group of macrocyclic antibacterial agents in the ansamycin family originally isolated from *Amycolatopsis mediterranei* soil bacterium (Sensi et al., 1959; Sensi et al., 1983). Their chemical structures generally consist of a naphthyl or a naphthoquinone moiety, an ansa ring, and sidechains at positions 3 and/or 4 of the naphthyl or naphthoquinone moiety (Figure 4). In the past decades, various rifamycin derivatives have been discovered from soil bacteria and have been created through semisynthesis (Sensi, et al., 1964a; Maggi, et al., 1965; Lester, 1972). One of

the most well-known and significant rifamycin derivatives is rifampin (rifampicin or Rif). Rif possesses not only the common structural core of most rifamycins, but also a specific (4-methyl-1-piperazinyl) iminomethyl side chain at position 3 of the naphthyl moiety. As discussed earlier, Rif plays a vitally important role in the treatment of TB (Aristoff et al. 2010).

In 2017, Ebright lab published a crystal structure of *Mtb* RNAP-promoter open complex with Rif bound to it (Lin et al., 2017). The resulting structure shows that Rif functions by binding to the Rif target, which is located adjacent to the RNAP active center on the β subunit (Figure 4) (Lisitsyn et al., 1984; Jin et al., 1988; Severinov et al., 1993; Campbell et al., 2001; Garibyan et al., 2003; Ho et al. 2009), on *Mtb* RNAP. Additionally, a series of crystal structures with Rif bound to the RNAP-promoter initial transcribing complex containing short RNA products, have shown that the inhibitory mechanism of Rif is to sterically obstruct the extension of the RNA product beyond a length of 2-3 nucleotides during initial transcription (McClure et al., 1978; Campbell et al., 2001; Artsimovitch et al., 2005; Feklistov et al., 2008).

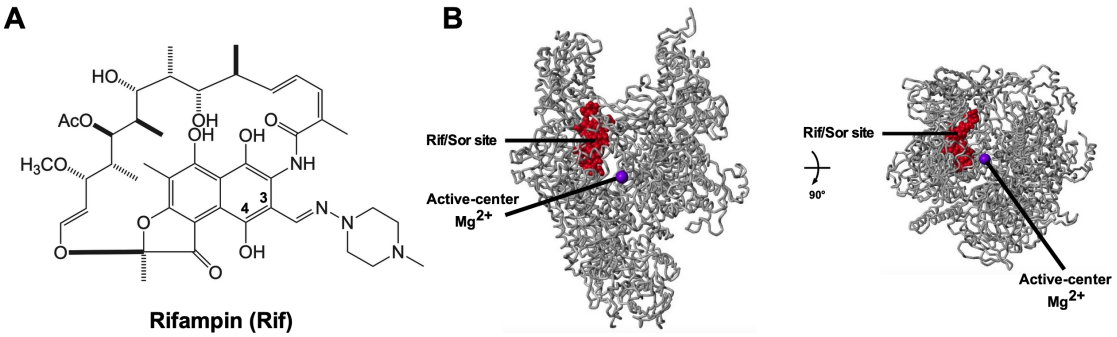

Figure 4. Structure and target of rifampin (Rif)

(A) Chemical structure of Rif.

(B) The Rif binding site is located adjacent to the RNAP active center on β subunit (gray ribbons, RNAP; Rif site, red surface; violet sphere, active-center Mg^{2+}) (Image modified from Degen, 2014).

Currently, the critical issue regarding the usage of Rif to treat TB is the

occurrence drug-resistance (Riley, 1993; Koul et al., 2011; Goldstein, 2014). The Rif binding site can be altered through the substitution of amino acid residues such that Rif no longer binds well to the RNAP enzyme. In order to overcome the development of Rif drug resistance, many researchers are attempting to redesign Rif derivatives in order to tolerate Rif resistant-substitutions without a loss of binding affinity; and to identify novel inhibitors that bind to and inhibit the RNAP enzyme through sites other than the Rif site (Floss et al., 2005; Chopra et al., 2007; Villain-Guillot et al., 2007; Forrest et al., 2010; Srivastava et al., 2011; Ma et al., 2016).

1.3.2 Sorangicin A

(+)-Sorangicin A (Sor) is a novel polyketide-derived macrocyclic-polyether antibiotic originally isolated from the myxobacterium *sorangium cellulosum* by Jansen et al. in 1985 (Jansen et al., 1985; Smith et al., 2009) (Figure 5). Similar to Rif, Sor inhibits bacterial RNAP, but does not inhibit eukaryotic and human RNAPs. Sor also possesses extraordinary antibiotic activity against both gram-positive and gram-negative bacteria (Irschik et al., 1987; Jansen et al., 1990). Mechanism of action studies have revealed that Sor inhibits transcription initiation at a step following the formation of RNAP-promoter open complex (RPo), and prevents the formation of RNA products longer than 2-4 nucleotides (Campbell et al., 2005; Xu et al., 2005; Ho et al., 2009). Therefore, the inhibitory mechanism of Sor is similar to that of Rif. Biochemical studies show that all Sor-resistant *E. coli* RNAP mutants exhibit cross-resistance to rifamycins, but only some Rif-resistant *E coli* mutants exist cross-resistance to Sor. This means that Sor and Rif are partially cross-resistant with each other, and suggests that the binding site of Sor overlaps with the Rif binding site (Rommele et al., 1990).

The structural determination of sorangicin in complex with *Thermus aquaticus* RNAP core enzyme illustrates that Sor binds to the same binding site as Rif in a pocket on the β subunit of RNAP (Campbell et al., 2005). All of the residues that Sor interacts with on RNAP are included in the residues that Rif contacts on RNAP (Ho et al., 2009). Although the Sor and Rif bind to the same binding site on RNAP, Sor has an advantageous ability to overcome some potential resistance substitutions arising from Rif binding site. In terms of chemical structure, the macrocycle of Sor (macrocyclic-polyether) is more flexible than the macrocycle of rifamycin (Campbell et al., 2005). The amino acid substitutions in the Rif binding pocket on RNAP are expected to alter the shape of the pocket. Through the conformational flexibility and reorientation, Sor is able to adapt to some of these changes in the pocket and overcome some Rif-resistance.

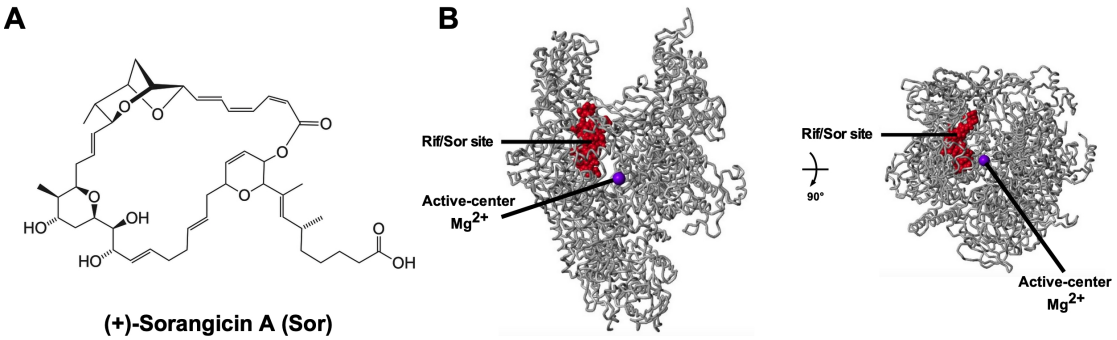

Figure 5. Structure and target of (+)-Sorangicin A (Sor)

(A) Chemical structure of Sor.

(B) The Sor binding site is same as the Rif binding site on β subunit (gray ribbons, RNAP; Sor site, red surface; violet sphere, active-center Mg^{2+}) (Image modified from Degen, 2014).

1.3.3 GE23077

GE23077 (GE) is a cyclic heptapeptide antibiotic originally isolated as a mixture of four components (A1, A2, B1 and B2) from the fermentation broth of the

soil bacterium *Actinomadura* sp. DSMZ 13491 in 2001 by Ciciliato et al. (Ciciliato et al., 2003; Ciciliato et al., 2004; Marazzi et al., 2005). The chemical structure of GE reveals that it contains four unusual amino acids: isoserine, α-aminomalonic acid, α,β-diaminopropanoic acid, and β,γ-dihydroxyglutamine, and three natural amino acids: serine, threonine, and valine (Figure 6). The differences in chemical structure between the four components are in the acyl group attached to the two different side chains on α,β-diaminopropanoic acid, and in the configuration of stereocenter on α-amino-malonic acid (Mariani et al., 2005). The inhibitory activities indicate that GE potently inhibits the bacterial RNAP transcription in both Gram-positive (*B. subtilis*) RNAP and Gram-negative (*E. coli*) RNAP (Ciciliato et al., 2004; Sarubbi et al., 2004). Due to the hydrophilic nature and the size of the cyclic peptide, GE has poor penetrating ability across the bacterial cell membrane. Hence, GE merely exhibits very narrow-spectrum antibacterial activity against *Moraxella catarrhalis* (Ciciliato et al., 2004).

The binding target of GE on RNAP has been identified through the isolation and sequencing of GE-resistant mutants; and subsequently confirmed through the crystal structure of *Thermus thermophiles* (*Tth*) RNAP holoenzyme in complex with GE (Zhang et al., 2014). Saturation mutagenesis experiments in *E. coli* indicate that GE-resistant mutants contain substitutions at only five different residues in the β subunit of RNAP located in the RNAP active-center region. These GE-resistant mutants do not have cross-resistance with Rif. The crystal structure of RNAP in complex with GE shows that the GE binding target is immediately adjacent to the Rif binding target, but does not significantly overlap it. The GE binding target overlaps the RNAP active-center i and i+1 sites, the β D2-loop and the β link region. The mechanism of inhibition for GE in RNAP is different from that of Rif and Sor: GE inhibits formation of the first phosphodiester bond in transcription initiation, that is

the first nucleotide-addition step (Zhang et al., 2014). GE is the first-known non-nucleoside RNAP inhibitor that functions through direct interaction with the RNAP active center.

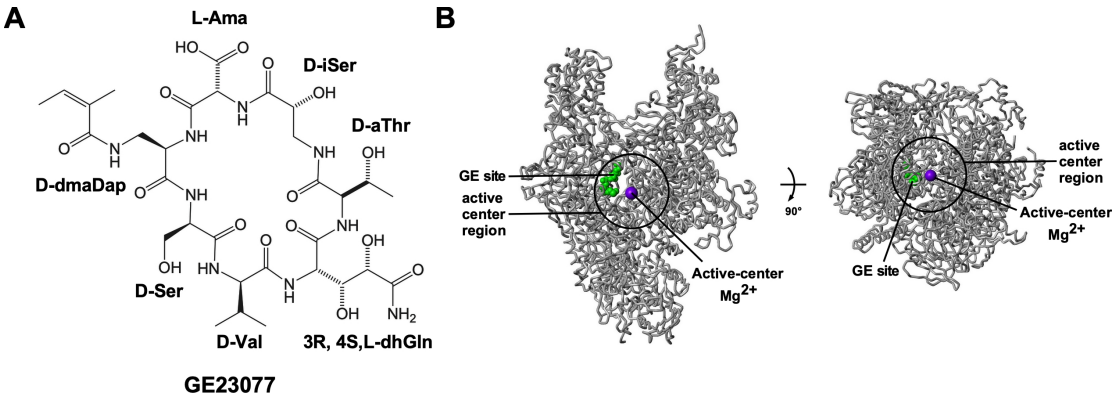

Figure 6. Structure and target of GE23077 (GE)

(A) Chemical structure of GE (D-iSer, D-isoserine; L-Ama, L-α-aminomalonic acid; D-dmaDap, D-N^{β}-(Z-2,3-dimethylacryloyl)-α,β-diaminopropanoic acid; L-dhGln, L-β,γ-dihydroxyglutamine; D-Ser, D-serine; D-aThr, D-*allo*-threonine; D-Val, D-valine).

(B) The GE binding site is located within the RNAP active-center region (gray ribbons, RNAP; GE site, green surface; violet sphere, active-center Mg^{2+}; black circle, active-center region) (Image modified from Zhang et al., 2014).

1.3.4 Nα-aroyl-N-aryl-phenylalaninamides (AAPs)

AAPs are a class of novel small-molecule inhibitors that inhibit *Mycobacterium tuberculosis* (*Mtb*) RNAP *in vitro* and *in vivo* (Ebright et al., 2018). The first AAP, which is named Nα-benzoyl-N-(2-methylphenyl)-phenylalaninamide (AAP1), was discovered through high-throughput screening of 114,260 synthetic compounds for inhibition of *Mtb* RNAP-σA holoenzyme in a fluorescence-detected transcription assay. The microplate-based Alamar Blue assays also showed that AAP1 inhibited the growth of *Mtb* in culture. AAP1 consists of three aromatic phenyl rings (A, B, and C ring) connected via two amide bonds, and possesses a chiral center on the α-carbon of phenylalanine (Figure 7). By using chiral chromatography, the D and L configurations of AAP1 could be isolated (Ebright et al., 2018). The results of

RNAP-inhibitory activity and antibacterial activity assays indicate that D-AAP1 (IC50: 1.5 μM, MIC: 3.13 μg/mL) is much more potent than L-AAP1 (IC50: 300 μM, MIC: >50 μg/mL), which means D-AAP1 possesses stereospecific activity against *Mtb*. D-AAP1 does not inhibit other bacterial RNAPs (*E. coli* and *Staphylococcus aureus*), and does not inhibit human RNAPs I/II/III. In culture, D-AAP1 exhibits potent activity against other mycobacteria, including *M. avium and M. smegmatis*; but it does not inhibit the growth of other bacterial species (*E. coli, S. aureus*, *A. baumannii*, etc.), nor does it inhibit the growth of mammalian cells (*Vero*) (Lin et al., 2017).

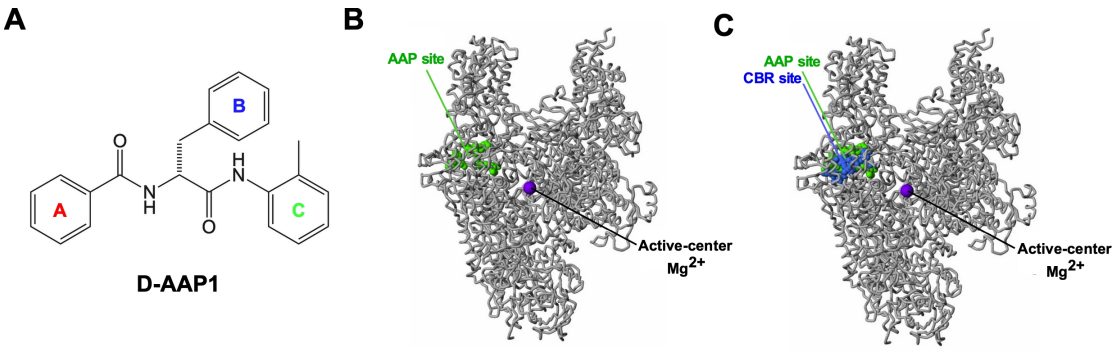

Figure 7. Structure and target of AAPs

(A) Chemical structure of D-AAP1.

(B) The AAP binding site is located in the RNAP bridge-helix N-terminus (gray ribbons, RNAP; AAP site, green surface; violet sphere, active-center Mg^{2+}).

(C) The AAP binding site is similar in location to the CBR binding site (gray ribbons, RNAP; AAP site, green surface; CBR site, blue surface; violet sphere, active-center Mg^{2+}).

The binding target of the AAPs has been determined through isolation and sequencing of AAP-resistant mutants, and subsequently verified through the crystal structure of D-AAP1 bound to an *Mtb* RNAP-promoter open complex (Lin et al., 2017). A previous graduate student and postdoc in the Ebright lab, Dr. Soma Mandal, performed the spontaneous resistance experiments in *M. smegmatis* and successfully isolated nineteen AAP-resistant mutants (Mandal, 2014). The sequencing results

indicate that all of the AAP-resistant mutants contain substitutions at one of ten residues in the RNAP β subunit, or at one of two different residues in the RNAP β' subunit. Mapping these AAP-resistant mutants onto the crystal structure of *T. thermophilus* RNAP reveals that they are located at the base of β subunit lobe and the N-terminus of β' subunit bridge-helix. To more comprehensively understand the AAP binding target, another former postdoc in the Ebright lab, Dr. Wei Lin, soaked D-AAP1 into pre-formed crystals of *Mtb* RNAP-RPo (Lin et al., 2017). The resulting structures clearly reveal that D-AAP1 binds to the N-terminus of RNAP bridge helix, which is also the binding site for the Gram-negative bacterial RNAP inhibitor CBR-703 (CBR). This binding site does not overlap with the RNAP active center (Feng et al., 2015; Lin et al., 2017). Due to the similarity in binding targets of AAPs and CBRs, the inhibitory mechanism of AAPs is expected to be similar to the inhibitory mechanism of CBRs, which is interference with bridge-helix conformational dynamics required for nucleotide addition.

1.4 Dual-targeted inhibitors of bacterial RNA polymerase

The design of dual-targeted inhibitors, in which two different drug molecules are covalently conjugated to form a single large molecule, has been a widely studied strategy for the potential treatment of bacterial infection (reviewed in Bremner et al., 2007; Pokrovskaya et al., 2010; Tevyashova et al., 2015; Klahn et al., 2017; Domalaon et al., 2018). In most cases, the two drug molecule components bind to different enzymatic targets and have different inhibitory mechanisms. The development of dual-targeted inhibitors could provide a critical solution for overcoming antibacterial drug resistance (Morphy et al., 2005; Barbachyn et al., 2008). By linking two drug moieties, the resistance arising from one of the targets contained

in the dual-targeted inhibitor can be overcome through its action on the other target. As a result, dual-targeted inhibitors also reduce the potential for resistance development.

There are several additional possible advantages in the development of dual-targeted inhibitors. Due to their dual mechanism of actions, the inhibitors may be able to enhance antibacterial potency via synergistic effects (Pokrovskaya et al., 2010). Moreover, the pharmacokinetic properties of dual-targeted inhibitors may be better than those of the individual components. Both components of dual-targeted inhibitor have matched availability, pharmacokinetics, tissue distribution, and ability of entry to bacterial-cell. In some cases, the dual-targeted inhibitor may have improved solubility and bioavailability in formulation vehicles, or possibly even reduced toxicities (Bremner et al., 2007; Barbachyn et al., 2008).

As mentioned earlier, several different bacterial RNAP inhibitors with identical or non-identical binding targets have been discovered. Dual-targeted inhibitors developed based on the known inhibitors, binding sites, and inhibitory mechanisms, can be categorized into three classes. Class I dual-targeted inhibitors contain functional components of inhibitors that are from two immediately adjacent, but non-overlapping binding sites (Maeda et al., 2006). According to their binding sites on bacterial RNAP, the relative positions of the Rif site and the GE site/RNAP active-center would fit into this class (Ho et al., 2009).

For the Class II dual-targeted inhibitors, both functional components on inhibitor are from two non-adjacent binding sites on RNAP (Maeda et al., 2006). Due to at least five different known inhibitor binding sites on bacterial RNAP, there are

many possibilities for two inhibitors from two nonadjacent binding sites. In order to overcome Rif resistance and improve the potency of AAP at the same time, the two components of the Class II dual-targeted inhibitors in our studies are primarily focused on the Rif site and AAP site/bridge-helix N-terminus (Lin et al., 2017).

Class III dual-targeted inhibitors contain two components covalently conjugated, whereby one would be an inhibitor that binds to bacterial RNAP, and the other component would bind to and restrain a different enzyme, such as DNA gyrase, bacterial topoisomerase II or IV, the ribosome, or another target (the inhibition of protein synthesis in bacterial cell) (Bozdogan et al., 2004; Zhi et al., 2006; Li et al., 2000; Robertson et al., 2008a; Robertson et al., 2008b). Recent literature has called attention to a promising dual-acting antibacterial agent, TNP-2092, a rifamycin-quinolone-derivative hybrid with potent activity against *Staphylococcus aureus* and *S. epidermidis* (Ma et al., 2016). Currently, TNP-2092 is being developed as an antimicrobial for the treatment of persistent bacterial infections, such as prosthetic joint infections, and is in phase III clinical trials. Therefore, the design of Class III dual-targeted inhibitor could also be a potential strategy to combat bacterial resistance.

Chapter 2:

Class I dual-targeted inhibitors of bacterial RNA polymerase (RifaGEs and SoraGEs)

RATIONALE

2.1 Relationship between GE and Rif, and GE and Sor

In 2014, Ebright lab published a crystal structure of *Thermus thermophilus* (*Tth*) RNA polymerase (RNAP) in complex with the cyclic-peptide antibiotic GE23077 (GE) at 3.3 Å resolution and confirmed the binding site of GE on *Tth* RNAP (Zhang et al., 2014; Ebright et al., 2016). In this structure, the GE binding site is immediately adjacent to the rifamycin (Rif) binding site without overlap. In subsequent work, a former postdoc in the Ebright lab, Dr. Yu Zhang, simultaneously soaked rifamycin SV (RifSV) and GE into a crystal of *Tth* RNAP-promoter open complex (RP_o) and successfully determined the structure (Zhang et al., 2014; Ebright et al., 2016). His results showed the electron density maps for RifSV in the Rif target and GE in the GE target in a crystal of RPo-RifSV-GE, bound at the same time, which means that both RifSV and GE can simultaneously bind to RNAP with no steric clash (Figure 8).

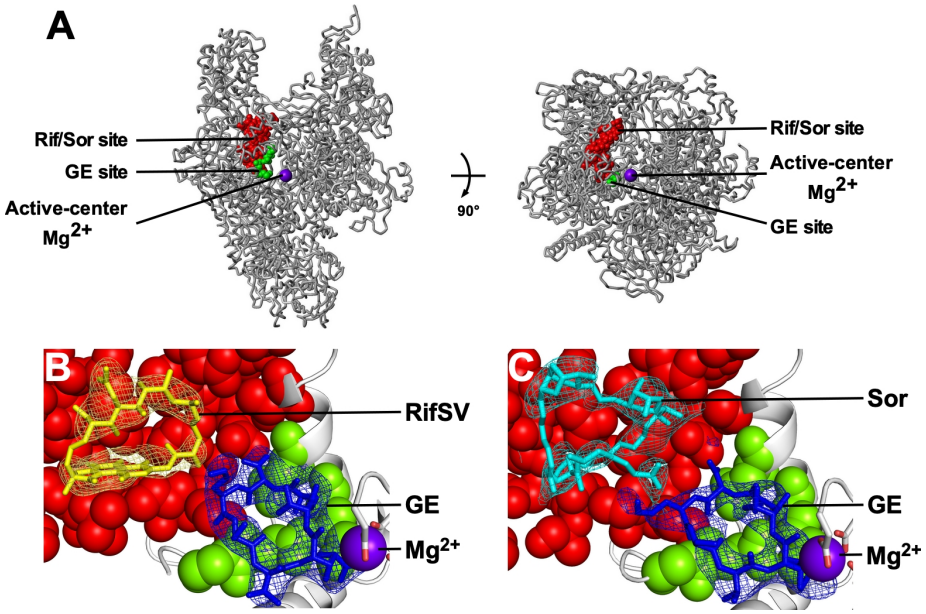

Figure 8. Targets of transcription inhibition by Rif/Sor and GE

(A) The Rif/Sor site is immediately adjacent to the GE site without overlap (Rif/Sor site, red surface; GE site, green surface; violet sphere, active-center Mg^{2+}) (Image modified from Zhang et al., 2014).

(B) Structure of *Tth* RNAP-RPo in complex with RifSV and GE. It reveals that RifSV binds to Rif/Sor site, and GE binds to GE site (yellow mesh, electron density for RifSV; yellow sticks, RifSV; blue mesh, electron density for GE; blue sticks, GE; violet sphere, active-center Mg^{2+}) (Image modified from Zhang et al., 2014).

(C) Structure of *Tth* RNAP-RPo in complex with Sor and GE. It reveals that Sor binds to Rif/Sor site, and GE binds to GE site (cyan mesh, electron density for Sor; cyan sticks, Sor; blue mesh, electron density for GE; blue sticks, GE; violet sphere, active-center Mg^{2+}).

As mentioned in the introduction, sorangicin A (Sor, macrocyclic polyether antibiotic), a non-Rif-related antibiotic, functions through the same binding site as Rif on RNAP (Campbell et al., 2005). Hence, Dr. Zhang also obtained a crystal structure of RPo with both Sor and GE bound at 3.8 Å resolution by soaking both substances into a crystal of *Tth* RP_o (Zhang and Ebright, unpublished). One of the essential insights from the crystal structures of RPo-RifSV-GE and RPo-Sor-GE is the positioning and distance of GE relative to RifSV and GE relative to Sor. Since Rif and Sor bound to RNAP are immediately adjacent to GE bound to RNAP, this suggests candidate positions and candidate linker lengths for covalent linkage of Rif and GE by zero- to four-atoms linker between Rif-C3/Rif-C4 and D-dmaDap of GE,

or covalent linkage of Sor and GE by zero- to four-atoms linker between carboxylic acid sidechain of Sor and D-dmaDap of GE to generate Class I dual-targeted inhibitors (RifaGEs or SoraGEs) (Zhang et al., 2014).

2.2 The difference between natural GE23077 and synthetic GE23077

In order to conjugate GE23077 (GE) to different Rif-targeted RNAP inhibitors, it requires a large quantity of GE. However, the quantity and source of the natural product GE are limited. Also, the amino acid residue of D-dmaDap on natural GE does not directly provide chemical reactivity and regiospecific conjugation that can link GE to Rif or Sor covalently (Mariani et al., 2005). Hence, the Ebright lab made many attempts to synthesize GE peptide analogs, and eventually contracted the total chemical synthesis of GE peptide analogs to a peptide synthesis company. As mentioned in the introduction, natural GE is a cyclic heptapeptide antibiotic with four unusual and three natural amino acids (Zhang et al., 2014). Usually, there is no difficulty obtaining the natural amino acids. However, sourcing a vendor and synthesizing unusual amino acids are challenging. To overcome these limitations, the Ebright lab found alternative options for particular functional groups on these four unusual amino acids for the synthetic GE peptide analogs.

Overall, there are four differences between the natural and the synthetic GE peptide analogs (Figure 9). Firstly, there is no chiral carboxyl group on the amino-malonic acid (Ama) residue of synthetic GE peptide analogs, because the carboxylic acid sidechain of L-Ama is labile under conditions required for conjugation chemistry. Secondly, the hydroxyl group on the D-iso-serine (iSer) residue of

synthetic GE peptide analogs is a non-chirality instead of D-configuration, because D-iSer racemizes under conditions required for conjugation chemistry. The *Z*-2,3-dimethylacryloyl group on D-α,β-diaminopropionic acid (D-Dap) residue of natural GE has been removed so that the primary amine on D-Dap can be conjugated to Rif or Sor directly, or can be introduced to different-length linkers between two moieties of a dual-targeted inhibitor. While natural GE has two chiral hydroxyl groups on the β- and γ-carbon of L-glutamine residue (3R,4S,L-dhGln), the synthetic GE peptide analogs have three different derivatives with zero (L-Gln), one (4S,L-hGln) or two (3R,4S,L-dhGln) hydroxyl groups because of the uncertain native stereochemistry on natural GE.

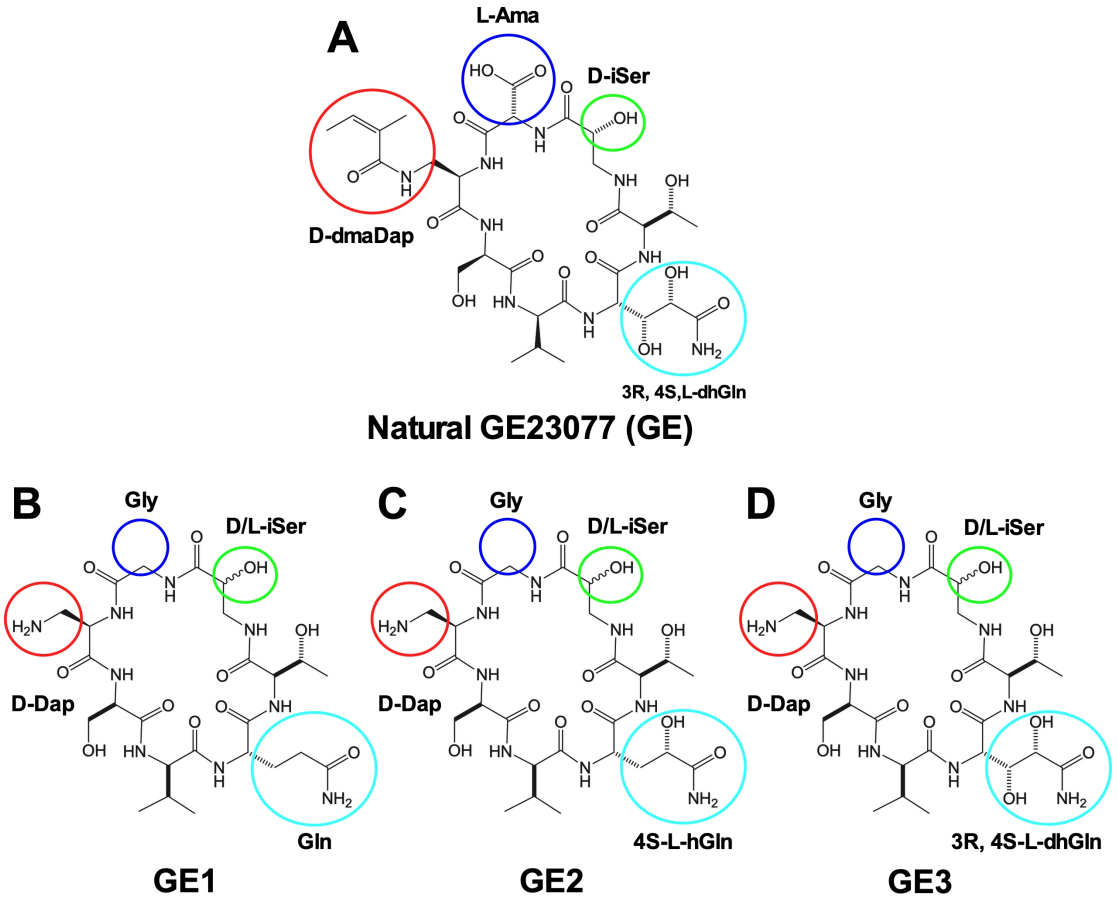

Figure 9. Four differences between GE23077 (GE) and synthetic GE peptide analogs

(A) Natural GE23077 with a *Z*-2,3-dimethylacryloyl group (red circle) on D-α,β-diaminopropionic acid (D-Dap), a chiral carboxyl group (blue circle) on L-amino-malonic acid (L-Ama), a chiral hydroxyl

group (green circle) on D-iso-serine (D-iSer), and two chiral hydroxyl groups (light blue circle) on β and γ carbon of glutamine (3R, 4S,L-dhGln).

(B)(C)(D) Synthetic GE23077 derivatives with an omitted *Z*-2,3-dimethylacryloyl group on D-α,β-diaminopropionic acid (D-Dap), an omitted carboxyl group on glycine (Gly), an achiral hydroxyl group on D/L-iso-serine (D/L-iSer), and a following glutamine (Gln) derivative (GE1, non-β,γ-dihydroxy glutamine; GE2, mono-γ-hydroxy glutamine; GE3, β,γ-dihydroxy glutamine).

2.3 Class I dual-targeted inhibitors

The crystal structures of RPo-RifSV-GE and RPo-Sor-GE reveal that the binding targets of Rif/Sor and GE are adjacent to each other, and that the RNAP inhibitors (RifSV and GE, or Sor and GE) bind on RNAP simultaneously and side-by-side. Both pieces of structural evidence suggest that it is possible to covalently join two separated inhibitors together and construct a Class I dual-targeted inhibitor (Zhang et al., 2014; Ebright et al., 2016). Conceptually, Class I dual-targeted inhibitor includes first moiety (Rif or Sor) that binds to a first site (Rif/Sor site) on RNAP and a covalently linked second moiety (GE) that binds to an adjacent site (GE site) on RNAP. Ideally, two moieties of the dual-targeted inhibitor could simultaneously interact with the two adjacent sites on RNAP.

There are several advantages of Class I dual-targeted inhibitors. Firstly, the Class I dual-targeted inhibitor is expected to exhibit extremely high binding affinity. The total binding free energy will be equal to or greater than the sum of the binding free energies of the two moieties. Secondly, because the Class I dual-targeted inhibitor binds to both Rif and GE targets, the RNAP inhibitory potency will be higher than that of either of the individual inhibitors. The last and most significant strength of Class I dual-targeted inhibitors is that they should have excellent ability to overcome resistance arising from a substitution in either of the two binding sites (Figure 10) (Zhang et al., 2014). Even if one of the binding sites has been mutated

(leading to a loss of binding affinity), the other target is still bound to one of moieties on a Class I dual-targeted inhibitor.

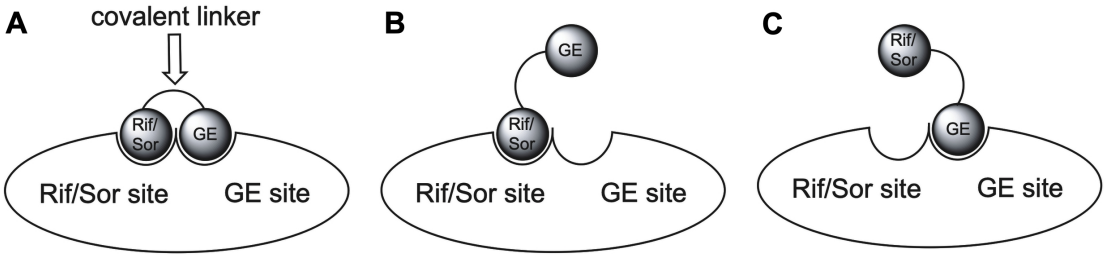

Figure 10. The concept and strategy for Class I dual-targeted inhibitor

(A) Two moieties (Rif and GE, or Sor and GE) of Class I dual-targeted inhibitor bind simultaneously to two adjacent binding sites (Rif/Sor site, and GE site) on wild-type RNAP (circle surface Rif/Sor = rifamycin/sorangicin; circle surface GE = synthetic GE peptide analogs).

(B) First moiety (Rif/Sor = rifamycin/sorangicin) of Class I dual-targeted inhibitor binds to first site (Rif/Sor site) on GE binding site mutated RNAP to overcome resistance.

(C) Second moiety (synthetic GE peptide analogs) of Class I dual-targeted inhibitor binds to second site (GE site) on Rif/Sor binding site mutated RNAP to overcome resistance.

EXPERIMENTAL DESIGN AND METHODS

2.4 Class I dual-targeted inhibitors of bacterial RNA polymerase: Linkage of a Rif/Sor-pocket ligand to a non-nucleotide ligand of the RNA polymerase active center

2.4.1 Synthetic strategy of rifamycin S conjugated to synthetic GE peptide analogs (RifaGE-3-GEs)

The crystal structure of RPo-RifSV-GE shows that the C3 sidechain of the naphthyl moiety on RifSV neighbors the D-dmaDap residue of natural GE, which suggests the possibility of constructing a dual-targeted inhibitor comprising a rifamycin derivative, connected through its C3 atom of the naphthyl moiety, and a GE, connected through its D-dmaDap residue. However, the functional groups on

RifSV and natural GE cannot be directly linked together. Therefore, to synthesize the rifamycin C3 conjugated to a synthetic GE peptide analog, we took 3-bromo-rifamycin S (Marchi and Montecchi, 1979; Zhang et al., 2014; Ebright et al., 2016) to react with a synthetic GE peptide analog. As mentioned before, the amino acid Dap residue on synthetic GE peptide analog has a primary amine with nucleophilicity. The 3-bromo-rifamycin S has a bromine as a leaving group on its C3 atom of the naphthyl moiety, which can undergo a nucleophilic substitution reaction with the primary amine of synthetic GE peptide analog to generate dual-targeted inhibitors (RifaGE-3-GEs) (Figure 11).

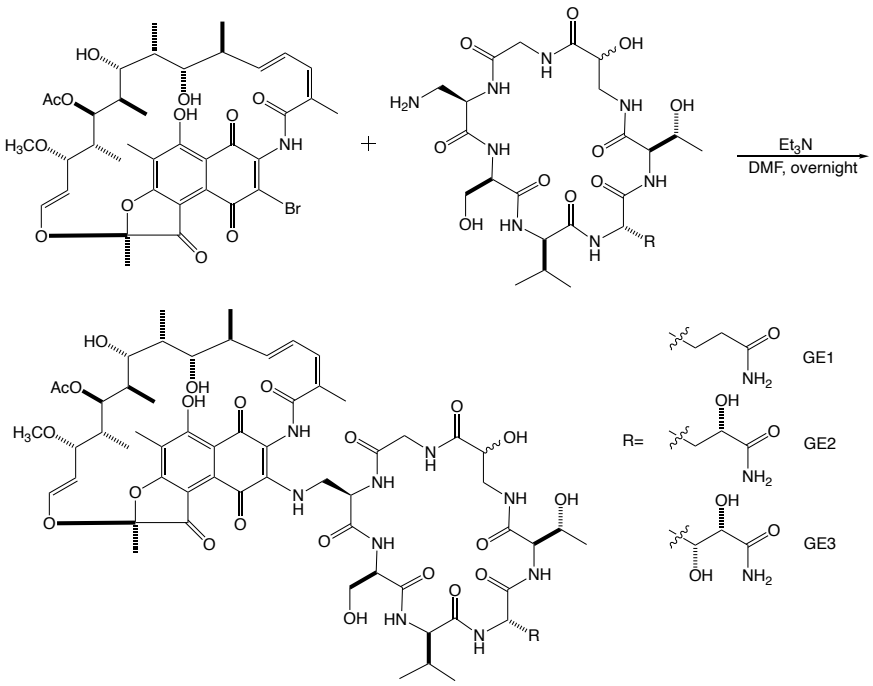

Figure 11. Synthetic route of RifS connected to synthetic GE peptide analogs

2.4.2 Synthetic strategy of rifamycin B conjugated to synthetic GE peptide analogs (RifaGE-4-GEs)

Rifamycin B (RifB), another compound in the rifamycin family, has a carboxyl group on the oxygen atom pendant to the naphthyl moiety C4 atom (Sensi

and Maggi, 1964b). The chemically reactive carboxyl group can react with the primary or secondary amine to form an amide linkage via an amide coupling reagent. Fortunately, all three synthetic GE peptide analogs in this thesis have a primary amine on the β-carbon of the Dap residue, which allows RifB, through the carboxylic acid group, to be covalently conjugated to synthetic GE peptide analogs, through the primary amine on the Dap residue, via the coupling reagent *N,N′*-dicyclohexylcarbodimide (DCC) (Figure 12) (Mustaev et al., 1994; Ebright et al., 2016).

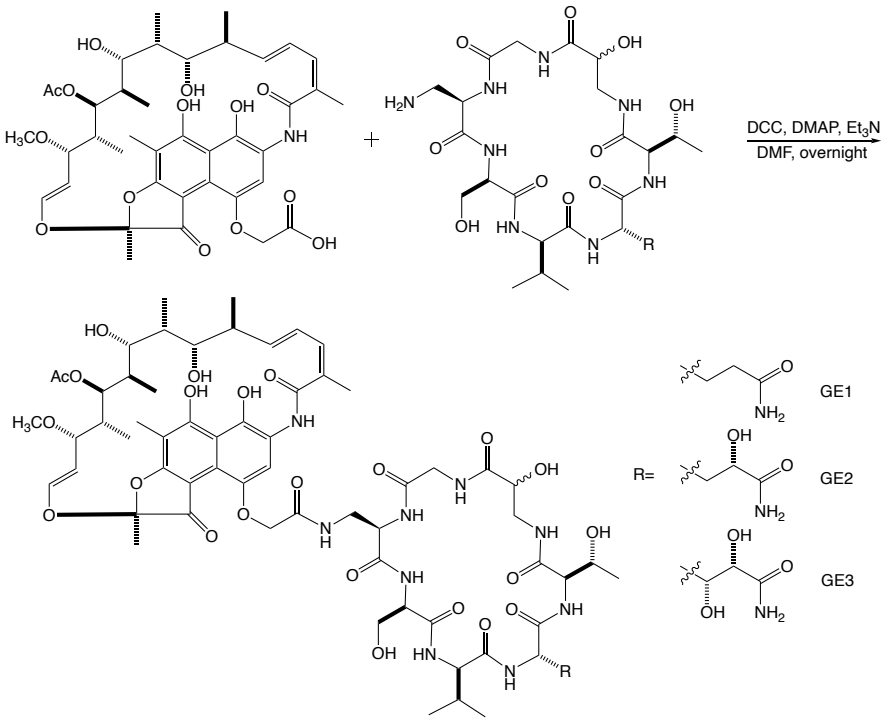

Figure 12. Synthetic route of RifB connected to synthetic GE peptide analogs

2.4.3 Synthetic strategy of sorangicin A conjugated to synthetic GE peptide analogs (SoraGE-GEs)

Sorangicin A (Sor), which is structurally unrelated to the rifamycin family, has a carboxyl group on the end of its hydrocarbon sidechain (Jansen et al., 1985). Within

the crystal of RPo-Sor-GE, the carboxyl group on sidechain of Sor is close to and pointed towards the D-dmaDap residue of GE (Zhang and Ebright, unpublished). To connect Sor to synthetic GE peptide analogs, the carboxyl group of Sor needs to be activated via carbonyl diimidazole (CDI) to form the carbonyl imidazolide intermediate. Since this kind of intermediate is highly reactive with primary amines, Sor can be covalently connected to synthetic GE derivatives to generate SoraGE-GEs (Ebright et al., 2016).

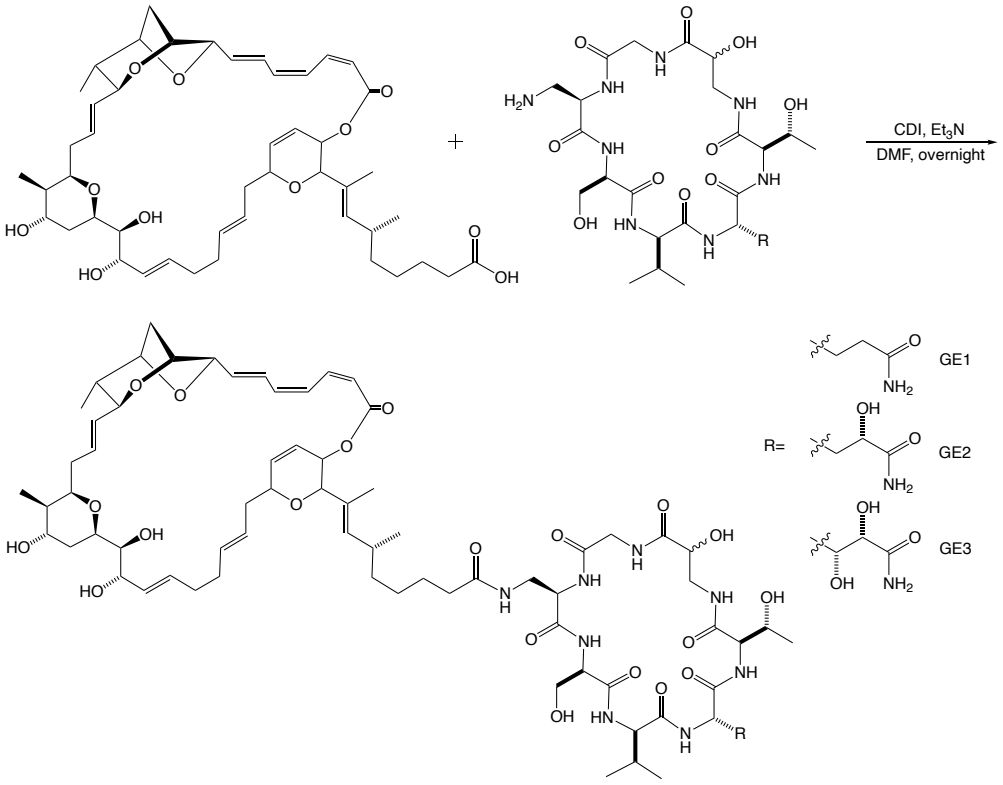

Figure 13. Synthetic route of Sor connected to synthetic GE peptide analogs

2.5 Class I dual-targeted inhibitors of bacterial RNA polymerase: characterization

All synthetic Class I dual-targeted inhibitors have been tested for their inhibition of bacterial RNAP. Specifically, a postdoc in the Ebright lab and I

performed biochemical evaluation of all Class I dual-targeted inhibitors via fluorescence-detected transcription assays to assess their ability against wild-type *E. coli* RNAP holoenzyme, Rif-resistant *E. coli* RNAP holoenzyme (RNAP derivatives containing β S531L or β H526D substitutions), and GE-resistant *E. coli* RNAP holoenzyme (RNAP derivatives containing β E565D or β N684K substitutions).

2.5.1 Assay of RNAP-inhibitory activity: ribogreen fluorescence-detected transcription assay

Fluorescence-detected RNA polymerase transcription assays were performed using a modification of the procedure in Kuhlman et al. (2004). Reaction mixtures contained (20 μL): 0-400 μM test compound, bacterial RNA polymerase holoenzyme (75 nM *E. coli* RNAP holoenzyme or 75 nM *E. coli* RNAP holoenzyme derivative), 20 nM DNA fragment containing the bacteriophage T4 N25 promoter (positions -72 to +367; prepared by PCR from plasmid pARTaqN25-340-tR2; Liu, 2007), 100 μM ATP, 100 μM GTP, 100 μM UTP, and 100 μM CTP, in transcription buffer (TB) (50 mM Tris-HCl, pH 8.0, 100 mM KCl, 10 mM $MgCl_2$, 1 mM DTT, 10 μg/mL bovine serum albumin, and 5.5% glycerol). Reaction components other than DNA and NTPs were pre-incubated for 10 min at 37°C. Reactions were carried out by addition of DNA, followed by incubation for 15 min at 37°C, after which NTPs were added and then incubated for 60 min at 37°C. DNA was removed by addition of 1 μL 5 mM $CaCl_2$ and 2 U DNaseI (Ambion, Inc.), followed by incubation 90 min at 37°C. RNA was quantified by addition of 100 μL RiboGreen RNA Quantitation Reagent (Life Technologies, Grand Island, NY; 1:500 dilution in 10 mM Tris- HCl, pH 8.0, 1 mM EDTA), followed by incubation for 10 min at 25°C, followed by measurement of fluorescence intensity (excitation wavelength = 485 nm and emission wavelength =

535 nm; GENios Pro microplate reader [Tecan, Männedorf, Switzerland]). Half-maximal inhibitory concentrations (IC50) were calculated by non-linear regression in SigmaPlot where IC50 is defined as the concentration of inhibitor resulting in 50% inhibition of RNA polymerase activity.

2.5.2 Structure determination: RPo + Class I dual-targeted inhibitor

The crystal structure was determined by soaking the Class I dual-targeted inhibitor into a pre-formed crystal of a of *T. thermophilus* (*Tth*) RNAP promoter transcription initiation complex, collecting X-ray diffraction data at a synchrotron beamline, solving the structure by molecular replacement using atomic coordinates for the structure of a of *Tth* RNAP promoter transcription open complex in the absence of Class I dual-targeted inhibitor as the search model, and refining the structure. These methods for crystal growth, crystal soaking, data collection, structure solution, and structure refinement for determination of a structure of Class I dual-targeted inhibitor bound to *Tth* RNAP promoter open complex were performed as in Zhang et al., 2014.

RESULTS

2.6 Class I dual-targeted inhibitors of bacterial RNA polymerase: Linkage of a Rif/Sor-pocket ligand to a non-nucleotide GE derivative ligand of the RNA polymerase active center

Using the strategies described above, I have synthesized most of compounds in this class. All of the Class I dual-targeted inhibitors were purified via reverse-phase

HPLC, and their molecular masses were confirmed via MALDI-TOF (Zhang et al., 2014).

2.6.1 Synthesis of {[D/L-iSer]-[N$^{\beta}$-desacyl-dmaDap]-[β,γ-dideshydroxy-dhGln]-[α-descarboxy-Ama]-GE23077}-{rifamycin S} (RifaGE-3-GE1)

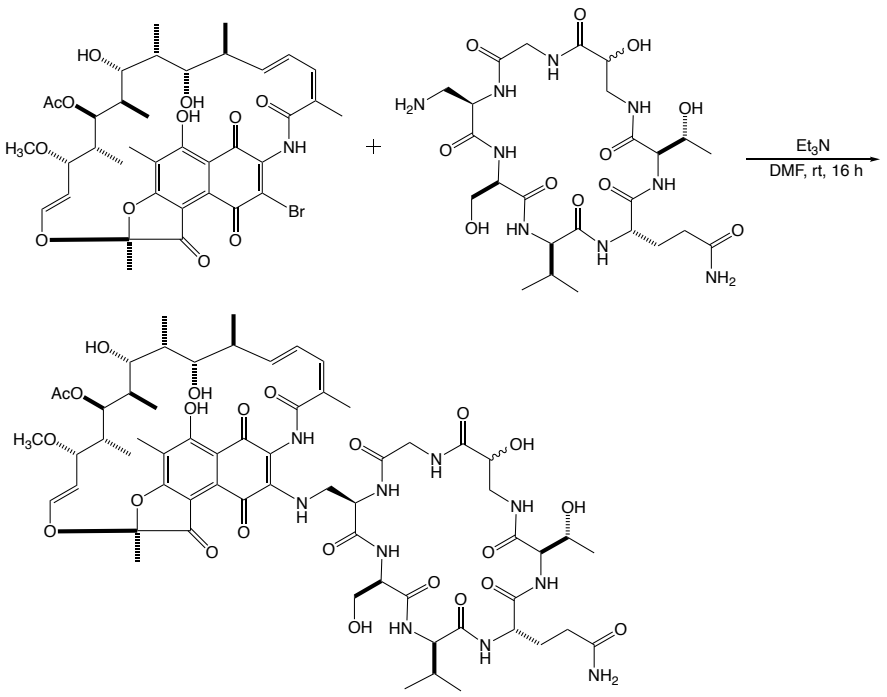

To a solution of [D/L-iSer]-[N$^{\beta}$-desacyl-dmaDap]-[β,γ-dideshydroxy-dhGln]-[α-descarboxy-Ama]-GE23077 (GE1; 1 mg; 1.55 µmole; Pepscan) in 100 µL DMF at room temperature, was added 3-bromo-rifamycin S (1.5 mg; 1.94 µmole) (Marchi and Montecchi, 1979) and triethylamine (0.65 µL; 4.64 µmole, Sigma-Aldrich), and the reaction mixture was stirred 16 h at room temperature. The reaction mixture was quenched with 100 µL water, evaporated to dryness, re-dissolved in 1 mL water, and centrifuged. The supernatant was purified by reversed-phase HPLC (Phenomenex C18, analytical; 0 min 10% B, 35 min 100% B, 45 min 100% B; A = 0.065% TFA in water, B = 0.05% TFA in acetonitrile, 1 mL/min).

Yield: 0.22 mg; 10%. MS (MALDI): calculated: *m/z* 1361.58 ($M + Na^+$); found: 1361.38.

2.6.2 Synthesis of {[D/L-iSer]-[N^{β}-desacyl-dmaDap]-[β-deshydroxy-dhGln]-[α-descarboxy-Ama]-GE23077}-{rifamycin S} (RifaGE-3-GE2)

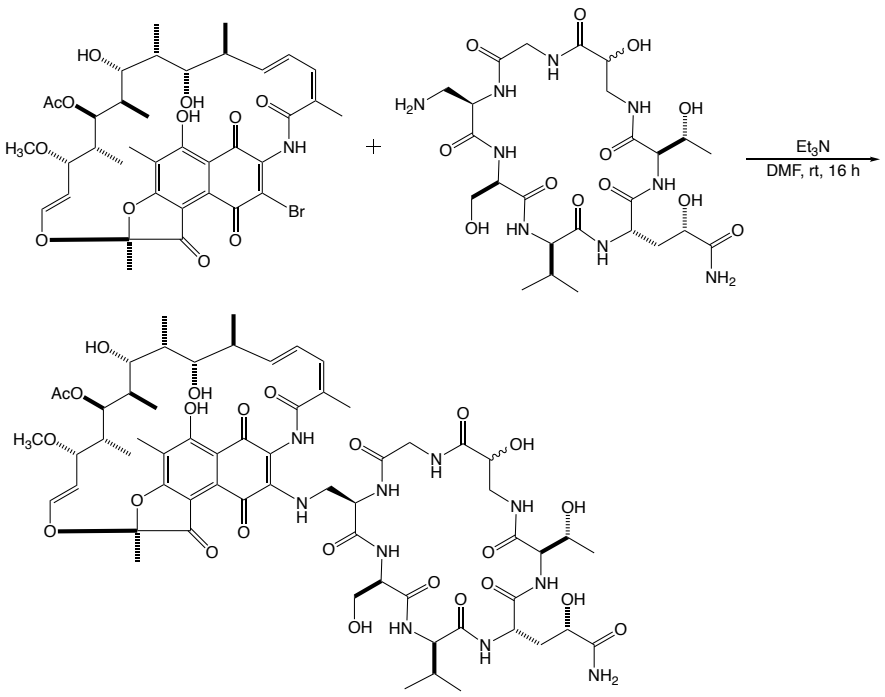

To a solution of [D/L-iSer]-[N^{β}-desacyl-dmaDap]-[β-deshydroxy-dhGln]-[α-descarboxy-Ama]-GE23077 (GE2; 1 mg; 1.51 µmole; Pepscan) in 100 µL DMF at room temperature, was added 3-bromo-rifamycin S (1.5 mg; 1.94 µmole) (Marchi and Montecchi, 1979) and triethylamine (0.63 µL; 4.52 µmole, Sigma-Aldrich), and the reaction mixture was stirred 16 h at room temperature. The reaction mixture was quenched with 100 µL water, evaporated to dryness, re-dissolved in 500 µL water and 500 µL MeOH, and centrifuged. The supernatant was purified by reversed-phase HPLC (Phenomenex C18, analytical; 0 min 10% B, 35 min 100% B, 40 min 100% B; A = water, B = acetonitrile, 1 mL/min).

Yield: 0.85 mg; 41%. MS (MALDI): calculated: *m/z* 1377.57 ($M + Na^+$); found: 1377.73.

2.6.3 Synthesis of {[D/L-iSer]-[N^{β}-desacyl-dmaDap]-[β,γ-dideshydroxy-dhGln]-[α-descarboxy-Ama]-GE23077}-{rifamycin B} (RifaGE-4-GE1)

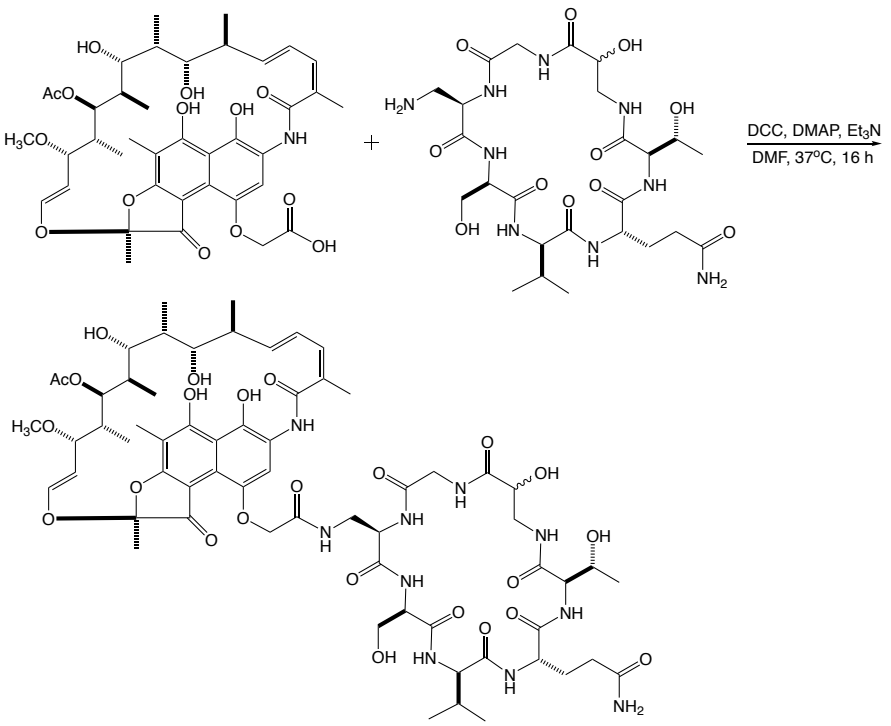

To a suspension of rifamycin B (4 mg; 5.29 μmole; AvaChem Scientific) in 75 μL anhydrous tetrahydrofuran at room temperature, was added *N,N′*-dicyclohexylcarbodiimide (DCC; 4 mg; 19.39 μmole; Sigma-Aldrich) in 25 μL anhydrous tetrahydrofuran, and the reaction mixture was mixed 1 h at room temperature by a nutator mixer. The reaction mixture was filtered off, and the filtrate was added to 1 mL anhydrous diethyl ether, yielding a yellow precipitate (Mustaev et al., 1994). The resulting yellow precipitate was re-dissolved in 100 μL DMF, added [D/L-iSer]-[N^{β}-desacyl-dmaDap]-[β,γ-dideshydroxy-dhGln]-[α-descarboxy-Ama]-GE23077 (GE1; 1 mg; 1.55 μmole; Pepscan) in 25 μL DMF, supplemented with 4-dimethylaminopyridine (0.018 mg; 0.15 μmole; Alfa Aesar) and triethylamine (0.43

µL; 3.09 µmole; Sigma-Aldrich), and the reaction mixture was incubated 16 h at 37°C on a nutator mixer. The reaction mixture was quenched with 100 µL water, evaporated to dryness, re-dissolved in 500 µL water and 500 µL MeOH. The product was purified through reversed-phase HPLC (Phenomenex C18, analytical; 0 min 10% B, 35 min 100% B, 40 min 100% B; A = 0.065% TFA in water, B = 0.05% TFA in acetonitrile, 1 mL/min).

Yield: first diastereomer: 0.12 mg, second diastereomer: 0.16 mg; 13%. MS (MALDI): calculated: first diastereomer *m/z* 1391.57 ($M + K^+$ - MeOH), second diastereomer *m/z* 1405.60 ($M + Na^+$); found: first diastereomer: 1391.78, second diastereomer: 1405.84.

2.6.4 Synthesis of {[D/L-iSer]-[N^{β}-desacyl-dmaDap]-[β-deshydroxy-dhGln]-[α-descarboxy-Ama]-GE23077}-{rifamycin B} (RifaGE-4-GE2)

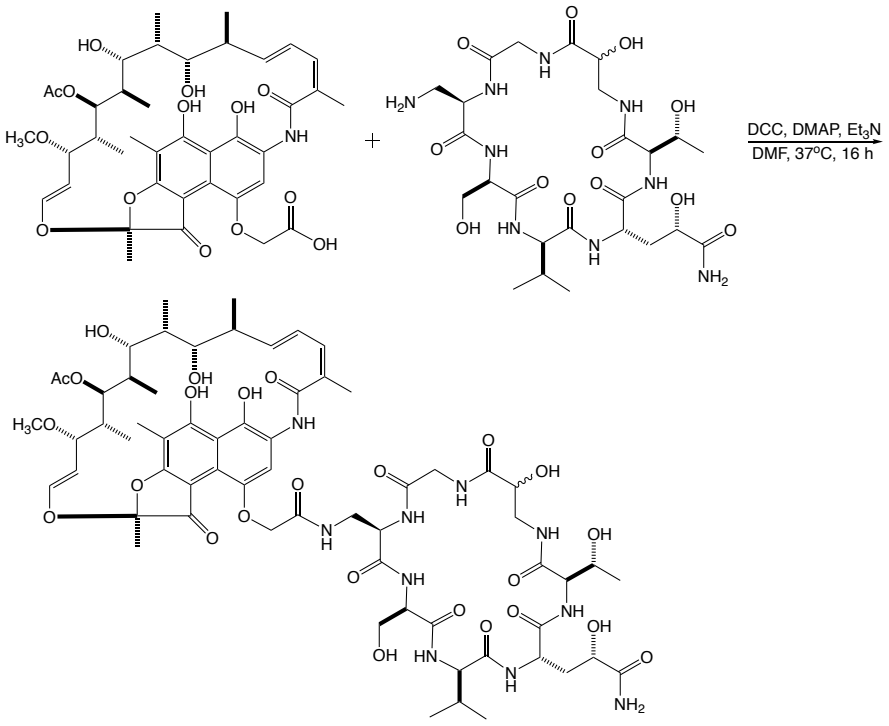

To a suspension of rifamycin B (4 mg; 5.29 µmole; AvaChem Scientific) in 75 µL anhydrous tetrahydrofuran at room temperature, was added *N,N′*-

dicyclohexylcarbodiimide (DCC; 4 mg; 19.39 μmole; Sigma-Aldrich) in 25 μL anhydrous tetrahydrofuran, after which the reaction mixture was incubated 1 h at room temperature on a nutator mixer. The reaction mixture was filtered off, and the filtrate was added to 1 mL anhydrous diethyl ether, yielding a yellow precipitate (Mustaev et al., 1994). The resulting yellow precipitate was re-dissolved in 100 μL DMF, added [D/L-iSer]-[N^{β}-desacyl-dmaDap]-[β-deshydroxy-dhGln]-[α-descarboxy-Ama]-GE23077 (GE2; 1 mg; 1.51 μmole; Pepscan) in 25 μL DMF, supplemented with 4-dimethylaminopyridine (0.018 mg; 0.15 μmole; Alfa Aesar) and triethylamine (0.42 μL; 3.01 μmole; Sigma-Aldrich), and then the reaction mixture was incubated 16 h at 37^{o}C on a nutator mixer. The reaction mixture was quenched with 100 μL water, evaporated to dryness, then re-dissolved in 500 μL water and 500 μL MeOH. The product was purified by reversed-phase HPLC (Phenomenex C18, analytical; 0 min 10% B, 35 min 100% B, 40 min 100% B; A = 0.065% TFA in water, B = 0.05% TFA in acetonitrile, 1 mL/min).

Yield: 0.33 mg; 17%. MS (MALDI): calculated: *m/z* 1421.60 ($M + Na^{+}$); found: 1421.65.

2.6.5 Synthesis of {[D/L-iSer]-[N^{β}-desacyl-dmaDap]-[β-deshydroxy-dhGln]-[α-descarboxy-Ama]-GE23077}-{sorangicin A} (SoraGE-GE2)

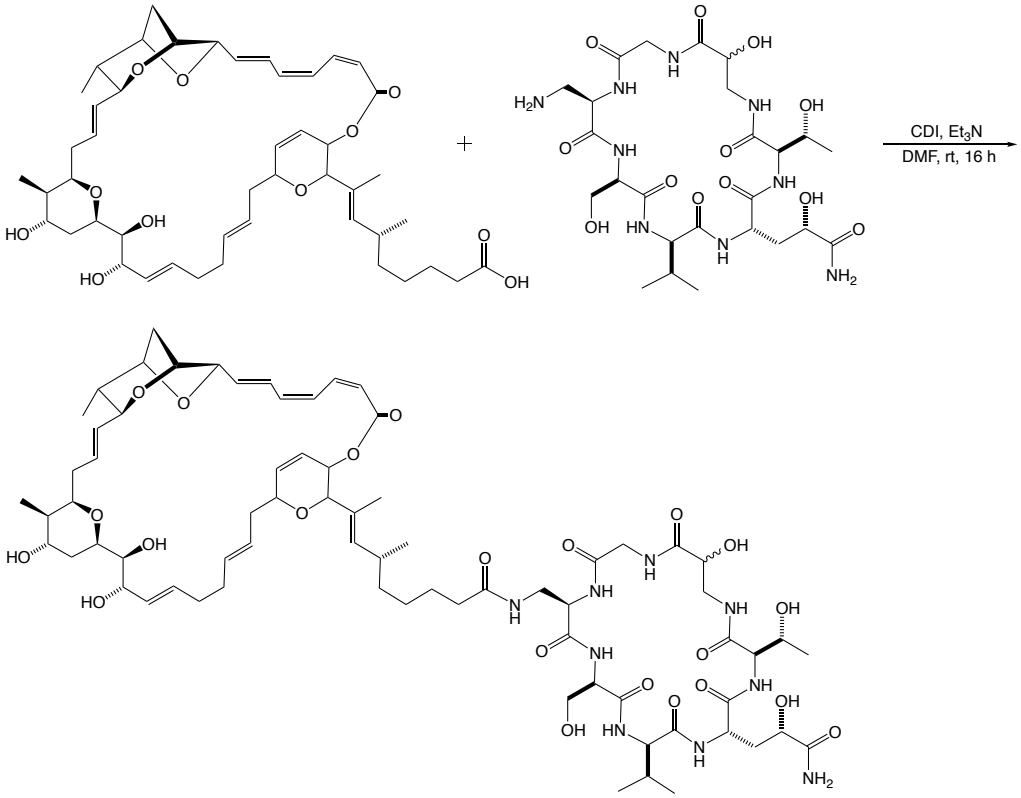

To a suspension of sorangicin A (1 mg; 1.24 µmole) in 200 µL dichloromethane at room temperature, was added carbodiimidazole (CDI; 0.4 mg; 2.48 µmole; Sigma-Aldrich) in 40 µL dichloromethane, after which the reaction was stirred 2 h at room temperature. The reaction mixture was evaporated to dryness, supplemented with [D/L-iSer]-[N^{β}-desacyl-dmaDap]-[β-deshydroxy-dhGln]-[α-descarboxy-Ama]-GE23077 (GE2; 1 mg; 1.51 µmole; Pepscan) in 100 µL DMF and triethylamine (1 µL; 7.17 µmole; Sigma-Aldrich), and stirred 16 h at room temperature. The reaction mixture was quenched with 100 µL water, evaporated to dryness, and re-dissolved in 500 µL water and 500 µL MeOH. The product was then purified by reversed-phase HPLC (Phenomenex C18(2), analytical; 0 min 100% A, 35 min 100% A; A = 0.1% formic acid in 75% MeOH and 25% water, 1 mL/min). Yield: 0.38 mg; 21%. MS (MALDI): calculated: m/z 1472.74 ($M + Na^{+}$); found: 1473.16.

2.6.6 Synthesis of {[D/L-iSer]-[N$^{\beta}$-desacyl-dmaDap]-[α-descarboxy-Ama]-GE23077}-{sorangicin A} (SoraGE-GE3)

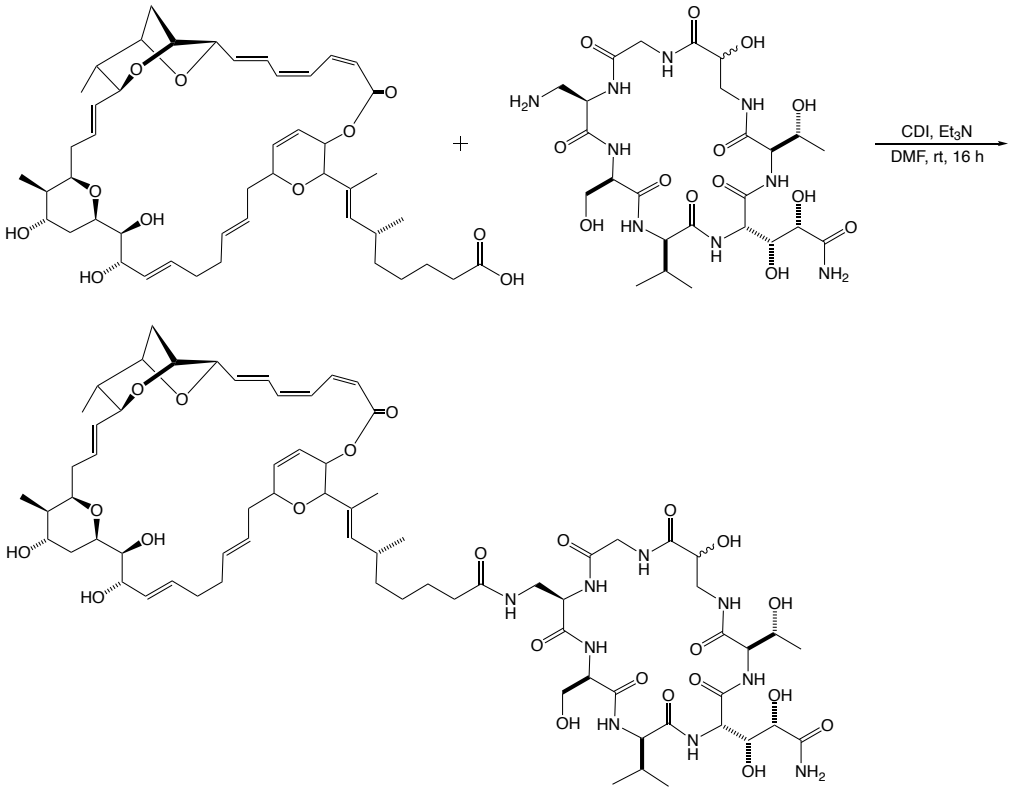

To a suspension of sorangicin A (1.2 mg; 1.49 μmole) in 200 μL dichloromethane at room temperature, was added carbodiimidazole (CDI; 0.4 mg; 2.48 μmole; Sigma-Aldrich) in 40 μL dichloromethane, after which the reaction was stirred 2 h at room temperature. The reaction mixture was evaporated to dryness, supplemented with [D/L-iSer]-[N$^{\beta}$-desacyl-dmaDap]-[α-descarboxy-Ama]-GE23077 (GE3; 1 mg; 1.46 μmole; Pepscan) in 100 μL DMF and triethylamine (1 μL; 7.17 μmole; Sigma-Aldrich), and stirred 16 h at room temperature. The reaction mixture was quenched with 100 μL water, evaporated to dryness, and re-dissolved in 500 μL water and 500 μL MeOH. The product was purified by reversed-phase HPLC (Phenomenex C18(2), analytical; 0 min 100% A, 35 min 100% A; A = 0.1% formic acid in 75% MeOH and 25% water, 1 mL/min).

Yield: 0.15 mg; 7%. MS (MALDI): calculated: m/z 1489.68 ($M + Na^+$); found: 1488.98.

2.7 Class I dual-targeted inhibitors of bacterial RNA polymerase: characterization

An essential purpose of constructing the Class I dual-targeted inhibitor is suppressing antibacterial drug resistance. The two moieties of a Class I dual-targeted inhibitor bind to the two adjacent binding sites on RNAP. Theoretically, these two should bind simultaneously to their targets on wild-type bacterial RNAP. However, if one of the two binding targets on bacterial RNAP is altered, that binding target cannot appropriately interact with its moiety. The non-mutated binding target, however, can still function and bind with the other moiety. Based on this hypothesis, the Class I dual-targeted inhibitor could overcome the resistance arising from a substitution in one of the binding targets on RNAP.

2.7.1 Assay of RNAP-inhibitory activity: Half-maximal inhibitory concentration (IC50)

2.7.1.1 Half-maximal inhibitory concentration (IC50) of RifaGE-3-GEs

In order to test the above hypothesis, Dr. David Degen from the Ebright lab and I assayed the RNAP-inhibitory activity for the inhibitors of RifS conjugated to two synthetic GE peptide analogs (GE1 and GE2) via ribogreen fluorescence-detected transcription assay. The results indicate that both RifaGE-3-GE1 and RifaGE-3-GE2 potently inhibit wild-type *E. coli* RNAP. Notably, one of the RifaGE-3-GEs inhibitors, namely the RifS connected to the synthetic GE peptide analog containing a

mono-γ-hydroxy glutamine (GE2; RifaGE-3-GE2), has wild-type-RNAP inhibitory activity equal to that of the individual components, RifSV and natural GE (Table 1). Also, both RifaGE-3-GE1 and RifaGE-3-GE2 inhibit wild-type *E. coli* RNAP >6,500-fold more potently than either of the synthetic GE peptide analogs (GE1 and GE2). We also tested both RifaGE-3-GE1 and RifaGE-3-GE2 against a Rif-resistant (Rif^R) *E. coli* RNAP (β S531L) and GE-resistant (GE^R) *E. coli* RNAPs (β E565D and β N684K). For the Rif^R *E. coli* RNAP (β S531L), only one inhibitor, RifS connected to the synthetic GE peptide analog containing a non-β,γ-dihydroxy glutamine (GE1; RifaGE-3-GE1), could inhibit Rif^R *E. coli* RNAP, 4.7-fold more potently than RifSV. Both RifaGE-3-GE1 and RifaGE-3-GE2 could not inhibit the Rif^R *E. coli* RNAP as effectively as the natural product GE. For the GE^R *E. coli* RNAPs (β E565D and β N684K), both dual-targeted inhibitors RifaGE-3-GEs not only potently overcame the resistance arising from GE target (10,000-fold more potently than any GE derivative), but also exhibited potency as high as that of RifSV (Table 1).

Table 1. Rifamycin SV, GE derivatives, and RifaGE-3-GEs: *E. coli* RNAP inhibitory activity

Compound name	*E. coli* RNAP IC50 (μM)	β S531L[a] *E. coli* RNAP IC50 (μM)	β E565D[b] *E. coli* RNAP IC50 (μM)	β N684K[b] *E. coli* RNAP IC50 (μM)
Rif				
RifSV	0.017	40	0.017	0.021
GE				
GE	0.017	0.009	>400	>400
GE1	>400	ND	>400	ND
GE2	>400	>400	>400	ND
RifaGE				
RifaGE-3-GE1	0.061	8.5	0.04	0.13
RifaGE-3-GE2	0.015	82	0.027	ND

[a] β S531L *E. coli* RNAP is a Rif-resistant mutant.

[b] β E565D *E. coli* RNAP and β N684K *E. coli* RNAP are the GE-resistant mutants.

2.7.1.2 Half-maximal inhibitory concentration (IC50) of RifaGE-4-GEs

To further improve the inhibitory activity of the Class I dual-targeted inhibitor, I attempted to conjugate the synthetic GE peptide analogs (GE1 and GE2) to another Rif-family RNAP inhibitor, rifamycin B (RifB). One interesting discovery during purification of the product was that there are two diastereomers formed in the reaction of RifB connected to the synthetic GE peptide analog containing a non-β,γ-dihydroxy glutamine (GE1; RifaGE-4-GE1). Hence, I decided to isolate both diastereomers separately and assay them individually. According to the IC50 results, both diastereomers of RifaGE-4-GE1 have good activity against wild-type *E. coli* RNAP *in vitro*; however, both diastereomers are 3.5- to 4-fold less potent than RifB and natural GE. Although there are no outstanding activities for RifaGE-4-GE1 against wild-type *E. coli* RNAP, the RifaGE-4-GE1 could still partly overcome the resistance arising from the Rif and GE targets. The IC50 results illustrate that both

diastereomers of RifaGE-4-GE1 inhibit Rif^R *E. coli* RNAP (β S531L) >4-fold more potently than individual RifB, inhibit GE^R *E. coli* RNAP (β E565D) >8,000-fold more potently than natural GE, and inhibit GE^R *E. coli* RNAP (β N684K) >2,800-fold more potently than natural GE (Table 2).

Table 2. Rifamycin B, GE derivatives, and RifaGE-4-GEs: *E. coli* RNAP inhibitory activity

Compound name	*E. coli* RNAP IC50 (μM)	β S531L[a] *E. coli* RNAP IC50 (μM)	β E565D[b] *E. coli* RNAP IC50 (μM)	β N684K[b] *E. coli* RNAP IC50 (μM)
Rif				
RifB	0.02	>100	0.22	0.3
GE				
GE	0.017	0.009	>400	>400
GE1	>400	ND	>400	ND
RifaGE				
RifaGE-4-GE1 diastereomer 1	0.068	19	0.038	0.12
RifaGE-4-GE1 diastereomer 2	0.076	23	0.049	0.14

[a] β S531L *E. coli* RNAP is a Rif-resistant mutant.

[b] β E565D *E. coli* RNAP and β N684K *E. coli* RNAP are the GE-resistant mutants.

2.7.1.3 Half-maximal inhibitory concentration (IC50) of SoraGE-GEs

Synthetic GE peptide analogs were not only conjugated to inhibitors that are the structurally-related to rifamycins, such as RifS and RifB, but were also linked to a non-Rif-related RNAP inhibitor, sorangicin A (Sor). Surprisingly, all resulting SoraGE-GEs dual-targeted inhibitors have higher RNAP-inhibitory potencies than Sor and natural GE alone (Table 3). All SoraGE-GEs inhibit wild-type *E. coli* RNAP ≥1.5-fold more potently than Sor. Moreover, SoraGE-GEs also have higher potencies against Rif^R *E. coli* RNAPs (β S526D and β S531L) and GE^R *E. coli* RNAP (β

E565D). All SoraGE-GEs potently inhibit Rif^R *E. coli* RNAP (β S526D, >500-fold more than Sor), Rif^R *E. coli* RNAP (β S531L, >18-fold more than Sor), and GE^R *E. coli* RNAP (β E565D, >13,000-fold more than natural GE and synthetic GE peptide analogs).

Table 3. Sorangicin A, GE derivatives, and SoraGE-GEs: *E. coli* RNAP inhibitory activity

Compound name	*E. coli* RNAP IC50 (μM)	β H526D[a] *E. coli* RNAP IC50 (μM)	β S531L[a] *E. coli* RNAP IC50 (μM)	β E565D[b] *E. coli* RNAP IC50 (μM)
Sor				
Sor	0.031	>100	0.6	0.033
GE				
GE	0.017	ND	0.009	>400
GE1	>400	ND	ND	>400
GE2	>400	ND	>400	>400
GE3	>400	ND	ND	ND
SoraGE				
SoraGE-GE1	0.016	0.037	0.032	0.029
SoraGE-GE2	0.009	0.035	0.02	0.029
SoraGE-GE3	0.019	0.19	ND	0.022

[a] β H526D *E. coli* RNAP and β S531L *E. coli* RNAP are Rif-resistant mutants.

[b] β E565D *E. coli* RNAP is a GE-resistant mutant.

2.8 Structural basis of transcription inhibition by Class I dual-targeted inhibitors

2.8.1 Rif and GE target: crystal structure of the RNAP-SoraGE complex

In order to further understand the binding of the Class I dual-targeted inhibitors to bacterial RNAP and their inhibition mechanism, Mr. Yu Liu, a graduate student in the Ebright lab, tried to soak various Class I dual-targeted inhibitors into

crystals of *T. thermophiles* (*Tth)* RNAP-promoter open complex (RP_o). He succeeded in determining two crystal structures, which are two different SoraGE-GEs in complex with *Tth* RNAP and promoter DNA at 3.3 Å and 3.9 Å resolution, respectively (Figure 14) (Ebright et al., unpublished).

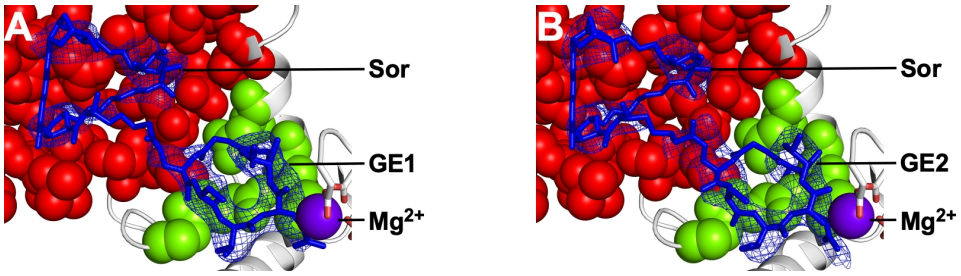

Figure 14. Crystal structure of *T. thermophilus* (*Tth*) RNAP bound to Class I dual-targeted inhibitors "SoraGE-GEs"

(A) View of the Rif/Sor and GE targets on *Tth* RNAP-RPo showing the electron densities for both Sor and GE1 moieties of Class I dual-targeted inhibitor (GE1, the synthetic GE peptide analog containing a non-β,γ-dihydroxy glutamine; resolution = 3.3 Å; Rfree = 0.32). The structure reveals that Sor moiety binds to Rif/Sor target (red surface), and GE1 moiety binds to GE target (green surface).

(B) View of the Rif/Sor and GE targets on *Tth* RNAP-RPo showing the electron densities for both Sor and GE2 moieties of Class I dual-targeted inhibitor (GE2, the synthetic GE peptide analog containing a mono-γ-hydroxy glutamine; resolution = 3.9 Å; Rfree = 0.28). The structure reveals that Sor moiety binds to Rif/Sor target (red surface), and GE2 binds to GE target (green surface).

The first crystal structure Mr. Liu obtained is the inhibitor of a Sor connected to a synthetic GE peptide analog containing a non-β,γ-dihydroxy glutamine (GE1; SoraGE-GE1) in complex with *Tth* RP_o. This structure confirms that both of the individual moieties on SoraGE-GE1 simultaneously bind to RNAP; Sor binds on the Rif site, synthetic GE1 binds on the GE site. Additionally, the crystal structure also shows that one molecule of SoraGE-GE1 interacts with one molecule of RNAP with a 1:1 stoichiometry. However, parts of the electron density maps for this SoraGE-GE1 inhibitor on RNAP, such as the carboxyl hydrocarbon sidechain of Sor, are not clear.

To gain clearer electron density maps for Class I dual-targeted inhibitors and thereby, provide further support for our hypothesis, Mr. Liu next soaked another

SoraGE inhibitor, a Sor connected to a synthetic GE peptide analog containing a mono-γ-hydroxy glutamine (GE2; SoraGE-GE2), into crystals of *Tth* RP_o complex. Again, he successfully obtained the crystal structure of RNAP-SoraGE-GE2 with the Sor and GE2 moieties interacting simultaneously with the Sor and GE sites. This crystal also shows more apparent electron density on the carboxyl hydrocarbon sidechain of Sor.

2.9 Discussion

The wild-type *E. coli* RNAP-inhibitory activities indicate that the Class I dual-targeted inhibitors containing a mono-γ-hydroxy glutamine (Gln) on synthetic GE peptide analog (GE2) are more potent than the Class I dual-targeted inhibitors containing a non-β,γ-dihydroxy glutamine on synthetic GE peptide analog (GE1). These results are consistent with our expectations. The crystal structure of RNAP-GE23077 defines each contact between GE and *T. thermophilus* RNAP (Zhang et al., 2014). It shows that the γ-hydroxy of Gln residue on GE directly makes a hydrogen bond with RNAP residue β Glu565, one of the highest-resistance-level GE^R substitutions (Zhang et al., 2014; Ebright et al., 2016). Hence, without this hydrogen bond contact between the inhibitors and RNAP, the wild-type RNAP-inhibitory activities could be worse.

The inhibitory activities against Rif^R *E. coli* RNAPs (β S526D and β S531L) and GE^R *E. coli* RNAPs (β E565D and β N684K) also demonstrate that the Class I dual-targeted inhibitors are able to overcome resistance arising from either the Rif/Sor or GE sites. Although the inhibitors of RifS connected to synthetic GE peptide analogs (RifaGE-3-GEs) and RifB connected to synthetic GE peptide analogs

(RifaGE-4-GEs) don't have exceptional inhibitory activities against Rif^R *E. coli* RNAP (β S531L), the RifaGE-3-GEs and RifaGE-4-GEs still are 4-fold to 5-fold more potent than the rifamycins (RifSV or RifB) alone. For the GE^R *E. coli* RNAP, all of the RifaGE-3-GEs and RifaGE-4-GEs have better or similar inhibitory activities as the rifamycins (RifSV or RifB) alone.

The most promising compounds within the Class I dual-targeted inhibitors are Sor conjugated to synthetic GE peptide analogs (SoraGEs). The IC50 results illustrate that all of the SoraGEs have extremely high activities against wild-type, Rif-resistant, and GE-resistant *E. coli* RNAPs. In particular, the inhibitor of Sor connected to the synthetic GE peptide analog containing a mono-γ-hydroxy glutamine (GE2; SoraGE-GE2) is the most potent of all Class I dual-targeted inhibitors we have synthesized and assayed. These results also demonstrate that the flexibility of molecule, and the binding interaction between inhibitor and RNAP, are two crucial elements when constructing potent Class I dual-targeted inhibitors.

The crystal structures of the RNAP-SoraGE complexes indicate that the entire SoraGE inhibitor can bind to the desired binding targets on RNAP without any issues. However, when Mr. Liu attempted to soak RifaGE-3-GEs and RifaGE-4-GEs into crystals of *T. thermophiles* RNAP-RPo, he could not obtain any crystal structures containing the RifaGEs bound to the complex. One possible explanation is the difference in flexibility between the ansamycin moiety in Rif derivatives and macrocyclic polyether moiety of Sor. As mentioned previously, Sor is a flexible molecule. It may allow SoraGEs to better tolerate changes to the Rif binding pocket on RNAP (Campbell et al., 2005). Additionally, the carboxyl hydrocarbon sidechain of Sor may also be a significant component of the interaction between SoraGE and

RNAP, since the sidechain could make two moieties of SoraGE less rigid. Through the sidechain, SoraGE could slightly adjust the relative distance and orientation between Sor and GE. Conversely, the ansamycin ring of Rif derivatives is inflexible. There is no flexible sidechain between RifS and synthetic GE peptide analogs. These factors may cause the RifaGE-3-GEs and RifaGE-4-GEs to not bind as tightly to RNAP.

2.10 Conclusion

All of the synthetic methods, biochemical data, and structural characterization of the Class I dual-targeted inhibitors support the conclusion that the Class I dual-targeted inhibitors were synthesized, function, and bind to RNAP as in our design. By taking advantage of specific functional groups on synthetic GE peptide analogs, rifamycin derivatives, and sorangicin A, the Class I dual-targeted inhibitors can be synthesized successfully. Although there are many different functional groups on synthetic GE peptide analogs, rifamycins, and sorangicin A, covalent conjugation can be conducted on the desired positions of each single inhibitor without destroying additional functional groups and losing the original functionality of the compound.

The *E. coli* RNAP-inhibitory activity results indicate that the Class I dual-targeted inhibitors are able to overcome the resistance arising from either the Rif/Sor or GE binding sites. This suggests that both of moieties on the inhibitor are bound to RNAP simultaneously and functioning as designed. Also, one half of the Class I dual-targeted inhibitor is still able to interact generally with its binding target when the other half of the inhibitor is not able to function, as is the case when there is a resistance substitution in one of the RNAP binding targets. Even if some of our

observed activities arise from trace amounts of cleaved rifamycins, Sor, and synthetic GE peptide analogs in the final samples, instead of the fully-conjugated inhibitors, the IC50 results could not be explained using this hypothesized model.

The crystal structures of the SoraGE-GEs in complex with bacterial RNAP further confirm that both of the moieties within the Class I dual-targeted inhibitors simultaneously interact with the GE and Rif/Sor targets on RNAP. The inhibition mechanism of Class I dual-targeted inhibitors must combine the behaviors of inhibiting both the GE and Rif/Sor targets. The structures also support our data showing that Class I dual-targeted inhibitors have high potency against wild-type and mutant RNAPs, and provide evidence of how inhibitors are capable of overcoming Rif/Sor-resistant or GE-resistant RNAPs. Hence, Class I dual-targeted inhibitors are a useful method to not only construct novel antibiotics, but also to overcome antibacterial drug resistance.

Chapter 3:

Class II dual-targeted inhibitors of bacterial RNA polymerase (RifaAAPs)

RATIONALE

3.1 Relationship between Rif and AAP

In 2017, Ebright lab published the first crystal structure of *Mycobacterium tuberculosis* (*Mtb*) RNA polymerase (RNAP)-promoter open complex (RP_o) with rifampin (Rif) at 4.3 Å resolution and confirmed the binding site of Rif on *Mtb* RNAP (Figure 15a) (Lin et al., 2017). This structure shows the binding site of Rif close to the RNAP active center and the interactions between *Mtb* RNAP and Rif. Additionally, the same publication reveals another crystal structure of *Mtb* RNAP in complex with a novel non-Rif-related small-molecule inhibitor (Nα-aroyl-N-aryl-phenylalaninamides, AAPs) of *Mtb* RNAP (Lin et al., 2017). The crystal structure of *Mtb* RNAP-RP_o with D-AAP1, which is one of the first three AAP compounds, indicates that the D-AAP1 functions through the bridge-helix N-terminus target of *Mtb* RNAP (Figure 15b) (Mandal, 2014; Lin et al., 2017; Ebright et al., 2018). Examining both crystal structures reveals that the binding site of D-AAP1 differs from the binding site of Rif on *Mtb* RNAP and that neither binding site is adjacent or proximal.

Based on the information provided, subsequently, a former postdoc in the Ebright lab, Dr. Wei Lin, simultaneously soaked both Rif and D-AAP1 into a crystal

of *Mtb* RNAP-RP_o and explicitly confirmed that Rif and D-AAP1 could bind to their binding sites on *Mtb* RNAP at the same time without influence and overlap with each other, which means that they should not compete with each other to bind simultaneously on RNAP and also that they exhibit no cross-resistance (Figure 15c) (Lin et al., 2017). Rif and AAP's ability to bind simultaneously to *Mtb* RNAP could potentially allow construction of dual-targeted inhibitors, wherein Rif is conjugated to AAP (RifaAAPs) to overcome the Rif-resistant *Mtb* RNAP.

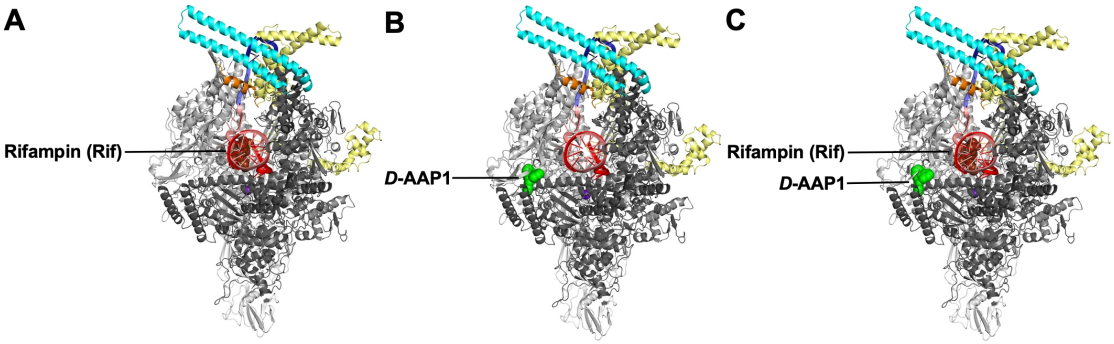

Figure 15. Targets of transcription inhibition by rifampin (Rif) and D-AAP1

(A) Structure of *Mtb* RNAP-RP_o in complex with rifampin (Rif, brown surface) (Image modified from Lin et al., 2017).

(B) Structure of *Mtb* RNAP-RP_o in complex with D-AAP1 (green surface) (Image modified from Lin et al., 2017).

(C) Structure of *Mtb* RNAP-RP_o in complex with both rifampin (Rif, brown surface) and D-AAP1 (green surface) (Image modified from Lin et al., 2017).

3.2 Non-Rif-related *Mtb* RNA polymerase inhibitors: Nα-aroyl-N-aryl-phenylalaninamides, IX-214a and IX-370a

From 2013 to 2016, Ebright's lab systematically synthesized and installed different substitutions at ortho, meta, and para positions of each phenyl ring (A, B, and C ring) on AAP (Figure 16a) (Ebright et al., 2018, Ebright et al., 2019). After synthesizing more than 600 different AAP analogs and combing all favorable substitutions to AAP, the most potent compound, IX-214a, was found in 2016 (Figure

16b) (Ebright et al., 2018). Following the chemical structure of IX-214a, we introduced two fluorine atoms to the R^1 position of A ring and the R^8 position of C ring on AAP, as well as a piperazinyl group to the R^6 position of C ring on AAP. Various *in vitro* analyses indicate that IX-214a has successfully increased the ligand-lipophilicity efficiency, metabolic stability, aqueous solubility and oral bioavailability. It could be a potential drug candidate for anti-*Mtb*; however, initial rodent studies illustrate that the IX-214a is not potent against *Mtb in vivo* (Ebright et al., unpublished).

The problems with IX-214a are that it still does not have high enough metabolic stability and oral bioavailability. To further improve the *in vitro* and *in vivo* potency so that the AAPs obtain high activity in mouse *Mtb* infection models, we introduced two deuterium atoms on the β-carbon of D-phenylalanine of IX-214a (R^3 and R^4 position) and retained all the beneficial substitutions from IX-214a (Ebright et al., 2019). Preparation of deuterated IX-214a eliminates the primary remaining metabolic inactivation site on the β-carbon of D-phenylalanine of IX-214a. According to the kinetic isotope effect (KIE), the carbon-deuterium bond can decrease the rate of bond cleavage in comparison with carbon-hydrogen bond in enzymic reactions (Guengerich, 2017). As a result, the deuterated IX-214a (called IX-370a, Figure 16c) should not only possess the outstanding *in vitro* potency as IX-214a, but should also exhibit greater metabolic stability, hydrolytic stability and pharmacokinetic properties than IX-214a. Various *in vitro* testing of IX-370a have shown that it indeed has higher potency than IX-214a. However, the mouse studies do not demonstrate that IX-370a superior activity against *Mtb in vivo* compared to the currently used anti-TB medicine "rifampin" (Ebright et al., unpublished).

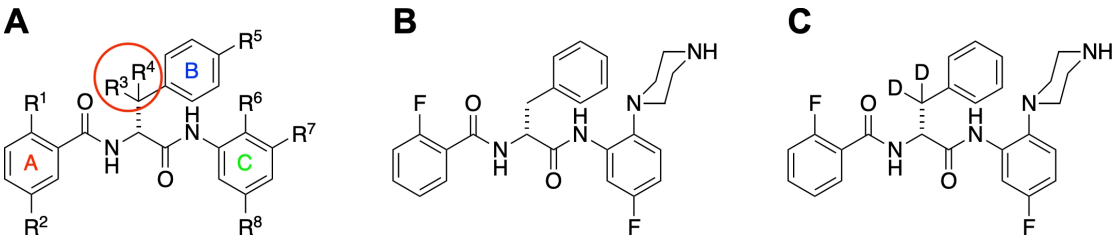

Figure 16. Chemical structure of AAPs

(A) Generic chemical structure of AAPs. The β-carbon of D-phenylalanine of AAP is the primary remaining metabolic inactivation site.

(B) Chemical structure of IX-214a with two fluorine atoms on R^1 and R^8 groups of AAP, and a piperazine on R^6 group of AAP.

(C) Chemical structure of IX-370a, the deuterated IX-214a, with two deuterium atoms on the β-carbon of D-phenylalanine.

3.3 Class II dual-targeted inhibitors

The crystal structure of RPo-Rif-AAP illustrates that the binding sites of Rif and AAP on *Mtb* RNAP are non-adjacent, and that both can function on their targets on RNAP at the same time (Lin et al., 2017). Hence, to take advantage of Rif and AAP's ability to bind simultaneously to RNAP and thereby overcome the *Mtb* drug resistance, it is possible to covalently conjugate Rif and AAP together and generate the Class II dual-targeted inhibitor (RifaAAPs) (Ebright et al., 2019).

Class II dual-targeted inhibitor comprises a first moiety (an inhibitor) that binds to a site on RNAP and covalently links to a second moiety (another inhibitor) that binds to a nonadjacent site on RNAP (Ebright and Wang, 2013). Although the binding sites of Class II dual-targeted inhibitors are not neighboring, both sites can be bound individually and simultaneously with two inhibitor molecules. The proposed function mechanism is that the first moiety of one molecule of inhibitor can interact with the first site on RNAP, and the second moiety can interact with another site (Ebright et al., 2019). Although the binding affinity and energy for Class II dual-

targeted inhibitors are not greater than that of Class I dual-targeted inhibitors, the Class II dual-targeted inhibitors still have several advantages.

Firstly, the Class II dual-targeted inhibitor is theoretically able to overcome resistance arising from either of two sites on RNAP (Figure 17) (Zhang et al., 2014). Even if one of the sites has resistant substitutions that prevent inhibitor binding, the other site still binds with an inhibitor. Secondly, as mentioned previously, IX-370a, a promising compound in all AAPs, has potency *in vitro* activity against *Mtb*, although it lacks superior activity in a mouse *Mtb* infection model with oral dosing. However, a RifaAAP conjugated inhibitor could bring benefit to IX-370a from Rif and improve the *in vivo* activity of IX-370a. (Bremner et al., 2007; Brötz-Oesterhelt and Brunner, 2008). Lastly, the RifaAAP conjugated inhibitor functions similarly to the co-administration of Rif and AAP (Forrest and Tamura, 2010). However, conjugating them is superior to co-administering them because the conjugation of two inhibitors could give both inhibitors the same pharmacokinetic property and contribute to additive antibacterial activity (Bremner et al., 2007; Tevyashova et al., 2015).

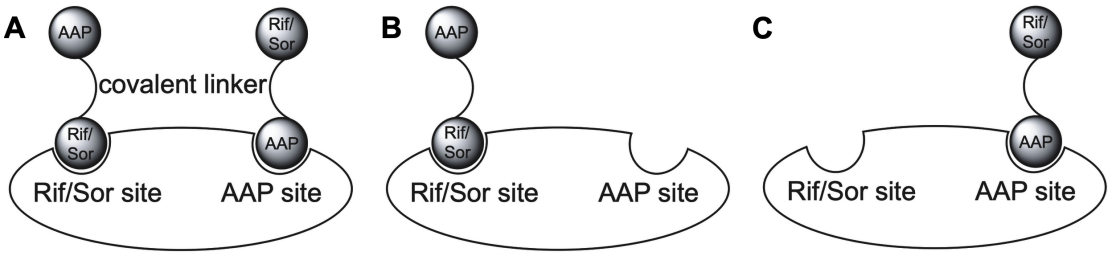

Figure 17. The concept and strategy for Class II dual-targeted inhibitor

(A) Two molecules (Rif and AAP, or Sor and AAP) of Class II dual-targeted inhibitor bind simultaneously to two non-adjacent binding sites (Rif/Sor site, and AAP site) on wild-type RNAP via first moiety (Rif or Sor) of one molecule of Class II dual-targeted inhibitor and second moiety (AAP) of another molecule of Class II dual-targeted inhibitor (circle surface Rif/Sor = rifamycin/sorangicin; circle surface AAP = AAP).

(B) One molecule of Class II dual-targeted inhibitor binds to first site (Rif/Sor site) on AAP binding site mutated RNAP via first moiety (Rif/Sor = rifamycin/sorangicin) of one molecule of Class II dual-targeted inhibitor to overcome resistance.

(C) Another molecule of Class II dual-targeted inhibitor binds to second site (AAP site) on Rif/Sor binding site mutated RNAP via second moiety (AAP) of another molecule of Class II dual-targeted inhibitor to overcome resistance.

EXPERIMENTAL DESIGN AND METHODS

3.4 Class II dual-targeted inhibitors of bacterial RNA polymerase: Linkage of a Rif/Sor-pocket ligand to a non-Rif-related ligand (AAP) of the RNA polymerase bridge-helix N-terminus target

3.4.1 Synthetic strategy of rifamycins conjugated to AAPs (RifaAAPs)

To synthesize Class II dual-targeted inhibitors, it is indispensable to determine the specific chemically-reactive functional groups on both moieties of rifamycin and AAP. As mentioned earlier, the binding sites of Rif and AAP are not adjacent (Lin et al., 2017). Hence, the position and direction of the connecting functional groups between Rif and AAP are not as significant as those of Class I dual-targeted inhibitors (Zhang et al., 2014; Ebright et al., 2016). However, the rifamycin and AAP must have functional groups that are able to react and form a covalent bond with each other so that the Class II dual-targeted inhibitors can be generated.

The chemical structure of IX-370a indicates that it has a piperazinyl group on its C ring. The secondary amine of piperazinyl group on IX-370a possesses excellent nucleophilicity and reacts readily with some particular functional groups, such as aldehyde via reductive amination, carboxylic acid via amide formation, and halogenoalkane via S_N2 reaction, respectively. Hence, the secondary amine of piperazinyl group on IX-370a is a feasible linkage between Rif and IX-370a. For the rifamycin derivatives, the 3-formyl rifamycin, rifamycin B, and 3-bromo-rifamycin S

all have particular functional groups with chemical reactivity with the secondary amine. Therefore, the rifamycin derivatives and IX-370a are able to be covalently conjugated together and generate RifaAAPs Class II dual-targeted inhibitors via chemical reactions (Ebright et al., 2019).

In order to further optimize the potency of RifaAAPs, one probable strategy is to modify the linker between Rif and AAP. The distinct length and composition of the linker can alter the pharmacological activity of the dual-targeted inhibitor. Ideally, if the linker causes both moieties to become more flexible on dual-targeted inhibitor, then the inhibitor will bind to their targets on RNAP more stably. Hence, a variety of different linkers could be installed between Rif and AAP. In particular, the alkane chain with sp^3 carbon-carbon single bond usually is quite flexible. Alternatively, using the alkane chain with piperazinyl group or glycine derivative as a linker could potentially improve the potency and solubility for the RifaAAPs.

3.5 Class II dual-targeted inhibitors of bacterial RNA polymerase: characterization

All of the synthesized Class II dual-targeted inhibitors have been tested for their inhibition of bacterial RNAP. The research technicians in the Ebright lab and I performed the biochemical evaluation for all Class II dual-targeted inhibitors via fluorescence-detected transcription assay to assess their ability against wild-type *Mtb* RNAP holoenzyme, Rif-resistant *Mtb* RNAP holoenzyme (RNAP derivative containing β S531L substitution), and AAP-resistant *Mtb* RNAP holoenzyme (RNAP derivatives derivative containing β R637C substitution).

All of the synthesized Class II dual-targeted inhibitors have also been tested for their inhibition of bacterial growth in culture. The minimum inhibitory concentration (MIC) was examined for all Class II dual-targeted inhibitors via microplate Alamar Blue assay to assess their ability against *Mycobacterium tuberculosis* (*Mtb*) H37Rv; rifampin-resistant *Mtb* isolates 20626 (rpoB-H'526'D), 4457 (rpoB-H'526'Y), and 14571 (rpoB-S'531'L).

Additionally, a few of the Class II dual-targeted inhibitors with promising activities were soaked into the equilibrating pre-formed crystals of *Mtb* RPo complex. The X-ray diffraction data of crystals will be collected at a synchrotron light source, and structures will be solved by molecular replacement.

3.5.1 Assay of RNAP-inhibitory activity: ribogreen fluorescence-detected transcription assay

Fluorescence-detected RNA polymerase assays were performed by a modification of the procedure in Kuhlman et al. (2004). Reaction mixtures contained (20 μL): 0-100 μM test compound, bacterial RNA polymerase core enzyme (75 nM *Mycobacterium tuberculosis* RNAP core enzyme or 75 nM *Mycobacterium tuberculosis* RNAP core enzyme derivative) (Lin et al., 2017), 300 nM *Mycobacterium tuberculosis* σA, 20 nM DNA fragment containing the bacteriophage T4 N25 promoter (positions -72 to +367; prepared by PCR from plasmid pARTaqN25-340-tR2; [Liu, 2007]), 100 μM ATP, 100 μM GTP, 100 μM UTP, 100 μM CTP, in transcription buffer (TB) (40 mM Tris-HCl, pH 8.0, 75 mM NaCl, 5 mM $MgCl_2$, 2.5 mM DTT, and 12.5% glycerol). Reaction components 75 nM *Mycobacterium tuberculosis* RNAP core enzyme, and 300 nM *Mycobacterium*

tuberculosis σA in TB were incubated in ice for 10 mins. Reaction components other than DNA and NTPs were pre-incubated for 10 min at 37°C. Reactions were carried out by addition of DNA and incubation for 5 min at 37°C, followed by addition of NTPs and incubation for 60 min at 37°C. DNA was removed by addition of 1 μL 5 mM $CaCl_2$ and 2 U DNaseI (Ambion, Inc.), followed by incubation for 90 min at 37°C. RNA was quantified by addition of 100 μl RiboGreen RNA Quantitation Reagent (Life Technologies, Grand Island, NY; 1:500 dilution in 10 mM Tris- HCl, pH 8.0, 1 mM EDTA), followed by incubation for 10 min at 25°C, and measurement of fluorescence intensity (excitation wavelength = 485 nm and emission wavelength = 535 nm; GENios Pro microplate reader [Tecan, Männedorf, Switzerland]) (Ebright et al., 2019). Half-maximal inhibitory concentrations (IC50) were calculated by non-linear regression in SigmaPlot. IC50 is defined as the concentration of inhibitor resulting in 50% inhibition of RNA polymerase activity.

3.5.2 Assay of RNAP-inhibitory activity: γ-[2'-(2-benzothiazoyl)-6'-hydroxybenzothiazole]-ATP (BBT-ATP) fluorescence-detected transcription assay

Reaction mixtures contained (20 μL): 0-400 μM test compound, bacterial RNA polymerase core enzyme (75 nM *Mycobacterium tuberculosis* RNAP core enzyme or 75 nM *Mycobacterium tuberculosis* RNAP core enzyme derivative) (Lin et al., 2017), 300 nM *Mycobacterium tuberculosis* σA, 20 nM DNA fragment containing the bacteriophage T4 N25 promoter (positions -72 to +367; prepared by PCR from plasmid pARTaqN25-340-tR2; [Liu, 2007]), 25 μM BBT-ATP (Jena Bioscience), 100 μM GTP, 100 μM UTP, and 100 μM CTP, in transcription buffer (TB) (50 mM Tris-

HCl, pH 8.0, 75 mM NaCl, 5 mM $MgCl_2$, 2.5 mM DTT, and 12.5% glycerol). Reaction components 75 nM *Mycobacterium tuberculosis* RNAP core enzyme, and 300 nM *Mycobacterium tuberculosis* σA in TB were incubated in ice for 10 mins. Reaction components other than DNA and NTPs were pre-incubated for 10 min at 37°C. Reactions were carried out by addition of DNA and incubation for 5 min at 37°C, followed by addition of NTPs (pre-mixed BBT-ATP, GTP, UTP and CTP) and incubation for 60 min at 37°C. Reactions were terminated, and profluorescent BBT-diphosphate produced during reactions was hydrolyzed to fluorescent BBT by addition of 1 μL 0.5 M AMPSO (Sigma-Aldrich) containing 0.5 U calf-intestinal alkaline phosphatase (New England BioLabs) and incubation for 20 min at 37°C (Mandal, 2014; Feng et al., 2015). Fluorescence emission intensities were measured by using a GENios Pro microplate reader ([Tecan Männedorf, Switzerland]; excitation wavelength = 415 nm; emission wavelength = 535 nm). Half-maximal inhibitory concentrations were calculated by non-linear regression in SigmaPlot (SPSS).

3.5.3 Assay of antibacterial activity: Microplate Alamar Blue assay

The minimum inhibitory concentrations for *M. tuberculosis* H37Rv; rifampin-resistant *M. tuberculosis* isolates 20626 (rpoB-H'526'd), 4457 (rpoB-H'526'Y), and 14571 (rpoB-S'531'L) against Class II dual-targeted inhibitors were quantified via microplate Alamar Blue assays as described (Collins and Franzblau, 1997).

3.5.4 Structure determination: RPitc + Class II dual-targeted inhibitor

The crystal structure was determined by soaking the Class II dual-targeted inhibitor into a pre-formed crystal of a *M. tuberculosis* RNAP promoter transcription

initiation complex, collecting X-ray diffraction data at a synchrotron beamline, solving the structure by molecular replacement using atomic coordinates for the structure of a *Mtb* RNAP promoter transcription initiation complex in the absence of Class II dual-targeted inhibitor as the search model, and refining the structure. These methods for crystal growth, crystal soaking, data collection, structure solution, and structure refinement for determination of a structure of Class II dual-targeted inhibitor bound to *M. tuberculosis* RNAP promoter transcription initiation complex were performed as in Lin et al., 2017.

RESULTS

3.6 Class II dual-targeted inhibitors of bacterial RNA polymerase: Linkage of a Rif/Sor-pocket ligand to a non-Rif-related ligand (AAP) of the RNA polymerase bridge-helix N-terminus target

3.6.1 Synthesis of 2-fluoro-*N*-(1-((5-fluoro-2-(piperazin-1-yl)phenyl)amino)-1-oxo-3-phenylpropan-2-yl)benzamide (IX-214)

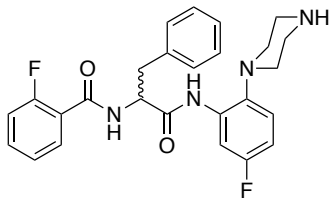

IX-214 was synthesized as in Ebright et al., 2018.

3.6.2 Synthesis of (*R*)-2-fluoro-*N*-(1-((5-fluoro-2-(piperazin-1-yl)phenyl)amino)-1-oxo-3-phenylpropan-2-yl-3,3-d2)benzamide (IX-370a)

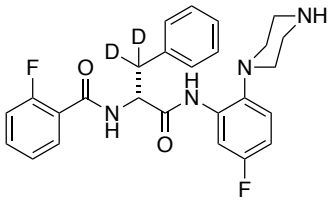

3.6.2.1 Synthesis of *t*-Butyl 4-(4-fluoro-2-nitrophenyl)piperazine-1-carboxylate

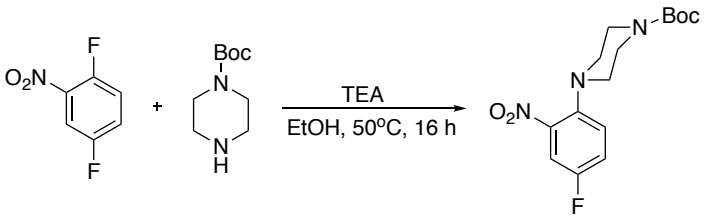

To a solution of 2,5-difluoronitrobenzene (3.2 mL; 29.5 mmol; Sigma-Aldrich) in ethanol (59 mL), was added 1-Boc-piperazine (6.05 g; 32.5 mmol; Sigma-Aldrich) and triethylamine (4.11 mL; 29.5 mmol; Sigma-Aldrich), and the reaction mixture was stirred 16 h at 50°C and then allowed to cool to room temperature. The reaction mixture was evaporated and then extracted with ethyl acetate (30 mL). The extract was dried over anhydrous sodium sulfate, filtered, and evaporated to dryness, and the crude product was purified by silica chromatography (ethyl acetate/hexanes gradient) (Ebright et al., 2018).

Yield: 6.18 g; 64%. ^{1}H NMR (500 MHz, $CDCl_3$): δ 7.51 (dd, 1H), 7.26-7.23 (m, 1H), 7.17 (dd, 1H), 3.56 (t, 4H), 2.95 (brs, 4H), 1.47 (s, 9H).

3.6.2.2 Synthesis of *t*-Butyl 4-(2-amino-4-fluorophenyl)piperazine-1-carboxylate

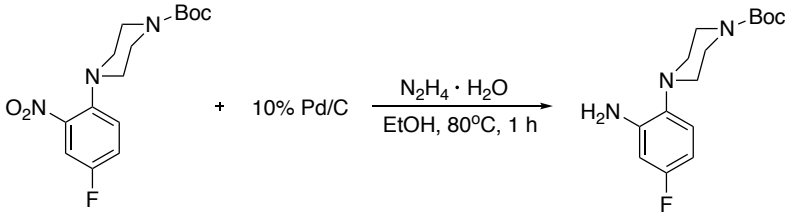

To a solution of *t*-butyl 4-(4-fluoro-2-nitrophenyl)piperazine-1-carboxylate (6.18 g; 19 mmol; Example 3.6.2.1) in ethanol (79 mL), was added 10% Pd/C (794 mg; Sigma-Aldrich) and hydrazine monohydrate (4.3 mL; 88.65 mmol; Sigma-Aldrich), after which the reaction mixture was stirred 1 h at 80°C. After cooling to room temperature, the reaction mixture was filtered through a pad of Celite 521 (Sigma-Aldrich). The filtrate was concentrated to an oil, re-dissolved in ethyl acetate (80 mL), dried over anhydrous sodium sulfate, filtered, and evaporated to dryness. The crude product was used in the next step without further purification (Ebright et al., 2018).

Crude yield: 5.62 g; 99%. ^{1}H NMR (500 MHz, $CDCl_3$): δ 6.90-6.86 (m, 1H), 6.44-6.36 (m, 2H), 4.13-4.09 (m, 2H), 3.55 (br, 4H), 2.78 (brs, 4H), 1.48 (d, 9H).

3.6.2.3 Synthesis of D-phenylalanine-3,3'-d_2

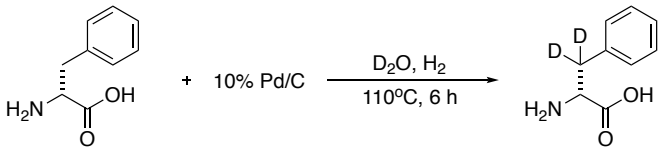

D-phenylalanine-3,3'-d_2 was prepared using procedures described for preparation of L-phenylalanine-3,3'-d_2 (Maegawa et. al., 2005). A suspension of D-phenylalanine (330 mg; 2 mmol; Chem-Impex) and 10% Pd/C (33 mg; Sigma-Aldrich) in deuterium oxide (8 mL; 99.9% D; Sigma-Aldrich) was heated 6 h at 110°C under H_2 (balloon). After cooling to room temperature, the reaction mixture was filtered through a pad of Celite 521 (Signa-Aldrich). The filtrate was concentrated to a solid, dissolved in 10 mL water and 10 mL methanol, and evaporated to yield D-phenylalanine-3,3'-d_2 (Maegawa et al., 2005). The crude product was used in the next step without further purification.

Crude yield: 316 mg; 95%. ^{1}H NMR (500 MHz, D_2O): δ 7.45-7.42 (m, 2H), 7.40-7.36 (m, 1H), 7.34-7.32 (m, 2H), 3.99 (s, 1H).

3.6.2.4 Synthesis of *N*-Fmoc-D-phenylalanine-3,3'-d_2

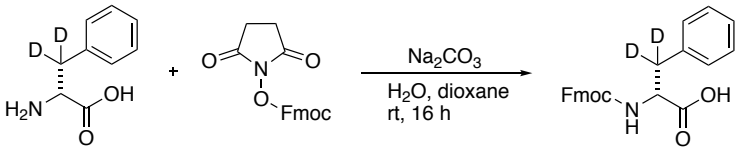

To a suspension of D-phenylalanine-3,3'-d_2 (1.19 g; 7.12 mmol; Example 3.6.2.3) in 10% sodium carbonate (8.4 mL; Fisher Scientific), was added Fmoc *N*-hydroxysuccinimide ester (2.64 g; 7.83 mmol; Chem-Impex) in dioxane (8.8 mL; Sigma-Aldrich). The reaction was stirred 16 h at room temperature, diluted with water (20 mL), and extracted with ethyl acetate (2 x 20 mL). The aqueous layer was poured into ethyl acetate (30 mL), acidified with 1 N HCl to pH 3, and extracted with ethyl acetate (3 x 30 mL). The pooled extracts were washed with 1 N HCl (2 x 30 mL), water (2 x 30 mL), and brine (30 mL), and then dried over anhydrous sodium sulfate, filtered, and evaporated. The crude product was directly used in the next step without further purification.

Crude yield: 2.41 g; 87%.

3.6.2.5 Synthesis of *t*-Butyl (*R*)-4-(2-(2-((((9H-fluoren-9-yl)methoxy)carbonyl)amino)-3-phenylpropanamido-3,3-d2)-4-fluorophenyl)piperazine-1-carboxylate

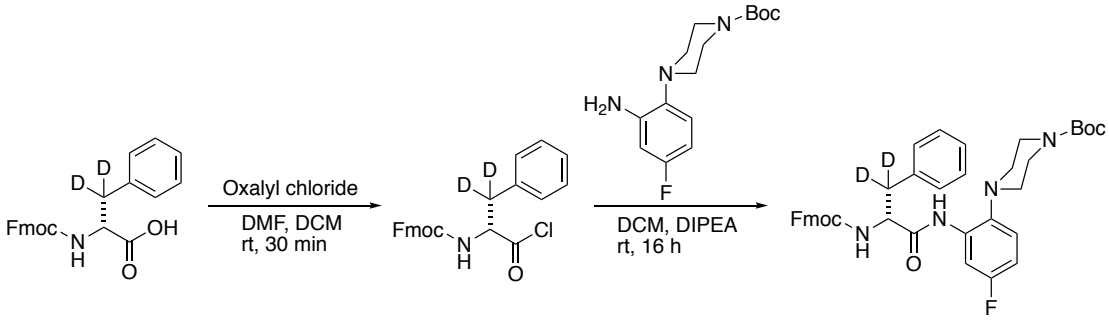

To a suspension of *N*-Fmoc-D-phenylalanine-3,3'-d_2 (2.41 g; 6.19 mmol; Example 3.6.2.4) in dichloromethane (28 mL), was added oxalyl chloride (0.79 mL; 9.28 mmol; Sigma-Aldrich) and dimethylformamide (60 μL), and the reaction mixture was stirred 30 min at room temperature under argon. The reaction mixture was evaporated to dryness, re-dissolved in dichloromethane (28 mL), supplemented with *t*-Butyl 4-(2-amino-4-fluorophenyl)piperazine-1-carboxylate (1.826 g; 6.18 mmol; Example) and *N*,*N*-diisopropylethylamine (1.6 ml; 9.19 mmol; Sigma-Aldrich), and stirred 16 h at room temperature under argon. The reaction mixture was washed with 0.5 M HCl (30 mL) and saturated sodium bicarbonate (30 mL), and was extracted with dichloromethane (3 x 30 mL). The pooled extracts were dried over anhydrous sodium sulfate, filtered, and evaporated to dryness, after which the product was purified by silica chromatography (ethyl acetate/hexanes gradient).
Yield: 2.9 g; 70%. MS (MALDI): calculated: *m*/*z* 666.79 ($M+H^+$); found: 667.25 ($M+H^+$).

3.6.2.6 Synthesis of *t*-Butyl (*R*)-4-(2-(2-amino-3-phenylpropanamido-3,3-d_2)-4-fluorophenyl)piperazine-1-carboxylate

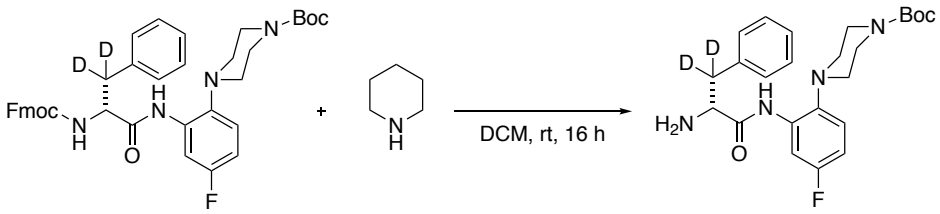

To a solution of *t*-butyl (*R*)-4-(2-(2-((((9*H*-fluoren-9-yl)methoxy)carbonyl)amino)-3-phenylpropanamido-3,3-d_2)-4-fluorophenyl)piperazine-1-carboxylate (2.9 g; 4.35 mmol; Example 3.6.2.5) in dichloromethane (34 mL; Sigma-Aldrich), was added piperidine (1.72 mL; 17.41 mmol; Sigma-Aldrich), and the reaction mixture was stirred 16 h at room temperature. The reaction mixture was evaporated to dryness, 1 N HCl was added to adjust pH to 7, and the reaction mixture was extracted with dichloromethane (3 x 30 mL). The pooled extracts were dried over anhydrous sodium sulfate, filtered, and evaporated, after which the product was purified by silica chromatography (ethyl acetate/hexanes gradient).

Yield: 1.82 g; 94%.

3.6.2.7 Synthesis of *t*-Butyl (*R*)-4-(4-fluoro-2-(2-(2-fluorobenzamido)-3-phenylpropanamido-3,3-d_2)phenyl)piperazine-1-carboxylate

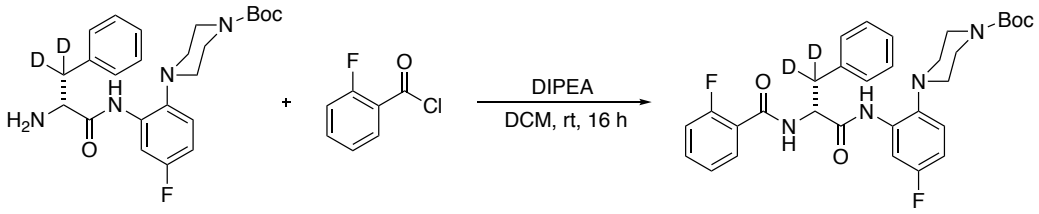

To a solution of *t*-butyl (*R*)-4-(2-(2-amino-3-phenylpropanamido-3,3-d_2)-4-fluorophenyl)piperazine-1-carboxylate (1.82 g; 4.1 mmol; Example 3.6.2.6) in dichloromethane (40 mL), was added 2-fluorobenzoyl chloride (0.74 mL; 6.2 mmol; Sigma-Aldrich) and *N*,*N*-diisopropylethylamine (1.1 mL; 6.32 mmol; Sigma-Aldrich), and the reaction mixture was stirred 16 h at room temperature under argon. The reaction mixture was diluted with dichloromethane (40 mL) and extracted with 0.5 N HCl (2 x 40 mL). The pooled extracts were dried over anhydrous sodium sulfate,

filtered, and evaporated, after which the product was purified by silica chromatography (ethyl acetate/ hexanes gradient).

Yield: 1.73 g; 75%.

3.6.2.8 Synthesis of (*R*)-2-fluoro-*N*-(1-((5-fluoro-2-(piperazin-1-yl)phenyl)amino)-1-oxo-3-phenylpropan-2-yl-3,3-d_2)benzamide (IX-370a)

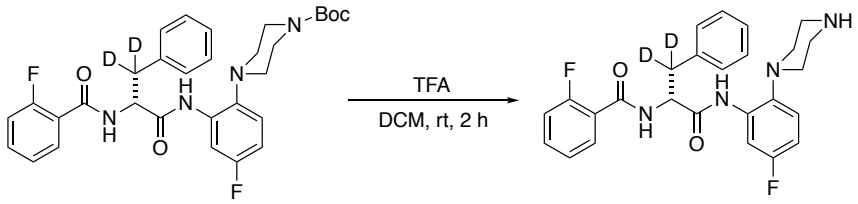

To *tert*-butyl (*R*)-4-(4-fluoro-2-(2-(2-fluorobenzamido)-3-phenylpropanamido-3,3-d_2)phenyl)piperazine-1-carboxylate (1.1 g; 1.93 mmol; Example 3.6.2.7) was added dichloromethane (10 mL) and trifluoroacetic acid (5 mL; Sigma-Aldrich), and the reaction mixture was stirred 2 h at room temperature. The reaction mixture was evaporated, and the crude product was purified by silica chromatography (methanol/dichloromethane gradient).

Yield: 1.02 g; 99%. ^{1}H NMR (500 MHz, $CDCl_3$): δ 9.16 (s, 1H), 8.25 (dd, 1H), 8.05 (td, 1H), 7.53-7.49 (m, 1H), 7.34-7.21 (m, 6H), 7.19-7.08 (m, 2H), 6.75 (td, 1H), 4.98 (dd, 1H), 3.19-3.14 (m, 4H), 2.85 (brs, 4H). MS (MALDI): calculated: *m*/*z* 467.53 ($M+H^+$); found: 467.27 ($M+H^+$).

3.6.3 Synthesis of 2-fluoro-*N*-(1-((5-fluoro-2-(4-(2-(piperazin-1-yl)ethyl)piperazin-1-yl)phenyl)amino)-1-oxo-3-phenylpropan-2-yl)benzamide (IX-402)

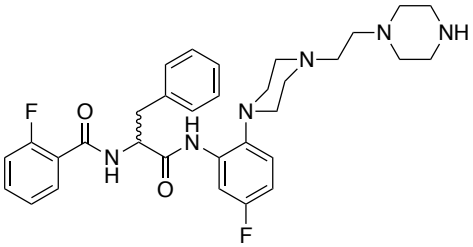

3.6.3.1 Synthesis of *t*-Butyl 4-(2-(4-(4-fluoro-2-(2-(2-fluorobenzamido)-3-phenylpropanamido)phenyl)piperazin-1-yl)ethyl)piperazine-1-carboxylate

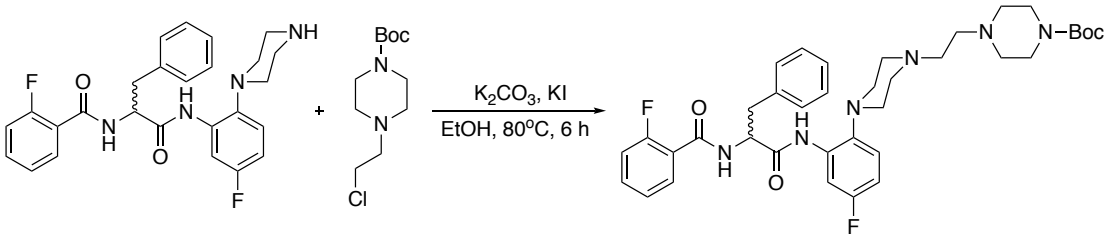

A suspension of IX-214 (30 mg; 0.065 mmol; Example 3.6.1), potassium carbonate (9 mg; 0.065 mmol), and potassium iodide (2 mg; 0.012 mmol) in ethanol (1 mL) was stirred 5 min at room temperature, was supplemented with *t*-butyl 4-(2-chloroethyl)piperazine-1-carboxylate (24.3 mg; 0.098 mmol; Acros Organics), and stirred 6 h at 80°C. The reaction mixture was evaporated, re-dissolved in 10 mL water, and extracted with dichloromethane (3 x 10 mL). The pooled extracts were dried over anhydrous sodium sulfate, filtered, and evaporated, and the product was purified by silica chromatography (methanol/dichloromethane gradient).

Yield: 34.4 mg; 79%.

3.6.3.2 Synthesis of 2-Fluoro-*N*-(1-((5-fluoro-2-(4-(2-(piperazin-1-yl)ethyl)piperazin-1-yl)phenyl)amino)-1-oxo-3-phenylpropan-2-yl)benzamide (IX-402)

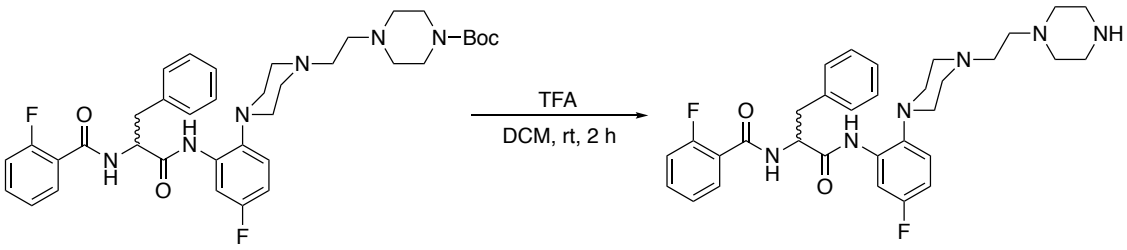

To *tert*-butyl 4-(2-(4-(4-fluoro-2-(2-(2-fluorobenzamido)-3-phenylpropanamido)-phenyl)piperazin-1-yl)ethyl)piperazine-1-carboxylate (34 mg; 0.05 mmol; Example 3.6.3.1), was added dichloromethane (0.5 mL) and trifluoroacetic acid (125 μL; Sigma-Aldrich), and the reaction mixture was stirred 2 h at room temperature. The reaction mixture was evaporated, and the crude product was purified by silica chromatography (methanol/dichloromethane/ammonium hydroxy gradient).

Yield: 9 mg; 30%. ^{1}H NMR (500 MHz, $CDCl_3$): δ 8.93 (s, 1H), 8.25 (dt, 1H), 8.11 (td, 1H), 7.51-7.49 (m, 1H), 7.41-7.38 (m, 1H), 7.29-7.26 (m, 4H), 7.23-7.21 (m, 1H), 7.17-7.13 (m, 1H), 7.06-7.03 (m, 1H), 6.72 (tt, 1H), 5.00-4.99 (m, 1H), 3.48 (d, 1H), 3.42-3.38 (m, 1H), 3.24-3.20 (m, 1H), 2.94 (d, 4H), 2.59-2.29 (m, 17H). MS (MALDI): calculated: *m*/*z* 577.69 ($M+H^+$); found: 577.17 ($M+H^+$).

3.6.4 Synthesis of rifamycin SV-(CHN)-IX-214 conjugate (IX-398)

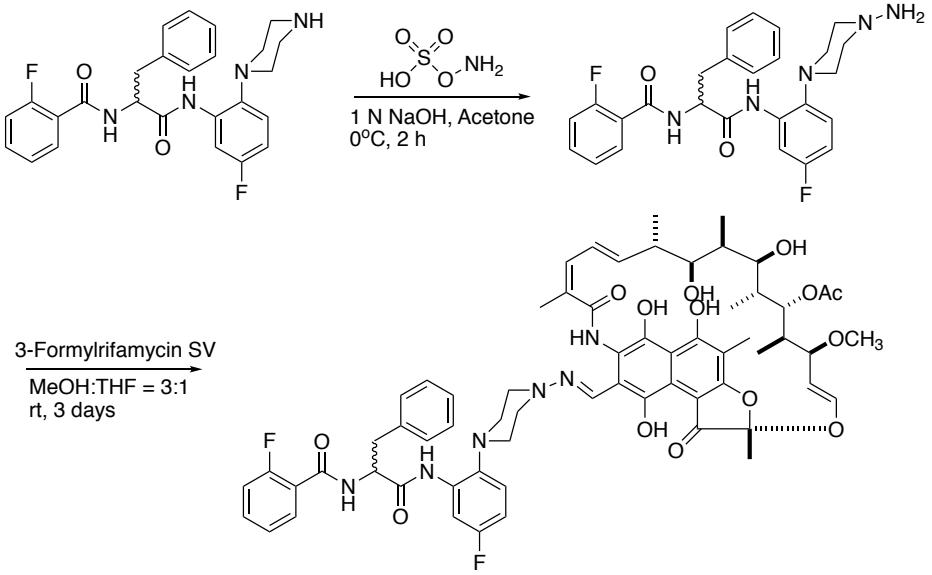

To a suspension of IX-214 (30 mg; 0.065 mmol; Example 3.6.1) in 0.5 mL 1 N NaOH at 0°C, was added acetone (0.25 mL) and hydroxyaminine-*O*-sulfuric acid in 20 µL water (9 mg; 0.08 mmol; Sigma-Aldrich; dissolved immediately before use), and the reaction mixture was stirred 2 h at 0°C and then allowed to come to room temperature. Following addition of glacial acetic acid (30 µL) to acidify the reaction mixture to pH 5, the reaction mixture was supplemented with ascorbic acid (6 mg; Sigma-Aldrich), methanol (1 mL), and 3-formylrifamycin SV freshly dissolved in 150 µL 3:1 v/v methanol/tetrahydrofuran (31 mg; 0.043 mmol; AvaChem Scientific), after which the reaction mixture was stirred 3 days at room temperature (Ma et al., 2016). The reaction mixture was evaporated to dryness, re-dissolved in 5 mL water, and extracted with dichloromethane (3 x 5 mL). The pooled extracts were dried over anhydrous sodium sulfate, filtered, and evaporated. The sample was dissolved in dichloromethane (2 mL) and 5% citric acid/0.5% ascorbic acid aqueous solution (2 mL), stirred 2 h at room temperature and extracted with dichloromethane (3 x 5 mL). The pooled extracts were collected, dried over anhydrous sodium sulfate, filtered, and evaporated, and the product was purified by silica chromatography (methanol/dichloromethane gradient).

Yield: 19.2 mg; 38%. MS (MALDI): calculated: *m/z* 1188.30 ($M+H^+$); found: 1209.27 ($M+Na^+$).

3.6.5 Synthesis of rifamycin SV-(CHN)-IX-370a conjugate (IX-404a)

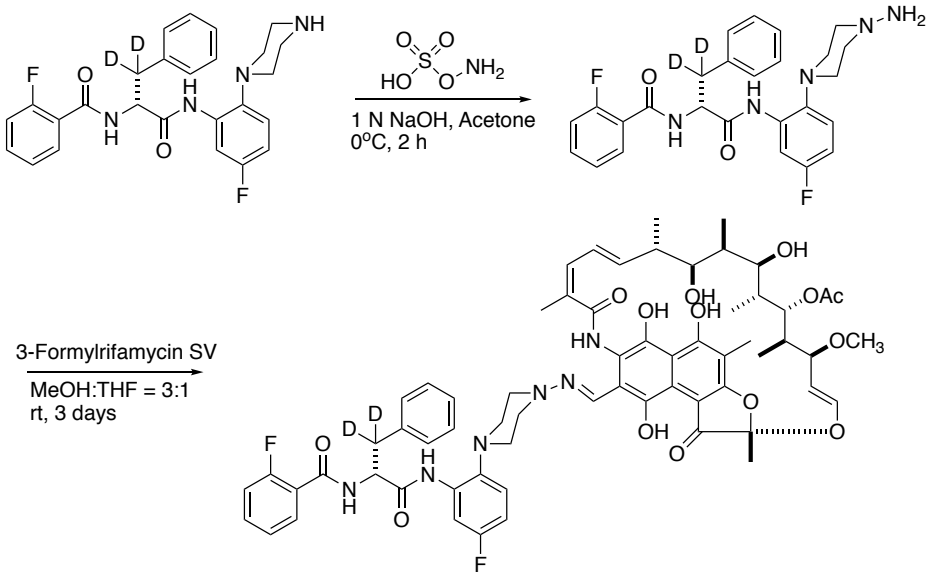

To a suspension of IX-370a (60 mg; 0.129 mmol; Example 3.6.2) in 1 mL 1 N NaOH at 0°C, was added acetone (0.8 mL) and hydroxyaminine-*O*-sulfuric acid in 40 µL water (15 mg; 0.132 mmol; Sigma-Aldrich; dissolved immediately before use), and the reaction mixture was stirred 2 h at 0°C and then allowed to come to room temperature. Following addition of glacial acetic acid (50 µL) to acidify the reaction mixture to pH 5, the reaction mixture was supplemented with ascorbic acid (12 mg; Sigma-Aldrich), methanol (2 mL), and 3-formylrifamycin SV freshly dissolved in 375 µL 3:1 v/v methanol/tetrahydrofuran (62 mg; 0.085 mmol; AvaChem Scientific), after which the reaction mixture was stirred 3 days at room temperature (Ma et al., 2016). The reaction mixture was evaporated to dryness, re-dissolved in 10 mL water, and extracted with dichloromethane (3 x 10 mL). The pooled extracts were dried over anhydrous sodium sulfate, filtered, and evaporated. The sample was dissolved in

dichloromethane (4 mL) and 5% citric acid/0.5% ascorbic acid aqueous solution (4 mL), stirred 2 h at room temperature and extracted with dichloromethane (3 x 10 mL). The pooled extracts were collected, dried over anhydrous sodium sulfate, filtered, and evaporated, and the product was purified by silica chromatography (methanol/dichloromethane gradient).

Yield: 33 mg; 32%. MS (MALDI): calculated: *m/z* 1190.32 ($M+H^+$); found: 1211.22 ($M+Na^+$).

3.6.6 Synthesis of rifamycin SV-(CHN)-IX-402 conjugate (IX-403)

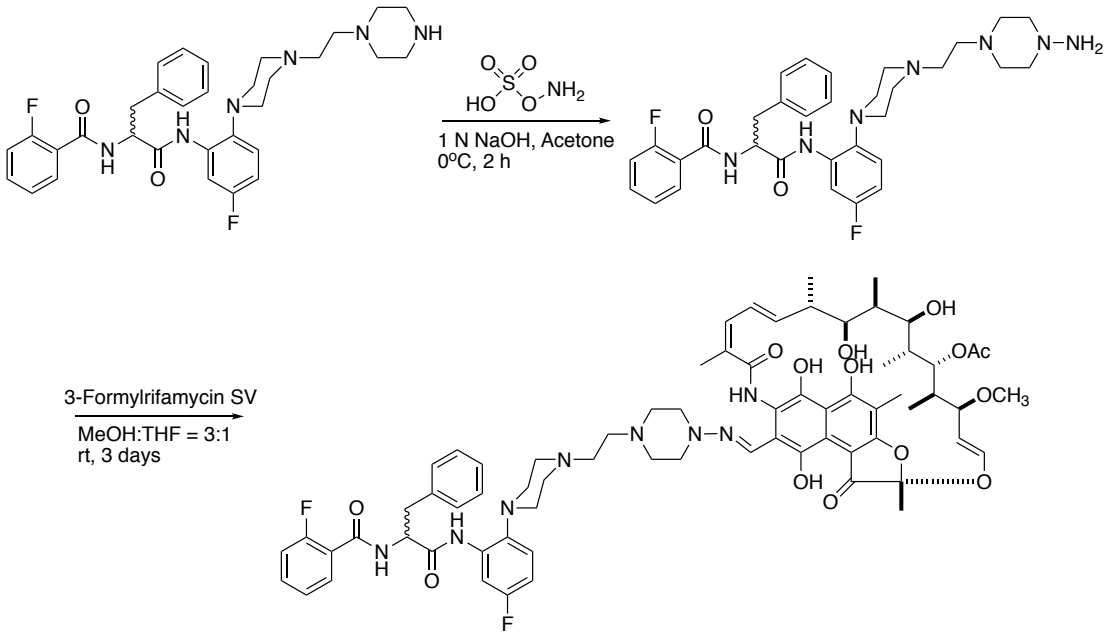

To a suspension of IX-402 (33 mg; 0.057 mmol; Example 3.6.3) in 0.6 mL 1 N NaOH at 0°C, was added acetone (0.3 mL) and hydroxyaminine-*O*-sulfuric acid in 20 µL water (8 mg; 0.071 mmol; Sigma-Aldrich; dissolved immediately before use), and the reaction mixture was stirred 2 h at 0°C and then allowed to come to room temperature. Following addition of glacial acetic acid (30 µL) to acidify the reaction mixture to pH 5, the reaction mixture was supplemented with ascorbic acid (6 mg; Sigma-Aldrich), methanol (1 mL), and 3-formylrifamycin SV freshly dissolved in 600

μL 3:1 v/v methanol/tetrahydrofuran (52 mg; 0.072 mmol; AvaChem Scientific), after which the reaction mixture was stirred 3 days at room temperature (Ma et al., 2016). The reaction mixture was evaporated to dryness, re-dissolved in 5 mL water, and extracted with dichloromethane (3 x 5 mL). The pooled extracts were dried over anhydrous sodium sulfate, filtered, and evaporated. The sample was dissolved in dichloromethane (2 mL) and 5% citric acid/0.5% ascorbic acid aqueous solution (2 mL), stirred 2 h at room temperature and extracted with dichloromethane (3 x 5 mL). The pooled extracts were collected, dried over anhydrous sodium sulfate, filtered, and evaporated, and the product was purified by silica chromatography (methanol/dichloromethane gradient).

Yield: 25.4 mg; 34%. MS (MALDI): calculated: m/z 1300.48 ($M+H^+$); found: 1267.31 (M-MeOH), 1299.31 ($M+H^+$).

3.6.7 Synthesis of rifamycin B-IX-370a conjugate (IX-408a)

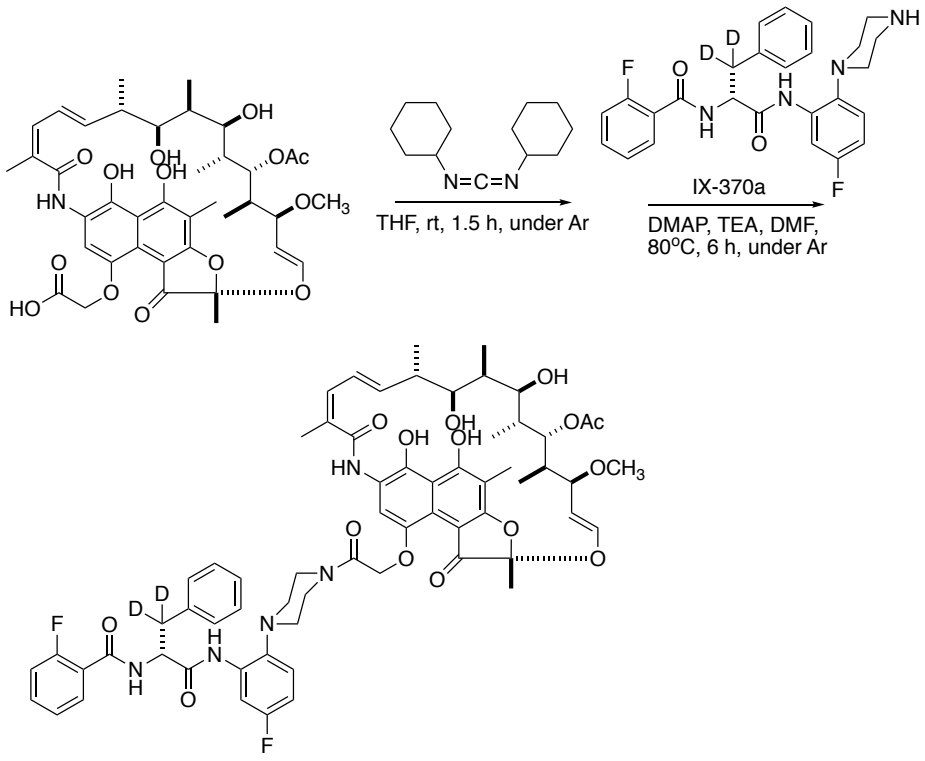

To a suspension of rifamycin B (150 mg; 0.20 mmol; AvaChem Scientific) in 3 mL tetrahydrofuran at room temperature under argon, was added a solution of *N,N′*-dicyclohexylcarbodiimide (150 mg; 0.73 mmol; Sigma-Aldrich) in 1 mL tetrahydrofuran, and the reaction mixture was stirred 1.5 h at room temperature. The reaction mixture was filtered off, and the filtrate was added to 25 mL anhydrous diethyl ether, yielding a yellow precipitate. The resulting yellow precipitate was dissolved in 3.75 mL dimethylformamide, and IX-370a (113 mg; 0.24 mmol; Example 3.6.2) in 2.8 mL dimethylformamide, 4-dimethylaminopyridine (2.4 mg; 0.02 mmol; Alfa Aesar), and triethylamine (0.056 mL; 0.4 mmol; Sigma-Aldrich) successively were added, and the reaction mixture was stirred 6 h at 80°C, and then evaporated to dryness. The product was purified by silica chromatography (methanol/dichloromethane gradient).

Yield: 94.6 mg; 40%. MS (MALDI): calculated: *m*/*z* 1205.33 ($M+H^+$); found: 1173.27 ($M+H^+$-MeOH).

3.6.8 Synthesis of rifamycin S-(CHN)-IX-370a conjugate (IX-476a)

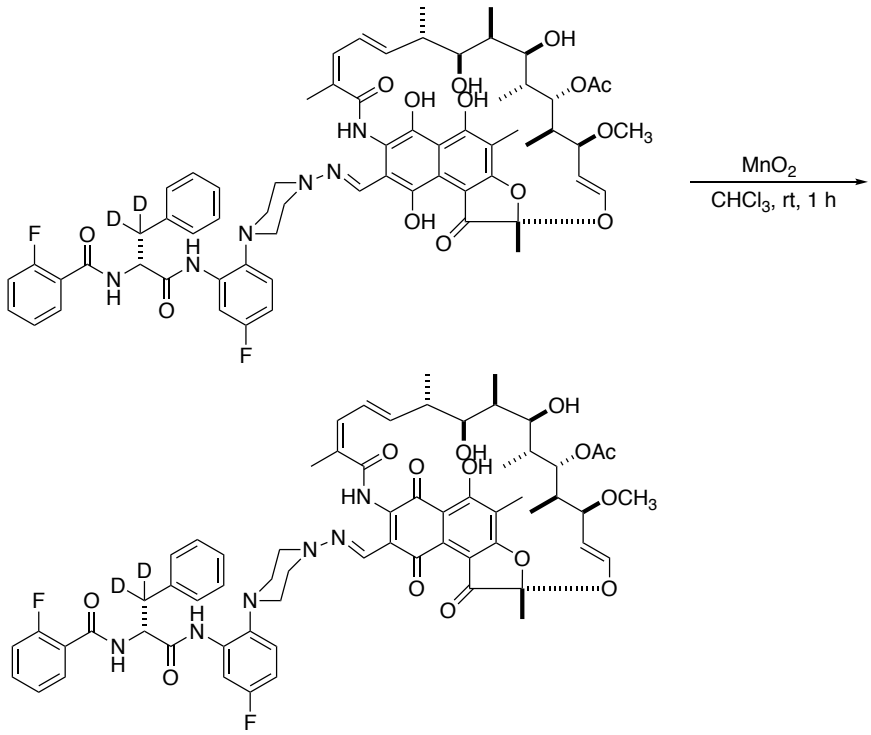

To a solution of IX-404a (100 mg; 0.084 mmol; Example 3.6.5) in 2 mL $CHCl_3$ at room temperature, was added 70% manganese(IV) oxide (261 mg; 2.1 mmol), and the reaction mixture was stirred 1 h at 25°C. The reaction mixture was filtered and evaporated to dryness, and the crude product was purified by silica chromatography (petroleum ether/ethyl acetate gradient).

Yield: 30.8 mg; 31%. ^{1}H NMR (400 MHz, $CDCl_3$): δ 13.10-12.50 (m, 1H), 10.64-10.20 (m, 1H), 9.09 (s, 1H), 8.31 (dd, 1H), 8.06 (dt, 1H), 7.61 (s, 1H), 7.43-7.35 (m, 1H), 7.35-7.27 (m, 6H), 7.26-7.20 (m, 2H), 7.10-6.89 (m, 4H), 6.75 (dt, 1H), 6.46 (brd, 1H), 6.11 (dd, 1H), 5.97 (brdd, 1H), 5.18-4.94 (m, 3H), 4.00-3.83 (m, 2H), 3.68-3.32 (m, 2H), 2.71 (brd, 6H), 2.50-2.02 (m, 12H), 1.85-1.75 (m, 5H), 1.52-1.37 (m, 2H), 1.11-0.78 (m, 11H), 0.51 (d, 3H), 0.16 (brd, 3H).

3.6.9 Synthesis of rifamycin SV-(CH_2)-IX-370a conjugate (IX-488a)

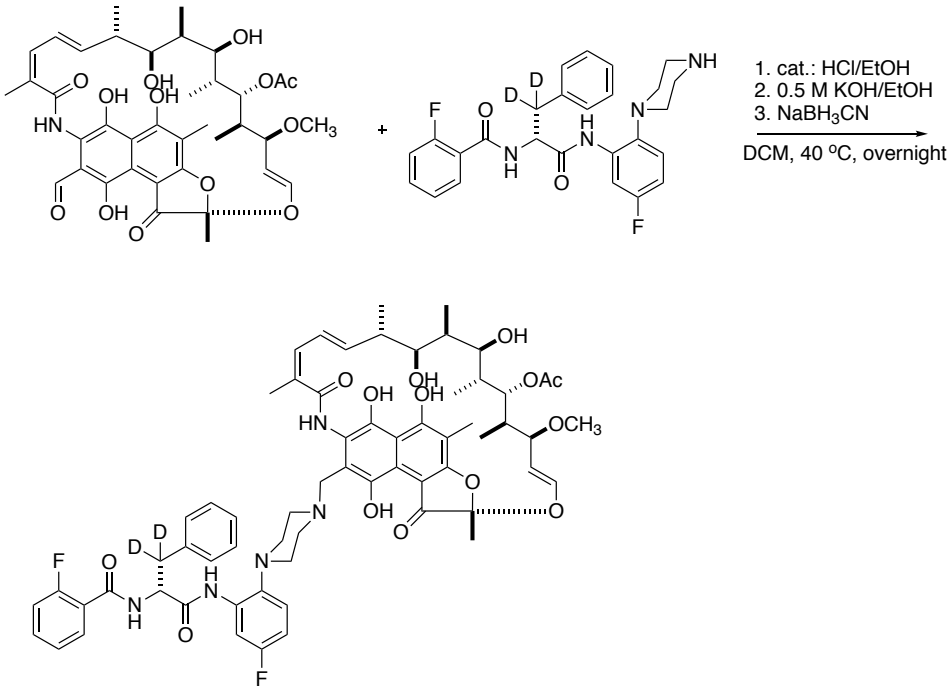

To a solution of 3-formylrifamycin SV (100mg; 0.138 mmol; AvaChem Scientific) in 20 mL dichloromethane at room temperature was added 2 µL 1:1 v/v 12N hydrogen chloride/ethanol. The IX-370a (78 mg; 0.167 mmol; Example 3.6.2) was neutralized with an equivalent amount of 0.5M KOH in ethanol solution, then added to the reaction solution. The reaction mixture was stirred 1.5 h at 40°C and then allowed to come to room temperature. Following addition of sodium cyanoborohydride (13mg; 0.207 mmol; Sigma-Aldrich), the reaction mixture was stirred overnight at 40°C. The mixture was evaporated to dryness, re-dissolved in 10 mL dichloromethane, and extracted with water (1 x 10 mL) and brine (1 x 10 mL). The pooled extracts were dried over anhydrous sodium sulfate, filtered, and evaporated, and the product was purified by silica chromatography (methanol/dichloromethane gradient and ethyl acetate/ hexanes gradient).

Yield: 29 mg; 18%. MS (LC-MS): calculated: *m/z* 1177.32 ($M+H^+$); found: 1177.6 ($M+H^+$).

3.6.10 Synthesis of rifamycin SV-(CHNNHCH$_2$CO)-IX-370a conjugate (IX-491a)

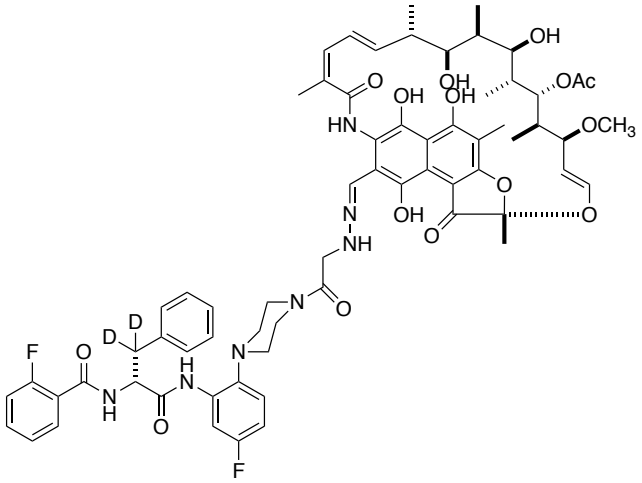

3.6.10.1 Synthesis of (*R*)-*N*-(1- ((2-(4-(2-bromoacetyl)piperazin-1-yl)-5-fluorophenyl)amino)-1-oxo-3-phenylpropan-2-yl-3,3-d_2)-2-fluorobenzamide

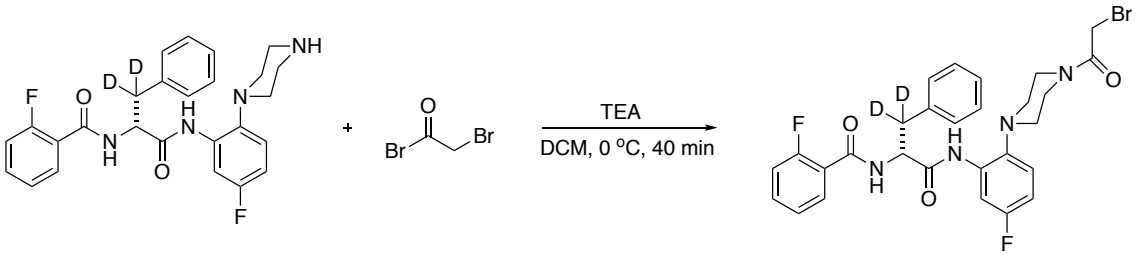

To a solution of IX-370a (200 mg; 0.43 mmol; Example 3.6.2) in 4 mL dichloromethane at 0°C under argon was added trimethylamine (0.15 mL; 1.08 mmol; Sigma-Aldrich), and the reaction mixture was stirred 15 minutes at 0°C. Following addition of a solution of bromoacetyl bromide (46 µl; 0.52 mmol; Acros Organics) in 1.2 mL dichloromethane, the reaction mixture was stirred 40 minutes at 0°C under argon. The reaction mixture was diluted with water (10 mL) and extracted with dichloromethane (3 x 10 mL); the pooled extracts were dried over anhydrous sodium

sulfate, filtered, and evaporated; and the product was purified by silica chromatography (ethyl acetate/hexanes gradient).

Yield: 152 mg; 60%. ^{1}H NMR (500 MHz, $CDCl_3$): δ 9.03 (s, 1H), 8.27 (dd, 1H), 8.08 (t, 1H), 7.54-7.50 (m, 1H), 7.37-7.26 (m, 5H), 7.14 (dd, 1H), 7.01 (dd, 1H), 6.74 (td, 1H), 5.00 (d, 1H), 3.83 (s, 2H), 3.40 (brs, 4H), 2.63-2.54 (m, 4H). MS (MALDI): calculated: m/z 588.46 ($M+H^+$); found: 587.10 ($M+H^+$).

3.6.10.2 Synthesis of Rifamycin SV-$CHNNH_2$

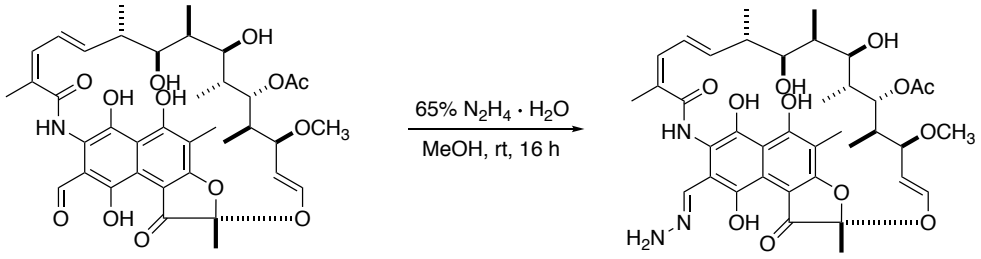

To 3-formylrifamycin SV (50 mg; 0.069 mmol; AvaChem Scientific), was added 1 mL methanol and 0.3 mL 65% hydrazine monohydrate (4.6 μL; 0.062 mmol; Sigma-Aldrich) in methanol, and the reaction mixture was stirred 16 h at room temperature. The reaction mixture was evaporated to dryness, and the crude product was used in the next step without further purification.

Crude yield: 42 mg; 82%.

3.6.10.3 Synthesis of rifamycin SV-($CHNNHCH_2CO$)-IX-370a conjugate (IX-491a)

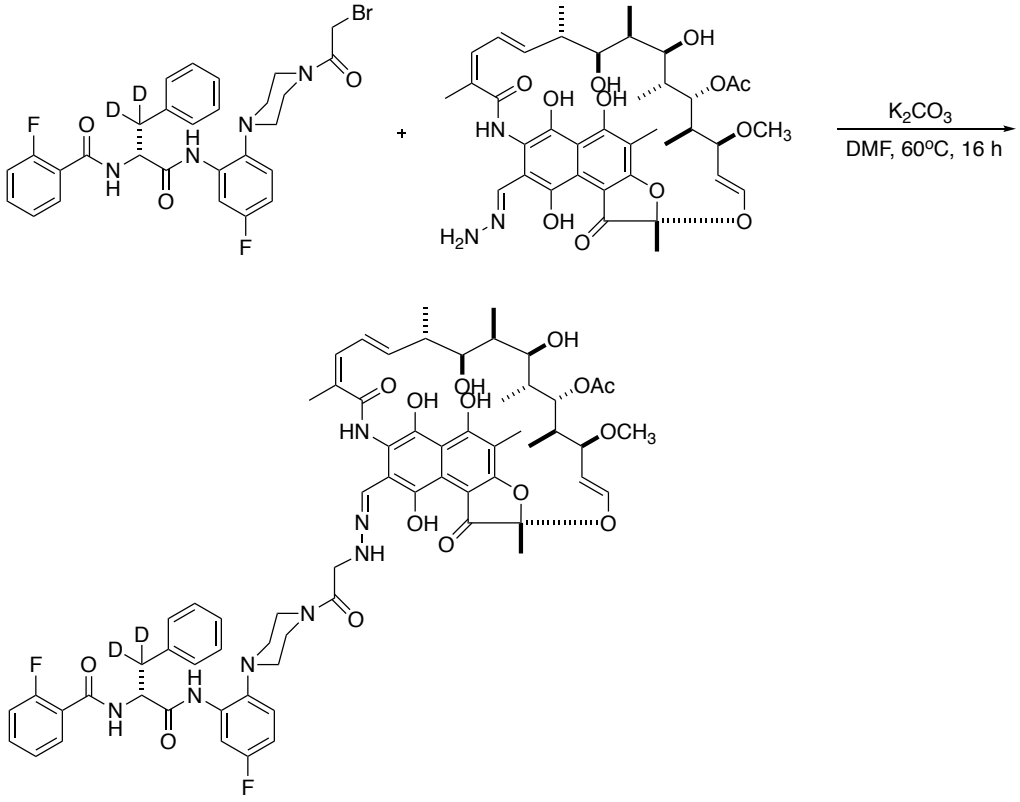

To a solution of rifamycin SV-CHNNH$_2$ (42 mg; 0.057 mmol; Example 3.6.10.2) in 1 mL DMF at room temperature was added potassium carbonate (9.4 mg; 0.068 mmol) and (*R*)-*N*-(1-((2-(4-(2-bromoacetyl)piperazin-1-yl)-5-fluorophenyl)amino)-1-oxo-3-phenylpropan-2-yl-3,3-d_2)-2-fluorobenzamide (33 mg; 0.056 mmol; Example 9.1), and the reaction mixture was stirred 16 h at 60°C under argon. The reaction mixture was evaporated to dryness, and the product was purified by silica chromatography (ethyl acetate/hexanes gradient).

Yield: 9.5 mg; 13%. MS (MALDI): calculated: *m*/*z* 1247.37 ($M+H^+$); found: 1268.49 ($M+Na^+$).

3.7 Class II dual-targeted inhibitors of bacterial RNA polymerase: characterization

Class II dual-targeted inhibitors' most important objective is to overcome anti-

TB drug resistance. Although both binding targets are not next to each other on *Mtb* RNAP for the Class II dual-targeted inhibitor, each binding target ideally should be bound with one molecular inhibitor.

3.7.1 Assay of RNAP-inhibitory activity: Half-maximal inhibitory concentration (IC50)

3.7.1.1 Half-maximal inhibitory concentration (IC50) of RifaAAPs Class II dual-targeted inhibitors

Several rifamycin derivatives conjugated to AAPs have been synthesized. In order to obtain data to prove whether the design and function of RifaAAPs meet our expectation (i.e. the ability to overcome the rifamycin resistance), we assayed the *Mtb* RNAP-inhibitory activity for RifaAAPs via ribogreen fluorescence-detected transcription assay and BBT-ATP fluorescent-detected transcription assay (Mandal, 2014; Feng et al., 2015; Ebright et al., 2019). The results illustrate that most of the RifaAAPs are able to potently inhibit wild-type *Mtb* RNAP as rifampin and rifamycin B. In particular, IX-404a has better inhibitory activity than rifampin. Also, the RifaAAPs are >10 to >100-fold more potent than individual AAP (IX-370a) against wild-type *Mtb* RNAP, meaning that the moiety of rifamycin derivative on RifaAAPs could effectively increase the activities (Table 4).

As previously mentioned, the most important goal for RifaAAPs is to overcome drug resistance. In addition to testing for RifaAAPs against wild-type *Mtb* RNAP, we also tested the RifaAAPs against Rif-resistant (Rif^R) *Mtb* RNAP and AAP-resistant (AAP^R) *Mtb* RNAP. We found all of the RifaAAPs could improve inhibition of Rif^R *Mtb* RNAP by approximately >5 to >100 times compared to rifampin and

rifamycin B. Although the activity of RifaAAPs is not as effective against Rif^R *Mtb* RNAP as IX-370a alone (as IX-370a has no resistance against Rif^R *Mtb* RNAP), they are still able to repress the resistance arising from Rif target mutations. For the AAP^R *Mtb* RNAP, the data further show that all of the RifaAAPs have no resistance against AAP^R *Mtb* RNAP. The inhibitory activities of RifaAAPs are as potent as rifampin and rifamycin B against AAP^R RNAP (Table 4).

Table 4. Rifampin, rifamycin B, AAP, and RifaAAPs: *M. tuberculosis* RNAP inhibitory activity

Compound name	*M. tuberculosis* RNAP IC50[a] (μM)	rpoB-S'531'L *M. tuberculosis* RNAP rifampin-resistant mutant IC50[a] (μM)	rpoB-R'637'C *M. tuberculosis* RNAP AAP-resistant mutant IC50[a] (μM)
Rif			
Rif	0.02	>100	0.02
RifB	0.02	>100	0.01
AAP			
IX-370a	1.1	0.3	4
RifaAAP			
IX-398	0.04	20	0.02
IX-404a	0.01	2	0.01
IX-408a	0.04	2	0.03
IX-476a	0.03	1.2	0.03
IX-488a	0.1	2.4	ND
IX-491a	0.03	1.1	0.01

[a] These relative values were determined by using either a ribogreen fluorescence–detected transcription assay or a BBT-ATP fluorescence-detected transcription assay.

3.7.2 Assay of antibacterial activity: Minimum inhibitory concentration (MIC)

3.7.2.1 Minimum inhibitory concentration (MIC) of RifaAAPs Class II dual-targeted inhibitors

The inhibition of *Mycobacterium tuberculosis* (*Mtb*) growth in culture for RifaAAPs has also been investigated via microplate Alamar Blue assay (Collins and Franzblau, 1997). All of the RifaAAPs have been tested against wild-type *Mtb* H37Rv growth and three different rifampin-resistant (Rif^R) *Mtb* growth in culture. The results show that most of the RifaAAPs have an outstanding minimum inhibitory concentration (MIC) against wild-type *Mtb* than their precursors, rifampin and rifamycin B. In particular, two of the RifaAAPs, IX-404a and IX-491a, are worth noting because they have lower MIC against wild-type *Mtb* than rifampin. Furthermore, all of the RifaAAPs have >3 to >16-fold more potency than individual IX-370a against the growth of wild-type *Mtb* in culture.

The most noteworthy and meaningful result of antibacterial activity for RifaAAPs is the inhibition of resistant *Mtb.* All of the RifaAAPs have been assayed against Rif^R *Mtb* 20626 (rpoB- H'526'D), *Mtb* 4457 (rpoB- H'526'Y), and *Mtb* 14571 (rpoB-S'531'L) growth in culture. As the table shows (Table 5), the rifampin and rifamycin B are not able to suppress the growth of Rif^R *Mtb*. However, all of the MIC results indicate that RifaAAPs could either partly or definitely overcome the growth of all three different Rif^R *Mtb* isolates approximately >2 to >256-fold more potently than rifampin and rifamycin B. Among all of the RifaAAPs we have discovered, IX-488a and IX-491a are the two most promising inhibitors against the development of Rif^R *Mtb* in culture within the category of Class II dual-targeted inhibitors. The results of MIC for IX-491a against three Rif^R *Mtb* suggest that IX-491a has excellent ability to suppress the resistance arising from Rif target. Especially for the strains of Rif^R *Mtb* 20626 (rpoB-H'526'D) and *Mtb* 4457 (rpoB-H'526'Y), IX-491a possesses much better antibacterial activity than not only rifampin but also IX-370a. Although the antibacterial activity of wild-type *Mtb* for IX-488a has 4-fold less potency than IX-

491a and rifampin, the MIC results of Rif^R *Mtb* indicate that IX-488a also overcomes resistance arising from Rif site. For the antibacterial activities of Rif^R *Mtb* 20626 (rpoB- H'526'D) and *Mtb* 4457 (rpoB-H'526'Y), IX-488a has >32 fold and >128 fold greater active than rifampin.

Table 5. Rifampin (Rif), rifamycin B (RifB), AAP, RifaAAPs: antibacterial activity

Compound Name	*Mtb* H37Rv MIC[a] (µg/ml)	rpoB-H'526'D *Mtb* 20626 rifampin-resistant MIC[a] (µg/ml)	rpoB-H'526'Y *Mtb* 4457 rifampin- resistant MIC[a] (µg/ml)	rpoB-S'531'L *Mtb* 14571 rifampin- resistant MIC[a] (ug/ml)
Rif				
Rif	0.063	>50	>50	>50
RifB	0.195	>50	50	>50
AAP				
IX-370a	0.78	0.78	1.56	0.78
RifaAAPs				
IX-398	0.25	12.5	3.13	6.25
IX-404a	0.048	25	3.13	19
IX-408a	0.097	12.5	3.13	19
IX-476a	0.156	>5	2.5	>5
IX-488a	0.195	1.56	0.39	3.13
IX-491a	0.048	0.39	0.195	3.13

[a]These relative values were determined by using Microplate Alamar Blue assay.

3.8 Structural basis of transcription inhibition by Class II dual-targeted inhibitors

3.8.1 Rif and AAP target: crystal structure of the RNAP-RifaAAP complex

To further comprehend the binding and interaction between Class II dual-targeted inhibitors and *Mycobacterium tuberculosis* (*Mtb*) RNAP, a former postdoc and a graduate student in the Ebright lab, Dr. Wei Lin and Mr. Yu Liu, tried to soak

IX-404a into crystals of *Mtb* RNAP-promoter initial transcribing complex (RPitc) and *Mtb* RNAP-promoter open complex (RP_o). After several attempts, they successfully obtained and built up a crystal structure, IX-404a in complex with *Mtb* RNAP, promoter DNA, and 2-nt RNA product at a resolution of 4.3 Å (Ebright et al., unpublished). The crystal structure unequivocally indicates that both Rif and AAP binding sites are simultaneously bound with an inhibitor on each site. Hence, for Class II dual-targeted inhibitors, there are typically two molecules of inhibitor (IX-404a) bound to one molecule of *Mtb* RNAP with a 2:1 stoichiometry (Figure 18) (Lin et al., unpublished).

The zoom-in structure on the Rif site of *Mtb* RNAP demonstrates that the first molecule of IX-404a can bind to Rif binding site through its Rif moiety. The electron density map also clearly shows that the IX-370a moiety on first molecule of IX-404a is connected to Rif moiety and bound closely to the Rif target, which means that the entire molecule (IX-404a) could perfectly occupy the Rif target on *Mtb* RNAP (Figure 18b). In addition, the second molecule of IX-404a has also been found on the AAP target of *Mtb* RNAP. The IX-370a moiety of IX-404a binds to the bridge-helix N-terminus target on RNAP through its AAP moiety. Also, both IX-370a and rifamycin moieties on whole IX-404a can be seen on AAP target according to the electron density map (Figure 18c).

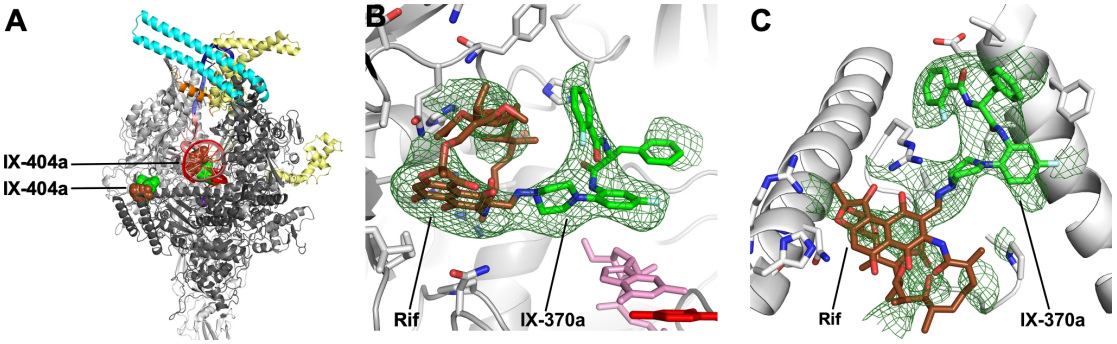

Figure 18. Targets of transcription inhibition by Class II dual-targeted inhibitors "RifaAAP, IX-404a"

(A) Structure of *Mtb* RNAP-RPitc2 in complex with two molecules of IX-404a (Rif moiety, brown surface; AAP moiety, green surface; resolution = 4.3 Å; Rfree = 0.27).

(B) View of the Rif target on *Mtb* RNAP-RPitc2 showing the electron densities for both Rif and AAP (IX-370a) moieties of Class II dual-targeted inhibitor "IX-404a". It reveals that one molecule of IX-404a binds to Rif target of *Mtb* RNAP through Rif moiety.

(C) View of the AAP target on *Mtb* RNAP-RPitc2 showing the electron densities for both AAP (IX-370a) and Rif moieties of Class II dual-targeted inhibitor "IX-404a". It reveals that another molecule of IX-404a binds to AAP target of *Mtb* RNAP through AAP moiety.

3.9 Discussion

The *M. tuberculosis* (*Mtb*) RNAP-inhibitory activities demonstrate that the Class II dual-targeted inhibitor of rifamycin derivative connected to AAP could effectively improve the IC50 of AAP or rifamycin derivative against wild-type and resistant *Mtb* RNAP. One possible improvement is to enable both AAP and rifamycin moieties to benefit from each other on the RifaAAP molecule. According to our understanding, rifampin potently inhibits the transcription of *Mtb* RNAP. The RifaAAP inhibitor is one kind of rifampin analog inhibitor. Hence, AAP can utilize the Rif to improve itself so that the RifaAAP could exhibit more potent activity than AAP. Still, the most serious problem for rifampin is drug-resistance. In the case of resistance arising from Rif site on *Mtb* RNAP, the AAP moiety on RifaAAP could bring benefit to Rif moiety and restrain the Rif-resistance.

IX-404a is one of the promising RifaAAP inhibitors. According to the

chemical structure of IX-404a, it is a combination inhibitor consisting of rifampin and IX-370a. The *Mtb* RNAP-inhibitory activities show that IX-404a has one-fold and 110-fold higher potency against wild-type *Mtb* RNAP than rifampin and IX-370a, respectively. Additionally, IX-404a is also able to overcome both Rif-resistant and AAP-resistant mutant RNAP. IX-404a potently inhibits Rif^R β S531L *Mtb* RNAP >50 fold more than Rif, and inhibits AAP^R β R637C *Mtb* RNAP >400 fold more than IX-370a (Table 4). This suggests that both rifampin and IX-370a can connect and work together to decrease or eliminate the resistances.

IX-491a is another promising RifaAAP inhibitor. Although the RNAP inhibitory-activities of IX-491a is similar to IX-404a, which has the best RNAP inhibitory-activities against wild-type and Rif^R *Mtb* RNAP, the antibacterial activities of IX-491a are more potent than IX-404a against the growth of Rif^R *Mtb* in culture. IX-491a exhibits almost same antibacterial activity against wild-type *Mtb* H37Rv as rifampin, and >16 fold better antibacterial activity against wild-type *Mtb* H37Rv than IX-370a. In addition, compared to rifampin, IX-491a also possesses >16 fold better antibacterial activity against Rif^R β S531L, >256 fold better antibacterial activity against Rif^R β H526Y, and >128 fold better antibacterial activity against Rif^R β H526D (Table 5). This further confirms that IX-491a is able to conquer all rifampin-resistant *Mtb* on antibacterial activities via AAP moiety on RifaAAP.

In terms of chemical structure, IX-404a differs from IX-398 with respect to its chirality on the α-carbon of phenylalanine and the deuteration on the β-carbon of phenylalanine on AAP moiety. IX-404a contains R configuration on the α-carbon of phenylalanine and di-deuterium on the β-carbon of phenylalanine. All of the IC50 and MIC results show that IX-404a not only has higher potency against wild-type (2-fold

higher), Rif^R (10-fold higher), and AAP^R (1-fold higher) *Mtb* RNAP than IX-398 (Table 4), but also exhibits superior antibacterial activity against *Mtb* H37Rv (5-fold higher) (Table 5). The different *Mtb* RNAP-inhibitory activities and antibacterial activities between IX-398 and IX-404a also match previous findings comparing IX-214 and IX-370a (R-form AAP is more active than S-form and racemic AAP).

The crystal structure of IX-404a has illustrated the ability of Class II dual-targeted inhibitors to overcome rifamycin-resistance caused by a mutation altering the Rif binding site on *Mtb* RNAP and the ability to overcome AAP-resistance caused by a mutation altering the bridge-helix N-terminus AAP binding site of RNAP. Although a mutation altering either Rif site or bridge-helix N-terminus AAP site on RNAP will prevent binding of one of two molecules of Class II dual-targeted inhibitor, the inhibition of bacterial transcription by another molecule of Class II dual-targeted inhibitor will continue.

3.10 Conclusion

The synthetic approaches reveal that the Class II dual-targeted inhibitors "RifaAAPs" have been successfully synthesized through directly conjugating rifamycin derivative to AAP, or indirectly connecting rifamycin derivative to AAP with a short linker. By way of the chemical reactions and reagents mentioned previously, the rifamycin derivative could be linked to AAP on the desired position without loss or destruction of any functional groups on RifaAAP. To retain the high potency and functionality for the RifaAAPs, it is essential to ensure that the chemical structures of both moieties on RifaAAP are not altered except at the junction of two moieties. Therefore, the analytical data support the evidence that the rifamycin

derivative and AAP have been connected together to generate the RifaAAPs as we designed.

The results of both inhibitory activity and antibacterial activity indicate that the Class II dual-targeted inhibitors "RifaAAPs" are superior to their parents, rifampin or AAP, against not only the wild-type *Mtb*, but also the resistant *Mtb*. These data suggest that the design of RifaAAP is on the right track. Given that resistant *Mtb* has been a global threat to human health, the strategy we have developed could effectively overcome this issue with respect to rifampin resistance. In particular, one of the moieties on RifaAAP can carry out their capabilities on RNAP no matter which one of the binding site has been mutated.

The crystal structure of IX-404a further verifies that RifaAAP could function through the desired targets on *Mtb* RNAP. Two molecules of IX-404a are able to interact individually with both Rif and AAP binding sites at the same time via their rifamycin moiety and AAP moiety, respectively. Moreover, the crystal structure also explains how the Class II dual-targeted inhibitor overcomes Rif resistance and AAP resistance: the structural evidence completely describes the inhibitory activity and antibacterial activity of Class II dual-targeted inhibitor. Hence, the development of Class II dual-targeted inhibitor is a useful solution to deal with resistant *Mtb*.

Chapter 4:

Discussion

4.1 Summary

This work characterizes the development and synthesis of both Class I and Class II dual-targeted inhibitors of bacterial RNA polymerase (RNAP). Both classes of dual-targeted inhibitor are able to effectively inhibit bacterial transcription through binding to either one or both of two non-identical targets on mutant or wild-type bacterial RNAP, respectively. Thanks to their dual-action capability, dual-targeted inhibitors not only show exceptionally high potencies against bacteria but also overcome resistance arising from one of two targets.

The experimental results of Class I dual-targeted inhibitors indicate that, in order to generate a dual-targeted inhibitor, a synthetic GE peptide analog and either a rifamycin or a sorangicin A can be covalently linked through the D-α,β-diaminopropionic acid residue (D-Dap) of synthetic GE peptide analog and any one of the following components: rifamycin C3 atom (rifamycin S), the carboxyl acid on rifamycin O4 sidechain (rifamycin B), or the carboxyl acid on the sidechain of sorangicin A. These Class I dual-targeted inhibitors have been shown to possess high RNAP-inhibitory potencies through contemporaneously binding to both adjacent GE and Rif/Sor sites, and excellent efficacy against target-based resistance through binding to one of GE and Rif/Sor sites. The structural basis of RNAP-SoraGE interaction further confirms that both Sor and GE moieties on Class I dual-targeted inhibitors are able to bind to RNAP at the same time.

The results of experimental trials of Class II dual-targeted inhibitors against *Mycobacterium tuberculosis* (*Mtb*) indicate that, to generate a dual-targeted inhibitor, a small-molecular anti-tuberculosis inhibitor "AAP" and a rifamycin can be covalently linked with or without a short linker between AAP and rifamycin through the piperazinyl moiety of AAP and either the formyl group on rifamycin C3 atom (rifaldehyde) or the carboxyl group on rifamycin O4 atom (rifamycin B). These Class II dual-targeted inhibitors have been demonstrated to have higher RNAP-inhibitory and antibacterial potencies than their parents, rifamycin and AAP, against both wild-type and mutant *Mtb* through binding to one of or both of non-adjacent AAP and rifamycin targets. The structural basis of RNAP-IX-404a interaction further illustrates that AAP and rifamycin binding targets on RNAP are able to be functioned through both AAP moiety of one molecule of IX-404a and rifamycin moiety of another molecule of IX-404a, respectively.

Class I and II dual-targeted inhibitors are potential approaches for the development of novel antibacterial agents. These dual-targeted inhibitors, functioning through one of or both of non-identical targets, are expected to overcome the current threat of drug-resistance because both classes of dual-targeted inhibitors are able to apply non-identical inhibitory mechanisms and pathways to restrain bacterial growth.

4.2 Class III dual-targeted inhibitors

One of this study's discoveries regarding Class II dual-targeted inhibitors is that the piperazinyl group on AAP could be attached to an enormous pharmacophore, such as a rifamycin derivative, to constitute a dual-action inhibitor without the loss of either RNAP-inhibitory activity or antibacterial activity against wild-type, rifamycin-

resistant and AAP-resistant *Mtb* (Ebright et al., 2019). The activity and functionality of the AAP moiety on the Class II dual-targeted inhibitors are not disrupted through the modification on the piperazinyl group. In other words, the piperazine substituent on AAP is tolerant of change, which also means there is an opportunity to improve the potency, metabolic stability, oral bioavailability, and pharmacological properties of AAP through its piperazinyl group.

As mentioned previously, the lead AAP compound (IX-370a) does not have superior activity against *Mtb in vivo*. To further optimize the AAP against wild-type and resistant *Mtb* and various *Mycobacterium* strains *in vitro* and *in vivo*, one potential approach is to apply AAP's advantages by covalently conjugating it to another pharmacophore (other than bacterial RNAP inhibitor) to form the dual-targeted inhibitor through its piperazine substituent (Ebright et al., 2019). According to Ma and Lynch (2016), researchers have developed a dual-acting antibacterial agent, TNP-2092, for the treatment of persistent bacterial infections. TNP-2092 is a conjugated inhibitor of a rifamycin derivative covalently connected to a quinolone derivative. The rifamycin moiety and quinolone moiety of TNP-2092 respectively play the role of a bacterial RNAP inhibitor and an inhibitor of bacterial DNA gyrase so that the TNP-2092 is able to potently inhibit both Rif-resistant and quinolone-resistant *S. aureus* (Robertson et al., 2008a; Robertson et al., 2008b; Ma and Lynch, 2016). Additionally, there are several classes of antibiotic have been explored as appropriate partners for the development of dual-action inhibitors against drug-resistance bacterial infection (Bremner et al., 2007; Pokrovskaya et al., 2010; Tevyashova et al., 2015; Klahn et al., 2017; Domalaon et al., 2018). Given these research findings and the feasibility of chemical reaction on the piperazinyl group of AAP, the possible pharmacophores of non-bacterial RNAP inhibitors for the

conjugation to AAP could include derivatives of fluoroquinolone, nitroimidazole, or oxazolidinone (Ding et al., 2007; Ma et al., 2007; Ding et al., 2010).

One well-known fluoroquinolone derivative that has been used as medication for treating tuberculosis and some bacterial infections, ciprofloxacin, functions through the inhibition of DNA gyrase and prevention of bacterial DNA synthesis (Bahl et al., 1997; Moadebi et al., 2007). Ciprofloxacin has a piperazinyl group with a free secondary amine on the C7 position of quinolone core. Hence, to conjugate AAP to ciprofloxacin, both single moieties could be attached together with a short linker through piperazine substituents on AAP and ciprofloxacin (Figure 19).

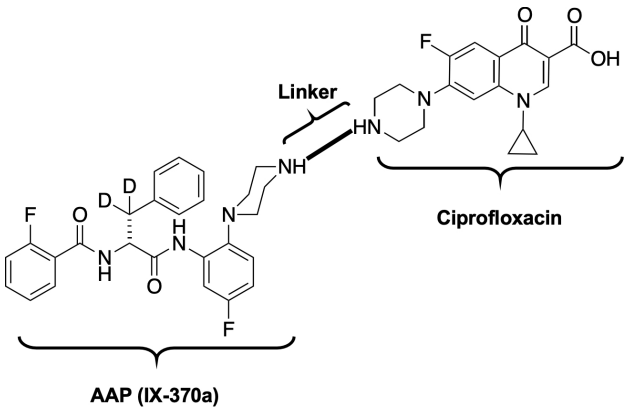

Figure 19. The conjugation of AAP (IX-370a) to fluoroquinolone derivatives
AAP could potentially be connected to ciprofloxacin through a linker on its piperazine moiety.

Some nitroimidazole derivatives have also been applied to combination therapy for tuberculosis (Mukherjee and Boshoff, 2011). These compounds, comprising nitro-containing heterocycles, are able to impede the production of mycolic acid and inhibit the biosynthesis of the bacterial cell wall for both aerobically replicating and anaerobically non-replicating *Mtb*. Pretomanid and delamanid are two approved nitroimidazole drugs for the combination treatment of multidrug-resistant tuberculosis (Matsumoto et al., 2006; Singh et al., 2008). The nitroimidazole moiety

on pretomanid and delamanid is an essential component for the activity against *Mycobacterium tuberculosis*: it is able to undergo the bioreductive activation pathway to cause DNA damage via a nitro radical anion (Mukherjee and Boshoff, 2011). Some of the nitroimidazole derivatives, which are highly related to the precursors of pretomanid and delamanid, are commercially available. These precursors could be the opportunities for AAP to be connected to the nitroimidazole moieties of pretomanid or delamanid to improve the activity (Figure 20). In addition, metronidazole, which has been found to inhibit both actively-replicating and non-replicating *Mtb* in combination treatment with rifampicin and isoniazid, is also one of the nitroimidazole derivatives (Mukherjee and Boshoff, 2011). There is a possibility to enhance the potency of AAP through the conjugation of AAP and metronidazole together.

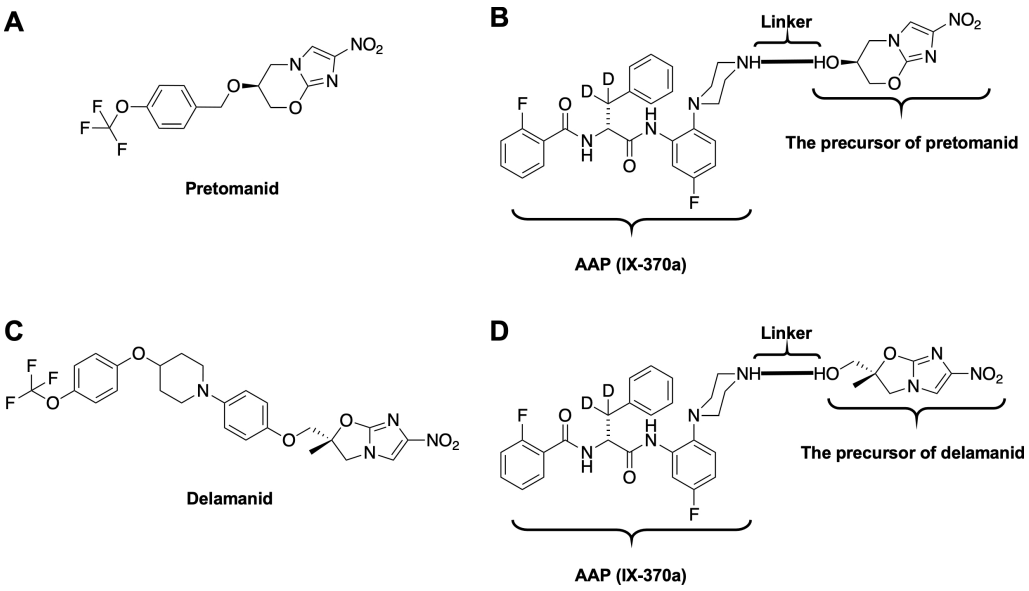

Figure 20. The conjugation of AAP (IX-370a) to nitroimidazole derivatives

(A) Chemical structure of pretomanid.

(B) AAP could potentially be connected to the precursor of pretomanid through a linker on its piperazine moiety.

(C) Chemical structure of delamanid.

(D) AAP could potentially be connected to the precursor of delamanid through a linker on its piperazine moiety.

The oxazolidinone-class antibacterial agents, which have been widely researched, have also shown potent activities against drug-resistant tuberculosis in both non-clinical and clinical studies of anti-TB drug development (Jadhavar et al., 2015). Linezolid, the first FDA approved oxazolidinone-antibiotic, has been found to be very effective in the combination therapy of multidrug-resistant tuberculosis with other anti-TB drugs (Schecter et al., 2010). The mechanism of action for linezolid is to inhibit the protein biosynthesis at the early phase of translation through binding to the ribosome. Because linezolid has a broad spectrum of activity and oral bioavailability, it could be a potential candidate to optimize the potency of AAP through the conjugation of the piperazinyl group on AAP and oxazolidinone derivatives (Figure 21).

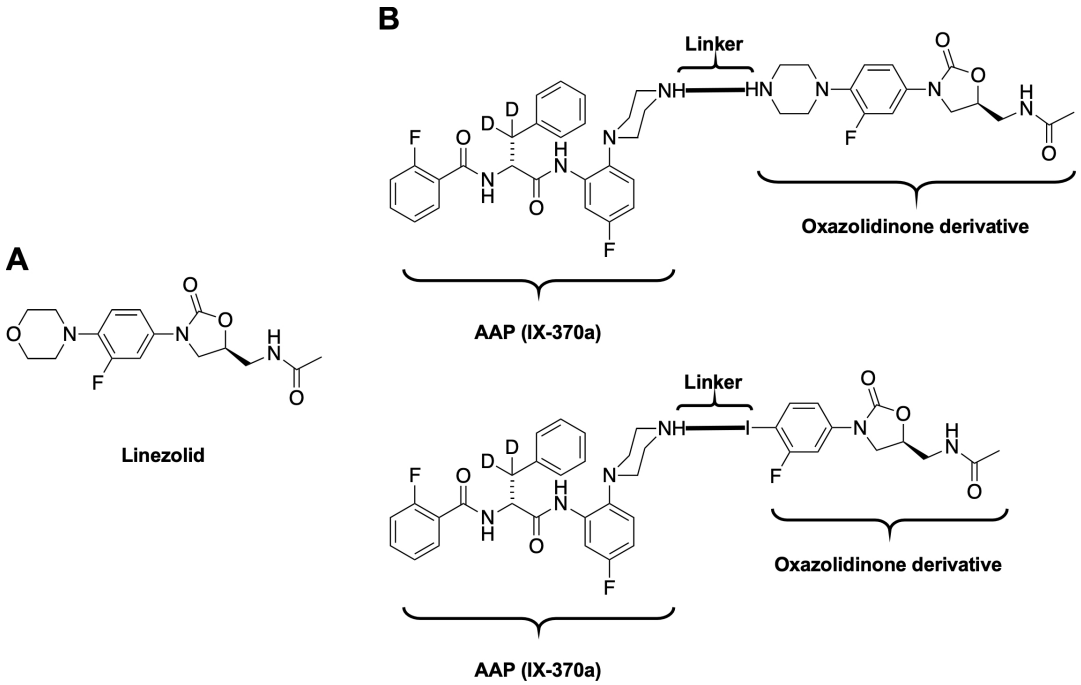

Figure 21. The conjugation of AAP (IX-370a) to oxazolidinone derivatives

(A) Chemical structure of Linezolid.

(B) AAP could potentially be connected to the oxazolidinone derivative through a linker on its piperazine moiety.

In summary, the discoveries of different classes of dual-targeted inhibitors

presented in this work provide not only significant strategies for combatting the currently ever-increasing threat of antibiotic drug resistance, but also crucial improvements to the disadvantages of single antibacterial agent (Bremner et al., 2007; Pokrovskaya et al., 2010; Tevyashova et al., 2015; Klahn et al., 2017; Domalaon et al., 2018). Several dual-targeted inhibitors in this work, provide exceptionally high potency and very low susceptibility to target-based resistances. Instead of looking for novel antibacterial agents with new binding targets on bacterial RNAP, the conjugation of two known bacterial RNAP inhibitors can also satisfy the urgent need to solve the resistance issue. Recently, three RifaAAPs (IX-404a, IX-488a, IX-491a) have been proven the excellent activities against *M. tuberculosis*. In the near future, hopefully, one of these can progress into clinical studies and succeed in the clinical setting.

References

Abbondanzieri, E.A., Greenleaf, W.J., Shaevitz, J.W., Landick, R., and Block, S.M. (2005). Direct observation of base-pair stepping by RNA polymerase. *Nature* **438**, 460-465.

Aristoff, P.A., Garcia, G.A., Kirchhoff, P.D., and Hollis Showalter, H.D. (2010). Rifamycins – obstacles and opportunities. *Tuberculosis* (Edinb) **90**, 94-118.

Artsimovitch, I., Chu, C., Lynch, A.S., and Landick, R. (2003). A new class of bacterial RNA polymerase inhibitor affects nucleotide addition. *Science* **302**, 650-654.

Artsimovitch, I., Vassylyeva, M.N., Svetlov, D., Svetlov, V., Perederina, A., Igarashi, N., Matsugaki, N., Wakatsuki, S., Tahirov, T.H., Vassylyev, D.G. (2005). Allosteric modulation of the RNA polymerase catalytic reaction is an essential component of transcription control by rifamycins. *Cell* **122**, 351-363.

Bae, B., Nayak, D., Ray, A., Mustaev, A., Landick, R., and Darst, S.A. (2015). CBR antimicrobials inhibit RNA polymerase via at least two bridge-helix cap-mediated effects on nucleotide addition. *Proc. Natl. Acad. Sci. USA* **112**, E4178-E4187.

Bahl, D., Miller, D.A., Leviton, I., Gialanella, P., Wolin, M.J., Liu, W., Perkins, R., and Miller, M.H. (1997). *In vitro* activities of ciprofloxacin and rifampin alone and in combination against growing and nongrowing strains of methicillin-susceptible and methicillin-resistant *Staphylococcus aureus*. *Antimicrob. Agents Chemother.* **41**, 1293-1297.

Barbachyn, M.R. (2008). Recent advances in the discovery of hybrid antibacterial agents. *Annu. Rep. Med. Chem.* **43**, 281-290.

Barry, C.E. 3rd, Boshoff, H.I., Dartois, V., Dick, T., Ehrt, S., Flynn, J., Schnappinger, D., Wilkinson, R.J., and Young, D. (2009). The spectrum of latent tuberculosis: rethinking the biology and intervention strategies. *Nat. Rev. Microbiol.* **7**, 845-855.

Borukhov, S., and Nudler, E. (2003). RNA polymerase holoenzyme: structure, function and biological implications. *Curr. Opin. Microbiol.* **6**, 93-100.

Bozdogan, B., and Appelbaum, P.C. (2004). Oxazolidinones: activity, mode of action, and mechanism of resistance. *Int. J. Antimicrob. Agents* **23**, 113-119.

Bremner, J.B., Ambrus, J.I., and Samosorn, S. (2007). Dual action-based approaches to antibacterial agents. *Curr. Med. Chem.* **14**, 1459-1477.

Brennan, C.A., Dombroski, A.J., and Platt T. (1987). Transcription termination factor rho is an RNA-DNA helicase. *Cell* **48**, 945-952.

Brötz-Oesterhelt, H., and Brunner, N.A. (2008). How many modes of action should an antibiotic have? *Curr. Opin. Pharmacol.* **8**, 564-573.

Brown, E.D., and Wright, G.D. (2016). Antibacterial drug discovery in the resistance era. *Nature* **529**, 336-343.

Campbell, E.A., Korzheva, N., Mustaev, A., Murakami, K., Nair, S., Goldfarb, A., and Darst, S.A. (2001). Structural mechanism for rifampicin inhibition of bacterial RNA polymerase. *Cell* **104**, 901-912.

Campbell, E.A., Muzzin, O., Chlenov, M., Sun, J.L., Olson, C.A., Weinman, O., Trester-Zedlitz, M., Darst, S.A. (2002). Structure of the bacterial RNA polymerase promoter specificity σ subunit. *Mol. Cell* **9**, 527-539.

Campbell, E.A., Pavlova, O., Zenkin, N., Leon, F., Irschik, H., Jansen, R., Severinov, K., and Darst, S.A. (2005). Structural, functional, and genetic analysis of sorangicin inhibition of bacterial RNA polymerase. *EMBO J.* **24**, 674-682.

Campbell, E.A., Westblade, L.F., Darst, S.A. (2008). Regulation of bacterial RNA polymerase σ factor activity: a structural perspective. *Curr. Opin. Microbiol*. **11**, 121-127.

Centers for Disease Control and Prevention (2019). The biggest antibiotic-resistant threats in the U.S.

Chakraborty, A., Wang, D., Ebright, Y.W., Korlann, Y., Kortkhonjia, E., Kim, T., Chowdhury, S., Wigneshweraraj, S., Irschik, H., Jansen, R., Nixon, B.T., Knight, J., Weiss, S., and Ebright, R.H. (2012). Opening and closing of the bacterial RNA polymerase clamp. *Science* **337**, 591-595.

Chellat, M.F., Riedl, R. (2017). Pseudouridimycin: the first nucleoside analogue that selectively inhibits bacterial RNA polymerase. *Angew. Chem. Int. Ed.* **56**, 13184-13186.

Chopra, I. (2007). Bacterial RNA polymerase: a promising target for the discovery of new antimicrobial agents. *Curr. Opin. Investig. Drug*s **8**, 600-607.

Ciciliato, I., Corti, E., Sarubbi, E., Stefanelli, S., Montanini, N., Marinelli, F., Kurz, M., and Selva, E. (2003). Antibiotics GE23077, pharmaceutically acceptable salts and compositions, and use thereof. US patent 6,586,393.

Ciciliato, I., Corti, E., Sarubbi, E., Stefanelli, S., Gastaldo, L., Montanini, N., Kurz, M., Losi, D., Marinelli, F., and Selva, E. (2004). Antibiotics GE23077, novel inhibitors of bacterial RNA polymerase. I. Taxonomy, isolation, and characterization. *J. Antibiot.* (Tokyo) **57**, 210-217.

Collins, L.A., and Franzblau, S.G. (1997). Microplate alamar blue assay versus BACTEC 460 system for high-throughput screening of compounds against *Mycobacterium tuberculosis* and *Mycobacterium avium*. *Antimicrob. Agents Chemother.* **41**, 1004-1009.

Cramer, P., Bushnell, D.A., and Kornberg, R.D. (2001). Structural basis of transcription: RNA polymerase II at 2.8 Ångstrom resolution. *Science* **292**, 1863-1876.

Cramer, P. (2002). Multisubunit RNA polymerases. *Curr. Opin. Structl. Biol.* **12**, 89-97.

Darst, S.A. (2001). Bacterial RNA polymerase. *Curr. Opin. Structl. Biol.* **11**, 155-162.

Darst, S.A. (2004). New inhibitors targeting bacterial RNA polymerase. *Trends Biochem. Sci.* **29**, 159-160.

Degen, D. (2014). Targets of transcription inhibition by the antibiotics lipiarmycin, GE23077, and salinamide. Ph.D. thesis, Rutgers University.

Degen, D., Feng, Y., Zhang, Y., Ebright, K.Y., Ebright, Y.W., Gigliotti, M., Vahedian-Movahed, H., Mandal, S., Talaue, M., Connell, N., Arnold, E., Fenical, W., and Ebright, R.H. (2014). Transcription inhibition by the depsipeptide antibiotic salinamide A. *eLife* **3**, e02451.

deHaseth, P.L., Zupancic, M.L., and Record, M.T. Jr. (1998). RNA polymerase-promoter interactions: the comings and goings of RNA polymerase. *J. Bacteriol.* **180**, 3019-3025.

Ding, C.Z., Ma, Z., Li, J., Harran, S., HE, Y., Minor, K.P., Kim, I.H., Longgood, J.C., Jin, Y., and Combrink, K.D. (2007). (*R*/*S*) Rifamycin derivatives, their preparations and pharmaceutical compositions. US Patent 7,226,931.

Ding, C.Z., Kim, I.H., Wang, J., Ma, Z., Jin, Y., Combrink, K.D., Lu, G., and Lynch, A.S. (2010). Nitroheteroaryl-containing rifamycin derivatives. US Patent 7,678,791.

Domalaon, R., Idowu, T., Zhanel, G.G., and Schweizer, F. (2018). Antibiotic hybrids: the next generation of agents and adjuvants against gram-negative pathogens? *Clin. Microbiol. Rev.* **31**, e00077-17.

Ebright, R.H. (2000). RNA polymerase: structural similarities between bacterial RNA polymerase and eukaryotic RNA polymerase II. *J. Mol. Biol.* **304**, 687-698.

Ebright, R.H. and Wang, D. (2013). Bipartite inhibitors of bacterial RNA polymerase. *US Patent* 8,372,839.

Ebright, R.H., Degen, D., Zhang, Y., Ebright, Y.W. (2016). Bipartite inhibitors of bacterial RNA polymerase. US Patent 9,415,112.

Ebright, R.H., Ebright Y.W., Mandal, S., Wilde, R., and Li, S. (2018). Antibacterial agents: N(alpha)-aroyl-N-aryl-phenylalaninamides. US Patent 9,919,998.

Ebright, R.H., Ebright, Y.W., and Lin, C.-T. (2019). Antibacterial agents: dual-targeted RNA polymerase inhibitors. PCT/US2019/033788.

Erie, D.A., Yager, T.D., and von Hippel, P.H. (1992). The single-nucleotide addition cycle in transcription: a biophysical and biochemical perspective. *Annu. Rev. Biophys. Biomol. Struct.* **21**, 379-415.

Feklistov, A., Mekler, V., Jiang, Q., Westblade, L.F., Irschik, H., Jansen, R., Mustaev, A., Darst, S.A., and Ebright, R.H. (2008). Rifamycins do not function by allosteric

modulation of binding of Mg^{2+} to the RNA polymerase active center. *Proc. Natl. Acad. Sci. USA* **105**, 14820-14825.

Feng, Y., Degen, D., Wang, X., Gigliotti, M., Liu, S., Zhang, Y., Das, D., Michalchuk, T., Ebright, Y.W., Talaue, M., Connell, N., Ebright, R.H. (2015). Structural basis of transcription inhibition by CBR hydroxamidines and CBR pyrazoles. *Structure* **23**,1470-1481.

Floss, H.G., and Yu, T.-W. (2005). Rifamycin-mode of action, resistance, and biosynthesis. *Chem. Rev.* **105**, 621-632.

Forrest, G.N., and Tamura, K. (2010). Rifampin combination therapy for nonmycobacterial infections. *Clin Microbiol. Rev.* **23**, 14-34.

Garibyan, L., Huang, T., Kim, M., Wolff, E., Nguyen, A., Nguyen, T., Diep, A., Hu, K., Iverson, A., Yang, H., and Miller, J.H. (2003). Use of the rpoB gene to determine the specificity of base substitution mutations on the *Escherichia coli* chromosome. *DNA Repair* (Amst.) **2**, 593-608.

Gillespie, S.H. (2002). Evolution of drug resistance in *Mycobacterium tuberculosis*: clinical and molecular perspective. *Antimicrob. Agents Chemother*. **46**, 267-274.

Gnatt, A.L., Cramer, P., Fu, J., Bushnell, D.A., and Kornberg, R.D. (2001). Structural basis of transcription: an RNA polymerase II elongation complex at 3.3 Å resolution. *Science* **292**, 1876-1882.

Goldstein, B.P. (2014). Resistance to rifampicin: a review. *J Antibiot.* **67**, 625-630.

Gross, C.A., Chan, C., Dombroski, A., Gruber, T., Sharp, M., Tupy, J., and Young, B. (1998) The functional and regulatory roles of sigma factors in transcription. *Cold Spring Harbor Symp. Quant. Biol.* **63**, 141-155.

Guengerich, F.P. (2017). Kinetic deuterium isotope effects in cytochrome P450 enzyme Reactions. *Methods Enzymol.* **596**, 217-237.

Ho, M.X., Hudson, B.P., Das, K., Arnold, E., and Ebright, R.H. (2009). Structures of RNA polymerase-antibiotic complexes. *Curr. Opin. Struct. Biol.* **19**, 715-723.

Hudson, B.P., Quispe, J., Lara-González, S., Kim, Y., Berman, H.M., Arnold, E., Ebright, R.H., and Lawson, C.L. (2009). Three-dimensional EM structure of an intact activator-dependent transcription initiation complex. *Proc. Natl. Acad. Sci. USA* **106**, 19830-19835.

Irschik, H., Jansen, R., Gerth, K., Hofle, G., and Reichenbach, H. (1987). The sorangicins, novel and powerful inhibitors of eubacterial RNA polymerase isolated from myxobacteria. *J. Antibiot.* (Tokyo) **40**, 7-13.

Jadhavar, P.S., Vaja, M.D., Dhameliya, T.M., and Chakraborti, A.K. (2015). Oxazolidinones as anti-tubercular agents: discovery, development and future perspectives. *Curr. Med. Chem.* **22**, 4379-4397.

Jansen, R., Wray, V., Irschik, H., Reichenbach, H., and Hofle, G. (1985). Isolation

and spectroscopic structure elucidation of sorangicin A, a new type of macrolide-polyether antibiotic from gliding bacteria. *Tetrahedon Lett.* **26**, 6031-6034.

Jansen, R., Schummer, D., Irschik, H., Hofle, G. (1990). Chemical modification of sorangicin A and structure-activity relationship I: carboxyl and hydroxyl group derivatives. *Liebigs Ann. Chem.* **1990**, 975-988.

Jin, D.J., and Gross, C.A. (1988). Mapping and sequencing of mutations in the *Escherichia coli* rpoB gene that lead to rifampicin resistance. *J. Mol. Biol.* **202**, 45-58.

Kapanidis, A.N., Margeat, E., Ho, S.O., Kortkhonjia, E., Weiss, S., and Ebright, R.H. (2006). Initial transcription by RNA polymerase proceeds through a DNA-scrunching mechanism. *Science* **314**, 1144-1147.

Klahn, P., and Bronstrup, M. (2017). Bifunctional antimicrobial conjugates and hybrid antimicrobials. *Nat. Prod. Rep.* **34**, 832-885.

Korzheva, N., Mustaev, A., Kozlov, M., Malhotra, A., Nikiforov, V., Goldfarb, A., and Darst, S.A. (2000). A structural model of transcription elongation. *Science* **289**, 619-625.

Koul, A., Arnoult, E., Lounis, N., Guillemont, J., and Andries, K. (2011). The challenge of new drug discovery for tuberculosis. *Nature* **469**, 483-90.

Kuhlman, P., Duff, H.L., and Galant, A. (2004). A fluorescence-based assay for multisubunit DNA-dependent RNA polymerases. *Analytical Biochemistry* **324**, 183-190.

Lane, W.J., and Darst, S.A. (2010a). Molecular evolution of multisubunit RNA polymerases: sequence analysis. *J. Mol. Biol.* **395**, 671-685.

Lane, W.J., and Darst, S.A. (2010b). Molecular evolution of multisubunit RNA polymerases: structural analysis. *J. Mol. Biol.* **395**, 686-704.

Lester, W. (1972). Rifampin: a semisynthetic derivative of rifamycin-a prototype for the future. *Annu. Rev. Microbiol.* **26**, 85-102.

Li, L., Chen, X., Fan, P., Mihalic, J.T., and Cutler, S. (2001). Antibacterial Agents. US patent 6,780,858.

Li, Q., Mitscher, L.A., and Shen, L.L. (2000). The 2-pyridone antibacterial agents: bacterial topoisomerase inhibitors. *Med. Res. Rev.* **20**,231-293.

Lin, M. (2017). Closing and opening of the RNA polymerase “Trigger Loop” in solution. Ph.D. thesis, Rutgers University.

Lin, W., Mandal, S., Degen, D., Liu, Y., Ebright, Y.W., Li, S., Feng, Y., Zhang, Y., Mandal, S., Jiang, Y., Liu, S., Gigliotti, M., Talaue, M., Connell, N., Das, K., Arnold, E., and Ebright, R.H. (2017). Structural basis of *Mycobacterium tuberculosis* transcription and transcription inhibition. *Mol. Cell* **66**,169-179.

Lin, W., Das, K., Degen, D., Mazumder, A., Duchi, D., Wang, D., Ebright, Y.W., Ebright, R.Y., Sineva, E., Gigliotti, M., Srivastava, A., Mandal, S., Jiang, Y., Liu, Y., Yin, R., Zhang, Z., Eng, E.T., Thomas, D., Donadio, S., Zhang, H., Zhang, C., Kapanidis, A.N., and Ebright, R.H. (2018). Structural basis of transcription inhibition by fidaxomicin (lipiarmycin A3). *Mol. Cell.* **70**, 60-71.

Lisitsyn, N.A., Gur'ev, S.O., Sverdlov, E.D., Moiseeva, E.P., and Nikiforov, V.G. (1984). Nucleotide substitutions in the rpoB gene leading to rifampicin resistance of *E. coli* RNA polymerase. *Bioorg. Khim.* **10**, 127-128.

Liu, B., Zuo, Y., and Steitz, T.A. (2016). Structures of *E. coli* σ^S-transcription initiation complexes provide new insights into polymerase mechanism. *Proc. Natl. Acad. Sci. USA* **113**, 4051-4056.

Liu, C. (2007). The use of single-molecule DNA nanomanipulation to study transcription kinetics. Ph.D. thesis, Rutgers University.

Lonetto, M., Gribskov, M., and Gross, C.A. (1992). The σ^{70} family: sequence conservation and evolutionary relationships. *J. Bacteriol.* **174**, 3843-3849.

Ma, C., Yang, X., and Lewis, P.J. (2016). Bacterial transcription as a target for antibacterial drug development. *Microbiol. Mol. Biol. Rev.* **80**, 139-160.

Ma, Z., Jin, Y., Li, J., Ding, C.Z., Minor, K.P., Longgood, J.C., Kim, I.H., Harran, S., Combrink, K., Morris, T.W. (2007). Rifamycin derivatives effective against drug-resistant microbes. US Patent 7,247,634.

Ma, Z., and Lynch, A.S. (2016). Development of a dual-acting antibacterial agent (TNP-2092) for the treatment of persistent bacterial infections. *J. Med. Chem.* **59**, 6645-6657.

Madariaga, M.G., Lalloo, U.G., and Swindells, S. (2008). Extensively drug-resistant tuberculosis. *Am. J. Med.* **12**, 835-44.

Maeda, D.Y., Mahajan, S.S., Atkins, W.M., and Zebala, J.A. (2006). Bivalent inhibitors of glutathione *S*-transferase: the effect of spacer length on isozyme selectivity. *Bioorg. Med. Chem. Lett.* **16**, 3780-3783.

Maegawa, T., Akashi, A., Esaki, H., Aoki, F., Sajiki, H., and Hirota, K. (2005). Efficient and selective deuteration of phenylalanine derivatives catalyzed by Pd/C. *SYNLETT* **5**, 845-847.

Maffioli, S., Candiani, G., Guglierame, P., Monciardini, P., Serina, S., and Donadio, S. (2015). Pseudouridimycin (PUM) and its derivatives. US patent 2015/0210740.

Maffioli, S.I., Zhang, Y., Degen, D., Carzaniga, T., Del Gatto, G., Serina, S., Monciardini, P., Mazzetti, C., Guglierame, P., Candiani, G., Chiriac, A.I., Facchetti, G., Kaltofen, P., Sahl, H.-G., Dehò, G., Donadio, S., and Ebright, R.H. (2017). Antibacterial nucleoside-analog inhibitor of bacterial RNA polymerase. *Cell* **169**, 1240-1248.

Maffioli, S.I., Sosio, M., Ebright, R.H., and Donadio, S. (2019). Discovery, properties, and biosynthesis of pseudouridimycin, an antibacterial nucleoside-analog inhibitor of bacterial RNA polymerase. *J. Ind. Microbiol. Biotechnol.* **46**, 335-343.

Maggi, N., Arioli, V., and Sensi, P. (1965). Rifamycins. XLI. A new class of active semisynthetic rifamycins. N-substituted aminomethyl derivatives of rifamycin SV. *J. Med. Chem.* **8**, 790-793.

Malinen, A., NandyMazumdar, M., Turtola, M., Malmi, H., Grocholski, T., Artsimovitch, I., and Belogurov, G.A. (2014). CBR antimicrobials alter coupling between the bridge helix and the β subunit in RNA polymerase. *Nat. Commun.* **5**, 3408.

Mandal, S. (2014). Novel small-molecule inhibitors of mycobacterial RNA polymerase "AAPs". Ph.D. thesis, Rutgers University.

Marazzi, A., Kurz, M., Stefanelli, S., and Colombo, L. (2005). Antibiotics GE23077, novel inhibitors of bacterial RNA polymerase. II. Structure elucidation. *J. Antibiot.* (Tokyo) **58**, 260-267.

Marchi, E., and Montecchi, L. (1979). Process for the preparation of 3 iodo- and 3 bromorifamycin S. US Patent 4,179,438.

Mariani, R., Granata, G., Maffioli, S., Serina, S., Brunati, C., Sosio, M., Marazzi, A., Vannini, A., Patel, D., White, R., and Ciabatti, R. (2005). Antibiotics GE23077, novel inhibitors of bacterial RNA polymerase. Part 3: Chemical derivatization. *Bioorg. Med. Chem. Lett.* **15**, 3748-3752.

Mariani, R., and Maffioli, S.I. (2009). Bacterial RNA polymerase inhibitors: an organized overview of their structure, derivatives, biological activity and current clinical development status. *Curr. Med. Chem.* **16**, 430-454.

Marston, H.D., Dixon, D.M., Knisely, J.M., Palmore, T.N., and Fauci, A.S. (2016). Antimicrobial Resistance. *JAMA* **316**, 1193-1204.

Matsumoto, M., Hashizume, H., Tomishige, T., Kawasaki, M., Tsubouchi, H., Sasaki, H., Shimokawa, Y., and Komatsu, M. (2006). OPC-67683, a nitro-dihydro-imidazooxazole derivative with promising action against tuberculosis *in vitro* and in mice. *PLoS Med.* **3**, e466.

McClure, W.R., and Cech, C.L. (1978). On the mechanism of rifampicin inhibition of RNA synthesis. *J. Biol. Chem.* **253**, 8949-8956.

Mekler, V., Kortkhonjia, E., Mukhopadhyay, J., Knight, J., Revyakin, A., Kapanidis, A.N., Niu, W., Ebright, Y.W., Levy, R., and Ebright, R.H. (2002). Structural organization of bacterial RNA polymerase holoenzyme and the RNA polymerase-promoter open complex. *Cell* **108**, 599-614.

Minakhin, L., Bhagat, S., Brunning, A., Campbell, E.A., Darst, S.A., Ebright, R.H., and Severinov, K. (2001). Bacterial RNA polymerase subunit ω and eukaryotic RNA polymerase subunit RPB6 are sequence, structural, and functional homologs and

promoter RNA polymerase assembly. *Proc. Natl. Acad. Sci. USA* **98**, 892-897.

Mitchison, D.A. (2000). Role of individual drugs in the chemotherapy of tuberculosis. *Int. J. Tuberc. Lung Dis.* 4, 796-806.

Moadebi, S., Harder, C.K., Fitzgerald, M.J., Elwood, K.R., and Marra, F. (2007). Fluoroquinolones for the treatment of pulmonary tuberculosis. *Drugs.* **67**, 2077-2099.

Mooney, R.A., Darst, S.A., and Landick, R. (2005). Sigma and RNA polymerase: an on-again, off-again relationship? *Mol. Cell* **20**, 335-345.

Morphy, R., and Rankovic, Z. (2005). Designed multiple ligands. An emerging drug discovery paradigm. *J. Med. Chem.* **48**, 6523-6543.

Mukherjee, T., and Boshoff, H. (2011). Nitroimidazoles for the treatment of TB: past, present and future. *Future Med. Chem.* **3**, 1427-1454.

Mukhopadhyay, J., Kapanidis, A., Mekler, V., Kortkhonjia, E., Ebright, Y.W., and Ebright, R.H. (2001). Translocation of σ70 with RNA polymerase during transcription: fluorescence resonance energy transfer assay for movement relative to DNA. *Cell* **106**, 453-463.

Mukhopadhyay, J., Das, K., Ismail, S., Koppstein, D., Jang, M., Hudson, B., Sarafianos, S., Tuske, S., Patel, J., Jansen, R., Irschik, H., Arnold, E., and Ebright, R.H. (2008). The RNA polymerase "switch region" is a target for inhibitors. *Cell* **135**, 295-307.

Murakami, K.S., Masuda, S., and Darst, S.A. (2002). Structural basis of transcription initiation: RNA polymerase holoenzyme at 4 Å resolution. *Science* **296**, 1280-1284.

Murakami, K.S., Masuda, S., Campbell, E.A., Muzzin, O., and Darst, S.A. (2002). Structural basis of transcription initiation: an RNA polymerase holoenzyme-DNA complex. *Science* **296**, 1285-1290.

Murakami, K.S., and Darst, S.A. (2003). Bacterial RNA polymerases: the wholo story. *Curr. Opin. Struct. Biol.* **13**, 31-39.

Mustaev, A., Zaychikov, E., Severinov, K., Kashlev, M., Polyakov, A., Nikiforov, V., and Goldfarb, A. (1994). Topology of the RNA polymerase active center probed by chimeric rifampicin-nucleotide compounds. *Proc. Natl. Acad. Sci. USA* **91**, 12036-12040.

Naryshkin, N., Revyakin, A., Kim, Y., Mekler, V., Ebright, R.H. (2000). Structural organization of the RNA polymerase-promoter open complex. *Cell* **101**, 601-611.

Nudler, E. (1999). Transcription elongation: structural basis and mechanisms. *J. Mol. Biol.* **288**, 1-12.

Ovchinnikov, Y.A., Monastyrskaya, G.S., Guriev, S.O., Kalinina, N.F., Sverdlov, E.D., Gragerov, A.I., Bass, I.A., Kiver, I.F., Moiseyeva, E.P., Igumnov, V.N., Mindlin, S.Z., Nikiforov, V.G., and Khesin, R.B. (1983). RNA polymerase rifampicin resistance mutations in *Escherichia coli*: sequence changes and dominance. *Mol. Gen.*

Genet. **190**, 344-348.

Pokrovskaya, V., and Baasov, T. (2010). Dual-acting hybrid antibiotics: a promising strategy to combat bacterial resistance. *Expert Opin. Drug Discov.* **5**, 883-902.

Record, M.T. Jr., Reznikoff, W., Craig, M., McQuade, K., and Schlax, P. (1996). Escherichia coli RNA polymerase (Eσ70), promoters, and the kinetics of the steps of transcription initiation, pp. 792-820. In Escherichia coli and Salmonella, F. C. Neidhardt (ed.), ASM Press, Washington, D.C.

Revyakin, A., Liu, C., Ebright, R.H., and Strick, T.R. (2006). Abortive initiation and productive initiation by RNA polymerase involve DNA scrunching. *Science* **314**, 1139-1143.

Richardson, J.P., and J. Greenblatt. (1996). Control of RNA chain elongation and termination, pp. 822-848. *In* F. C. Neidhardt (ed.), *Escherichia coli and Salmonella: Cellular and Molecular Biology*, 2nd ed. ASM Press, Washington, D.C.

Riley, L.W. (1993). Drug-resistant tuberculosis. *Clin. Infect. Dis.* **17** (Suppl 2), S442-S446.

Robertson, G.T., Bonventre, E.J., Doyle, T.B., Du, Q., Duncan, L., Morris, T.W., Roche, E.D., Yan, D., and Lynch, A.S. (2008a). *In vitro* evaluation of CBR-2092, a novel rifamycin-quinolone hybrid antibiotic: studies of the mode of action in Staphylococcus aureus. *Antimicrob. Agents Chemother.* **52**, 2313-2323.

Robertson, G.T., Bonventre, E.J., Doyle, T.B., Du, Q., Duncan, L., Morris, T.W., Roche, E.D., Yan, D., and Lynch, A.S. (2008b). *In vitro* evaluation of CBR-2092, a novel rifamycin-quinolone hybrid antibiotic: microbiology profiling studies with staphylococci and streptococci. *Antimicrob. Agents Chemother.* **52**, 2324-2334.

Rommele, G., Wirz, G., Solf, R., Vosbeck, K., Gruner, J., Wehrli, W. (1990). Resistance of *Escherichia coli* to rifampicin and sorangicin A-a comparison. *J. Antibiot*. (Tokyo) **43**, 88-91.

Ross, W., Gosink, K.K., Salomon, J., Igarashi, K., Zou, C., Ishihama, A., Severinov, K., and Gourse, R.L. (1993) A third recognition element in bacterial promoters: DNA binding by the α subunit of RNA polymerase. *Science* **262**, 1407-1413.

Ruff, E.F., Record, M.T. Jr., Artsimovitch, I. (2015). Initial events in bacterial transcription initiation. *Biomolecules* **5**, 1035-1062.

Saecker, R.M., Record, M.T. Jr., and deHaseth, P.L. (2011). Mechanism of bacterial transcription initiation: RNA polymerase-promoter binding, isomerization to initiation-competent open complexes, and initiation of RNA synthesis. *J. Mol. Biol.* **412**, 754-771.

Sarubbi, E., Monti, F., Corti, E., Miele, A., and Selva, E. (2004). Mode of action of the microbial metabolite GE23077, a novel potent and selective inhibitor of bacterial RNA polymerase. *Eur. J. Biochem.* **271**, 3146-3152.

Schecter, G.F., Scott, C., True, L., Raftery, A., Flood, J., and Mase, S. (2010). Linezolid in the treatment of multidrug-resistant tuberculosis. *Clin. Infect. Dis.* **50**, 49-55.

Sensi, P., Margalith, P., and Timbal, M.T. (1959). Rifamycin, a new antibiotic; preliminary report. *Farmaco. Sci.* **14**, 146-147.

Sensi, P., Maggi, N., Ballotta, R., Fürész, S., Pallanza, R., and Arioli, V. (1964a). Rifamycins. XXXV. Amides and Hydrazides of Rifamycin B. *J. Med. Chem.* **7**, 596-602.

Sensi, P., and Maggi, N. (1964b). Rifamycin B hydrazides. US Patent 3,197,468.

Sensi, P. (1983). History of the development of rifampin. *Rev. Infect. Dis.* **5** (Suppl. 3), 402-406.

Severinov, K., Soushko, M., Goldfarb, A., and Nikiforov, V. (1993). Rifampicin region revisited. New rifampicin-resistant and streptolydigin-resistant mutants in the β subunit of *Escherichia coli* RNA polymerase. *J. Biol. Chem.* **268**, 14820-14825.

Singh, R., Manjunatha, U., Boshoff, H.I.M., Ha, Y.H., Niyomrattanakit, P., Ledwidge, R., Dowd, C.S., Lee, I.Y., Kim, P., Zhang, L., Kang, S., Keller, T.H., Jiricek, J., and Barry, C.E. 3rd (2008). PA-824 kills nonreplicating *Mycobacterium tuberculosis* by intracellular NO release. *Science* **322**, 1392-1395.

Smith, A.B., Dong, S., Brenneman, J.B., and Fox, R.J. (2009) Total synthesis of (+)-sorangicin A. *J. Am. Chem. Soc.* **131**, 12109-12111.

Sosio, M., Gaspari, E., Iorio, M., Pessina, S., Medema, M.H., Bernasconi, A., Simone, M., Maffioli, S.I., Ebright, R.H., and Donadio, S. (2018). Analysis of the pseudouridimycin biosynthetic pathway provides insights into the formation of C-nucleoside antibiotics. *Cell Chem. Biol.* **25**, 540-549.

Sosunov, V., Sosunova, E., Mustaev, A., Bass, I., Nikiforov, V., and Goldfarb, A. (2003). Unified two-metal mechanism of RNA synthesis and degradation by RNA polymerase. *EMBO J.* **22**, 2234-2244.

Srivastava, A., Talaue, M., Liu, S., Degen, D., Ebright, R.Y., Sineva, E., Chakraborty, A., Druzhinin, S.Y., Chatterjee, S., Mukhopadhyay, J., Ebright, Y.W., Zozula, A., Shen, J., Sengupta, S., Niedfeldt, R.R., Xin, C., Kaneko, T., Irschik, H., Jansen, R., Donadio, S., Connell, N., and Ebright, R.H. (2011). New target for inhibition of bacterial RNA polymerase: 'switch region'. *Curr. Opin. Microbiol.* **14**, 532-543.

Tevyashova, A.N., Olsufyeva, E.N., and Preobrazhenskaya, M.N. (2015). Design of dual action antibiotics as an approach to search for new promising drugs. *Russ. Chem. Rev.* **84**, 61-97.

Tupin, A., Gualtieri, M., Roquet-Banères, F., Morichaud, Z., Brodolin, K., and Leonetti, J.-P. (2010). Resistance to rifampicin: at the crossroads between ecological, genomic and medical concerns. *Int. J. Antimicrob. Agents* **35**, 519-523.

Vassylyev, D.G., Sekine, S.-i., Laptenko, O., Lee, J., Vassylyeva, M.N., Borukhov,

S., and Yokoyama, S. (2002). Crystal structure of a bacterial RNA polymerase holoenzyme at 2.6 Å resolution. *Nature* **417**, 712-719.

Vassylyev, D.G., Vassylyeva, M.N., Perederina, A., Tahirov, T.H., and Artsimovitch, I. (2007a). Structural basis for transcription elongation by bacterial RNA polymerase. *Nature* **448**, 157-162.

Vassylyev, D.G., Vassylyeva, M.N., Zhang, J., Palangat, M., Artsimovitch, I., and Landick, R. (2007b). Structural basis for substrate loading in bacterial RNA polymerase. *Nature* **448**, 163-168.

Villain-Guillot, P., Bastide, L., Gualtieri, M., and Leonetti, J.-P. (2007). Progress in targeting bacterialtranscription. *Drug Discov. Today* **12**, 200-208.

von Hippel, P.H. (1998). An integrated model of the transcription complex in elongation, termination, and editing. *Science* **281**, 660-665.

Wang, D. (2008). Ensemble fluorescence resonance energy transfer analysis of RNA polymerase clamp conformation. Ph.D. thesis, Rutgers University.

Wang, Y., Severinov, K., Loizos, N., Fenyö, D., Heyduk, E., Heyduk, T., Chait, B.T., and Darst, S.A. (1997). Determinants for *Escherichia coli* RNA polymerase assembly within the β subunit. *J. Mol. Biol.* **270**, 648-662.

Williams, D.L., Waguespack, C., Eisenach, K., Crawford, J.T., Portaels, F., Salfinger, M., Nolan, C.M., Abe, C., Sticht-Groh, V., and Gillis, T.P. (1994). Characterization of rifampin resistance in pathogenic mycobacteria. *Antimicrob. Agents Chemother.* **38**, 2380-2386.

World Health Organization (2019a). No time to wait: securing the future from drug-resistant infections.

World Health Organization (2019b). Global tuberculosis report 2019.

Xu, M., Zhou, Y.N., Goldstein, B.P., and Jin, D.J. (2005). Cross-resistance of *Escherichia coli* RNA polymerases conferring rifampin resistance to different antibiotics. *J. Bacteriol.* **187**, 2783-2792.

Zhang, G., Campbell, E.A., Minakhin, L., Richter, C., Severinov, K., and Darst, S.A. (1999). Crystal structure of *Thermus aquaticus* core RNA polymerase at 3.3 Å resolution. *Cell* **98**, 811-824.

Zhang, Y., Feng, Y., Chatterjee, S., Tuske, S., Ho, M.X., Arnold, E., and Ebright, R.H. (2012). Structural Basis of Transcription Initiation. *Science* **338**, 1076-1080.

Zhang, Y., Degen, D., Ho, M., Sineva, E., Ebright, K.Y., Ebright, Y.W., Mekler, V., Vahedian-Movahed, H., Feng, Y., Yin, R., Tuske, S., Irschik, H., Jansen, R., Maffioli, S., Donadio, S., Arnold, E., and Ebright, R.H. (2014). GE23077 binds to the RNA polymerase 'i' and 'i+1' sites and prevents the binding of initiating nucleotides. *eLife* **3**, e02450.

Zhi, C., Long, Z.-Y., Manikowski, A., Comstock, J., Xu, W.-C., Brown, N.C., Tarantino, P.M. Jr., Holm, K.A., Dix, E.J., Wright, G.E., Barnes, M.H., Butler, M.M., Foster, K.A., LaMarr, W.A., Bachand, B., Bethell, R., Cadilhac, C., Charron, S., Lamothe, S., Motorina, I., and Storer, R. (2006). Hybrid antibacterials. DNA polymerase-topoisomerase inhibitors. *J. Med. Chem.* **49**, 1455-1465.

Zhu, W., Haupenthal, J., Groh, M., Fountain, M., and Hartmann, R. (2014). New insights into the bacterial RNA polymerase inhibitor CBR703 as a starting point for optimization as an anti-infective agent. *Antimicrob. Agents Chemother.* **58**, 4242-4245.